A GENERALIZED APPROACH TO THE DESIGN AND OPTIMIZATION OF SYMMETRICAL MICROWAVE FILTERS FOR COMMUNICATIONS SYSTEMS

Chandra M. Kudsia

A Thesis

in

The Faculty

of

Engineering

Presented in Partial Fulfillment of the Requirements
for the degree of Doctor of Philosophy
Concordia University
Montreal, Québec, Canada

November 1978

for my parents

ABSTRACT

ABSTRACT

A GENERALIZED APPROACH TO THE DESIGN AND OPTIMIZATION OF SYMMETRICAL MICROWAVE FILTERS FOR COMMUNICATIONS SYSTEMS

Chandra M. Kudsia, Ph.D.
Concordia University, 1978

The work described in this thesis was motivated by the continuing demands of the satellite communications industry for ever-more efficient filtering at microwave frequencies. Techniques and computer software have been developed to analyze and design the general class of lumped, doubly terminated, low-pass prototype filter networks for an arbitrary set of amplitude constraints. The objective function is defined in terms of the practical parameters of transmission or reflection loss in decibels (dB) at frequencies of attenuation poles and zeros-referred to as the critical frequencies of the general transmission function. The gradients of the objective and constraint functions are derived analytically. Two separate optimization programs are developed; one using the direct-search technique of the SIMPLEX method, and the other, a gradient strategy employing new Fletcher's algorithm. With the proper formulation of the problem, the gradient method has shown remarkable efficiency. Its flexibility is demonstrated by generating the known classes of filter functions such as Chebyshev and

elliptic in about 2 to 6 seconds of CPU time as special cases of the general optimization problem. The effect of dissipation is examined in detail, and included in the prototype low-pass and all-pass networks. This model is then used to derive practical filters and all-pass networks.

From the optimized critical frequencies of the prototype network, practical coupled-cavity band-pass filters are synthesized, using the basic technique described by Atia et al. New closed-form relationships are derived for the couplings of given-order filters in a dual-mode configuration in terms of the eigenvalues of the symmetric coupling matrix with excess couplings, if any, as parameters. This significantly reduces the matrix manipulations and provides a ready means to optimize the couplings to realize a less sensitive practical network. For narrow-band application, microwave filter structure can then be derived in terms of the distributed elements, as described by Cohn. The theoretical work and the associated computer software developed in the thesis were put to practical test in generating filter and multiplexer trade-offs for the upcoming Canadian Domestic Satellite (ANIK-C) in the 12 GHz frequency band. The optimized designs were realized in a dual-mode configuration with TE_{103} as the mode of propagation. The measured results agree closely with the theoretical response.

ACKNOWLEDGEMENTS

ACKNOWLEDGEMENTS

I wish to thank Dr. M.N.S. Swamy who encouraged me to join this program and agreed to be my supervisor. His encouragement and advice during the course of this work are deeply appreciated.

I feel grateful to my friend and ex-colleague, Virendra K. Jha, who nudged me to join this course and later helped me in dealing with the optimization problem. Thanks are also due to another ex-colleague, S. Kallianteris, with whom I had many interesting discussions on dual-mode realization of microwave filters and who provided some of the measured data on such units. I take special pleasure in thanking all my colleagues at Com Dev Limited, for providing me with the most stimulating environment to pursue my research. This added significantly to the quality and practical usefulness of this thesis. I also wish to thank Miss Margaret Stredder for her par-excellence in typing this manuscript.

Last, but not least, I thank my wife, Wendy, and our three children, Shari, Rajeev, and Dev, who often missed me on the weekends and late evenings during the course of this study.

TABLE OF CONTENTS

TABLE OF CONTENTS

LIST OF FIGURES

LIST OF FIGURES

LIST OF TABLES

LIST OF TABLES

LIST OF IMPORTANT ABBREVIATIONS AND SYMBOLS

LIST OF IMPORTANT ABBREVIATIONS AND SYMBOLS

a_i	i^{th} attenuation zero of the transfer function
b_i	i^{th} attenuation pole of the transfer function
dB	decibels
s	complex frequency variable
ω	real frequency variable in radians/second
f	real frequency variable in hertz
ω_1	pass-band band-width of low-pass prototype filter with respect to maximum ripple in the pass-band.
ω_3	stop-band band-width of low-pass prototype filter with respect to minimum attenuation in the stop-band
R_1, A_1	return loss and transmission loss in dB with respect to pass-band band-width ω_1
ω'_c	cut-off frequency of the low-pass prototype filter
R_3, A_3	return loss and transmission loss in dB with respect to stop-band band-width ω_3
R(j), T(j)	return loss and transmission loss in dB at the j^{th} attenuation minima or maxima
P_t	transmitted power per unit incident power
P_r	reflected power per unit incident power
P_{max}	maximum available power
F(s)	characteristic polynomial containing attenuation zeros
P(s)	characteristic polynomial containing attenuation poles

$E(s)$	Hurwitz polynomial
$K(s)$	characteristic polynomial of the transfer function
F	characteristic factor in dB
k	characteristic coefficients
n	number of poles in the transfer function
ε	ripple factor
ρ	reflection coefficient
t	transmission coefficient
S_k	$k^{\underline{th}}$ pole or zero of a given function
σ_k	real part of S_k
ω_k	imaginary part of S_k
β	phase in radians
τ	group delay in seconds
Q	quality factor
Q_0	unloaded quality factor
δ	dissipation factor
U	objective function
U_{art}	artificial objective function
ϕ	equality constraints
Φ	inequality constraints
H	Hessian matrix
δ_{ij}	Kronecker delta
I	identity matrix
M_{ij}	mutual coupling

M_e	even-mode coupling matrix
N	third index of operating mode
λ_g	guide wave-length
λ_c	cut-off wave-length of the wave-guide
Y_0	characteristic admittance of the guide
B	susceptance of irises
B/Y_0	normalized susceptance
ℓ	length of wave-guide cavity
VSWR	voltage standing wave ratio
λ	free space wave-length
$\lambda_1, \lambda_2, \ldots$	eigen values of the coupling impedance matrix

CHAPTER I

INTRODUCTION

CHAPTER I

INTRODUCTION

The recent past has witnessed an enormous growth of the commercial communications satellite industry. This has put economic pressures on satellite operators to increase the communications capacity within the allocated band-widths. One of the areas pressed hard to accomplish this has been the channelization of the available bandwidth through ever more efficient passive filtering. This has had the effect of an unprecedented activity in this area and has resulted in significant improvements in microwave filters and multiplexing networks. This trend is expected to continue - especially in the 14/11 GHz and 30/20 GHz frequency bands which are now available for satellite communication.

For satellites in the late sixties and early seventies, the bulk of RF filters used were direct-coupled waveguide band-pass filters based on the classic paper by Cohn [1]. For some applications in the L and S-band transponders, inter-digital filters were used based upon the works of Matthaei [2,3]. The paper by Wenzel [4] on inter-digital band-pass filters paved the way for subsequent work on general inter-digital filters. Subsequently,

Rhodes described the stepped digital elliptic function filters [5] and linear phase filters [6]. Rhodes also realized a waveguide linear phase filter in a folded-type structure [7].

Levy [8] described waveguide band-pass filters that realized a single pair of real-axis or transmission zeros. Prior to the work of Rhodes and Levy, Kurzrok [9, 10] reported the realization of 3 and 4-pole filters in waveguide and coax structures with bridge couplings to realize transmission zeros or real-axis zeros. In the early seventies, Comsat Laboratories performed pioneering work in realizing waveguide filters using two orthogonal modes in the same waveguide cavity. This resulted not only in the saving of volume and weight, which are critical parameters for space application, but also helped to realize generalized filter functions which can be used to optimize the communication channel performance. The simplicity of such a construction has virtually eliminated other types of structures to realize generalized response functions.

The early work in this area was performed by Blachier [11] and later generalized and significantly expanded by Atia and Williams [12,13,14]. The use of higher order propagation modes to achieve low loss was also advanc-

ed by Atia and Williams [15] in a single mode structure and later by Kallianteris and O'Donovan [16] in a dual-mode configuration. Nearly all narrow-band band-pass filters for space application utilize a dual-mode configuration using a dominant mode of propagation in 4,6 and 8 GHz frequency band and higher order propagation modes in 12 GHz and higher frequency bands.

There are two basic areas to improve the performance of passive electric filters. One is to optimize the response function for a given amplitude and phase or group delay requirements. This is accomplished most conveniently by dealing with the low-pass prototype network. Practical filters in the lower frequencies that are characterized by lumped elements or narrow-band filters at higher frequencies using distributed elements, can then be derived by using simple frequency transformations. The second area for advancing the state-of-the-art is in the physical realization of the response functions. This normally implies the lowest cost for application in ground-based equipment. For space application, achieving the minimum weight and high reliability are as important as the cost.

With the above background, the work carried out during the course of this thesis has been directed:

(a) Toward the development of computer programs to conduct filter and multiplexer tradeoffs under optimal conditions, so as to obviate the need of having to deal with specific filter functions, and

(b) Toward generalizing the approach to designing narrow-band band-pass microwave filters for space application.

These objectives have been met with the successful application of the results of this thesis to the design and optimization of the input and output multiplexing networks for the upcoming Canadian Domestic Satellite ANIK-C.

The thesis is divided into seven chapters. Following the Introduction, Chapter II is devoted to reviewing the basic characteristics of doubly terminated filter networks. Special emphasis has been placed on the relationships that relate the pole-zero configuration of the basic low-pass prototype structure to such practical parameters as insertion loss in dB and group delay in nanoseconds, and so on. The concept of unified design charts and of the tradeoff that exists, dB for dB, between the isolation in stopband and return loss in pass-band is highlighted.

The effect of dissipation on low-pass prototype networks is considered in detail in Chapter III. Expressions are derived for the equivalent low-pass prototype dissipation factors for the low-pass; high-pass, band-pass and band-stop filters.

The same concept is extended to derive equivalent dissipation factors for the normalized frequency variable of lumped and distributed all-pass networks. The inclusion of dissipation factors for the prototype low-pass and all-pass networks provides the models to derive the practical filters and all-pass networks through the use of frequency transformations.

These last two chapters provide an adequate backgorund for Chapter IV, which is devoted to the determination of pole-zero configuration for the most general class of doubly terminated, low-pass prototype filter networks. This is accomplished by developing computer-aided optimization programs in conjunction with analytic techniques to analyze and optimize lumped, doubly terminated, and low-pass prototype filter networks for an arbitrary set of amplitude constraints. The programs make use of the finite number of attenuation poles and zeros (referred to as the critical frequencies) of the transmission function as independent variables. The objective function is defined in terms of the practical parameters of transmission loss or return loss

or both in decibels (dB) at the critical frequencies or others, if required. The gradients of the objective function along with the inequality and equality constraints, if any, are derived analytically. Algorithms are developed that minimize the number of independent variables and constraint functions without loss of generality. Two separate optimization programs are developed; one based on the direct-search using the Simplex method, the other using a gradient strategy employing new Fletcher's algorithm. The programs have demonstrated the intended flexibility in generating new realizable filter functions. The well-known functions such as Butterworth, Chebyshev or the elliptic responses, can be derived as special cases of the generalized transfer function. With appropriate constraints to ensure physical realizability, this provides a tool to conduct filter trade-offs under optimal conditions. The technique is completely general, and is capable of generating new types of filter functions determined solely by the overall system requirements. Low-pass prototype characteristics of some new filter functions which are likely to have a practical application, are provided to aid filter designers in Chapter V.

Filter synthesis for band-pass filters is carried out using the basic technique described by Atia et al. [14] in Chapter VI. Closed-form expressions are derived for

the coupling coefficients in terms of the eigen values of the generalized coupling matrix which, in turn, are related to the pole-zero configuration of the prototype network. If the required couplings are greater than the degrees of freedom of the network in realizing a given response, then an arbitrary choice of excess couplings is used as parameters to optimize the coupling coefficients in realizing a less sensitive structure. For narrow-band application, the microwave filter structure is then derived in terms of the distributed elements, as described by Cohn [1]. Computer software has been developed that generates a susceptance matrix from the coupling matrix. The susceptance values are related to the physical dimensions of the irises or other tuning elements, either by such expressions as derived in Marcuvitz [17], or by generating susceptance versus physical dimensions of practical irises for a range of values. The derived susceptance matrix can be used to realize a dominant or higher order TE_{11N} or TE_{10N} propagation modes for the realization of filters in single or dual-mode waveguide structures. Practical examples of filters realized in a dual-mode configuration in the 12 GHz frequency band adequately demonstrate the accuracy of the computer software and the closed-form relationships for mutual-couplings developed in this thesis.

The last chapter describes the conclusions of this thesis. The original work carried out is reviewed. The areas of any future research where this thesis could be of value are highlighted.

A brief description of the computer programs with typical outputs is included in the Appendix.

CHAPTER II

CHARACTERIZATION OF DOUBLY TERMINATED FILTER NETWORKS

CHAPTER II

CHARACTERIZATION OF DOUBLY-TERMINATED FILTER NETWORKS

2.1 POWER TRANSFER AND PROPERTIES OF CHARACTERISTIC POLYNOMIALS

The basic properties of doubly terminated loss-less coupling networks are described in many classical textbooks [18,19,20]. These properties will be briefly reviewed here with an emphasis on those aspects which form the basis of research described in this thesis.

Filter networks considered here are terminated in resistors of equal value to effect a maximum power transfer. Such is the requirement in general communications systems. A loss-less doubly terminated two-port network is described in Figure 2.1. The maximum available power P_{max} from the ideal voltage source E is $E^2/4R_1$. Power P_2, delivered to the load R, is $|V_2|^2/R_2$. Therefore,

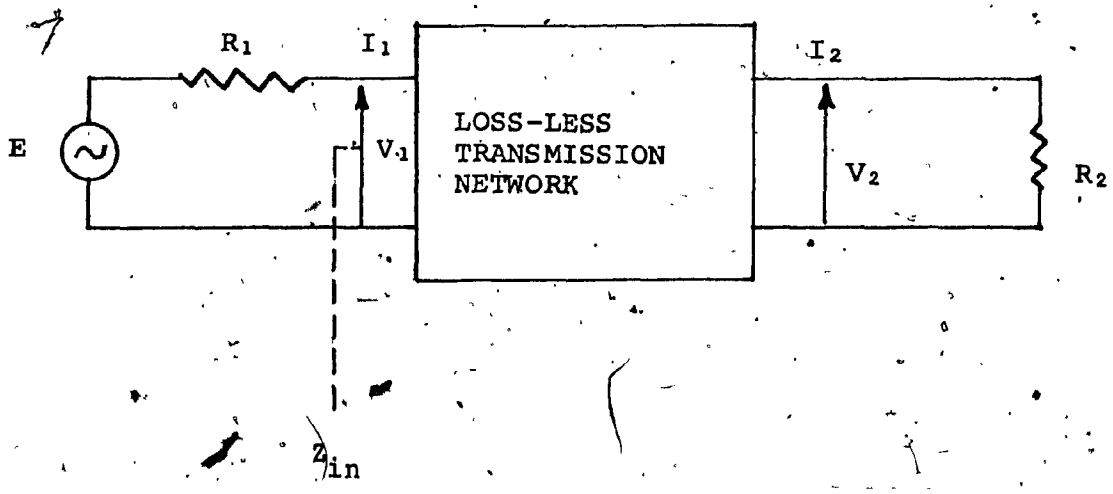

FIG. 2.1 DOUBLY TERMINATED LOSS-LESS TRANSMISSION NETWORK

$$\frac{P_{max}}{P_2} = \left| \frac{1}{2} \cdot \sqrt{R_2/R_1} \cdot \frac{E}{V_r} \right|^2 \qquad (2.1)$$

$$= \frac{1}{4} \cdot \left| \frac{E}{V} \right|^2 \quad \text{for } R_1 = R_2 \qquad (2.2)$$

For passive, loss-less two-port networks, P_2 can be equal to or less than P_{max}. For such networks, therefore, it is most convenient to define the characteristic function K(s) [21,22,23] by

$$\frac{P_{max}}{P} = 1 + \left| K(s) \right|^2_{s=j\omega} \qquad (2.3)$$

For lumped, linear and time-invariant circuits considered here, K(s) is a rational function in s with real coefficients. The ratio $\frac{P_{max}}{P_2}$ is defined by the transmission function H(s) where

$$\left| H(s) \right|^2_{s=j\omega} = 1 + \left| K(s) \right|^2_{s=j\omega} \qquad (2.4)$$

H(s) is also referred to as the transducer function and the above relationship is known as the "Feldtkeller equation". It may be written in the alternative form

$$H(s)\,H(-s) = 1 + K(s)\,K(-s)$$

since all network functions are rational in s with real coefficients. For the same reasons, the transmission function and the characteristic functions may be expressed as the ratio of polynomials in the form

$$H(s) = \frac{E(s)}{P(s)} \qquad (2.5)$$

and

$$K(s) = \frac{F(s)}{P(s)} \qquad (2.6)$$

The functions must satisfy the following conditions if they are to correspond to a realizable reactive network:

- $E(s)$, $F(s)$ and $P(s)$ must be rational functions of s with real coefficients
- $E(s)$ must be a Hurwitz polynomial, i.e., its zeros must lie in the left-half plane of s
- $P(s)$ is a pure even or pure odd polynomial
- The degree of $E(s)$ is greater than or equal to that of either $F(s)$ or $P(s)$

Furthermore, $\left|H(s)\right|_{s=j\omega} \geq 1$ must be satisfied for networks consisting of passive elements implying that the power delivered to the load can never exceed the maximum available power from the source.

An alternative form of Feldtkeller equation may then be expressed as

$$E(s)\ E(-s) = F(s)\ F(-s) + P(s)\ P(-s) \qquad (2.7)$$

It is to be noted that only two polynomials are necessary to define the transmission function completely. The third polynomial can be derived from the Feldtkeller relation, as above.

2.2 REFLECTION AND TRANSMISSION COEFFICIENTS

The reflection coefficients for two-port networks are defined by

$$\rho_1(s) = \frac{Z_{in} - R_2}{Z_{in} + R_1} \qquad (2.8)$$

and

$$\rho_2(s) = \frac{Z_{in} - R_1}{Z_{in} + R_2} \qquad (2.9)$$

For equally terminated networks,

$$\rho_1(s) = \rho_2(s) = \rho(s) = \frac{Z_{in} - R}{Z_{in} + R} \qquad (2.10)$$

where

$$R_1 = R_2 = R$$

For loss-less two-port networks, it is easily shown that

$$|\rho(j\omega)|^2 = 1 - \frac{P_2}{P_{max}} = \frac{\text{Reflected Power}}{\text{Available Power}} \qquad (2.11)$$

Similarly, the transmission coefficient $t(j\omega)$ is given by

$$|t(j\omega)|^2 = \frac{\text{Transmitted Power}}{\text{Available Power}} \qquad (2.12)$$

or

$$|t(j\omega)|^2 = \frac{P_2}{P_{max}} = 1 - |\rho(j\omega)|^2 \qquad (2.13)$$

and

$$|\rho(j\omega)|^2 + |t(j\omega)|^2 = 1 \qquad (2.14)$$

In terms of the characteristic polynomials,

$$\rho(s) = \frac{F(s)}{E(s)} \qquad (2.15)$$

and

$$t(s) = \frac{P(s)}{E(s)} \qquad (2.16)$$

Another interesting relationship that relates transmitted and reflected powers is easily derived as

$$\left|K(s)\right|^2_{s=j\omega} = \frac{\left|\rho(j\omega)\right|^2}{\left|t(j\omega)\right|^2} \qquad (2.17)$$

$$= \frac{P_r}{P_t} \qquad (2.18)$$

where

P_r is the reflected power, and

P_t is the transmitted power

2.3 CHARACTERISTIC POLYNOMIALS FOR IDEALIZED LOW-PASS PROTOTYPE NETWORKS

It is normal practice in filter theory to deal with ideal, normalized, low-pass prototype transmission functions. It has the simplest form and provides the model from which all types of practical filters can be derived through the use of frequency transformations. The effect of losses associated with the elements of the network and their frequency dependence, if it is significant, can then be incorporated to determine the true response. There is little loss of accuracy, as long as these effects are small, which is indeed the case for most practical applications. We follow a similar approach in the work described in this thesis.

Figure 2.2 depicts the response of an ideal low-pass filter. Such a filter has zero loss below the cut-off frequency, and infinite loss for all higher frequencies.

Such a response cannot be satisfied with finite circuit elements and consequently, the more practical form, as described in Figure 2.3, is chosen. Here, the loss is less than a prescribed limit α_p in the frequency band $o<\omega<\omega_c$ referred to as the pass-band and above a certain prescribed value α_s in the frequency range $\omega_s<\omega<\infty$ which is referred to as the stop-band.

In practical communications systems, filter requirements call for low loss in the pass-band and high loss in other frequency bands. Such a requirement can best be achieved by assigning all zeros of K(s) to the $j\omega$-axis in the pass-band region and all poles of K(s) to the $j\omega$-axis in the high loss frequency bands. For some practical specifications, poles of K(s) have non $j\omega$-axis location. This results in improved phase and group delay response in the pass-band at the expense of attenuation in the stop-band. Such a tradeoff is sometimes beneficial for the overall system requirements. The zeros of K(s), however, are invariably required to lie on the $j\omega$-axis in the pass-band region for most practical applications. This is to ensure low loss in the pass-band of the filter. With these considerations in mind, we shall deal with the characteristic function K(s)

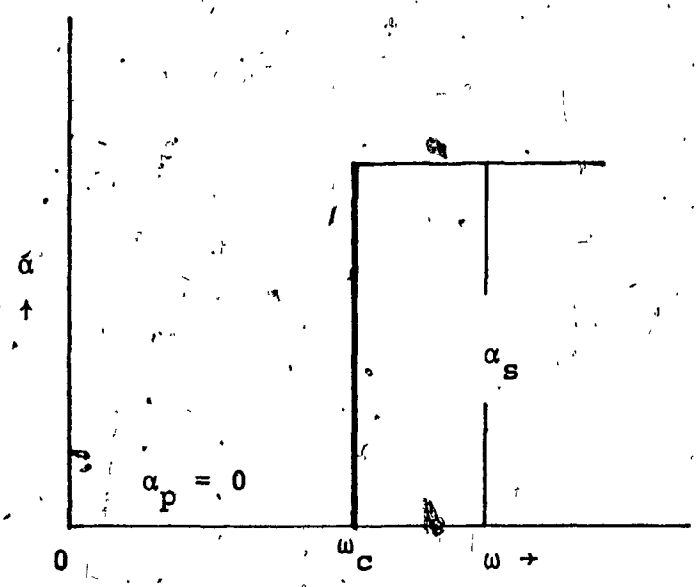

FIG. 2.2 IDEAL LOW-PASS AMPLITUDE RESPONSE

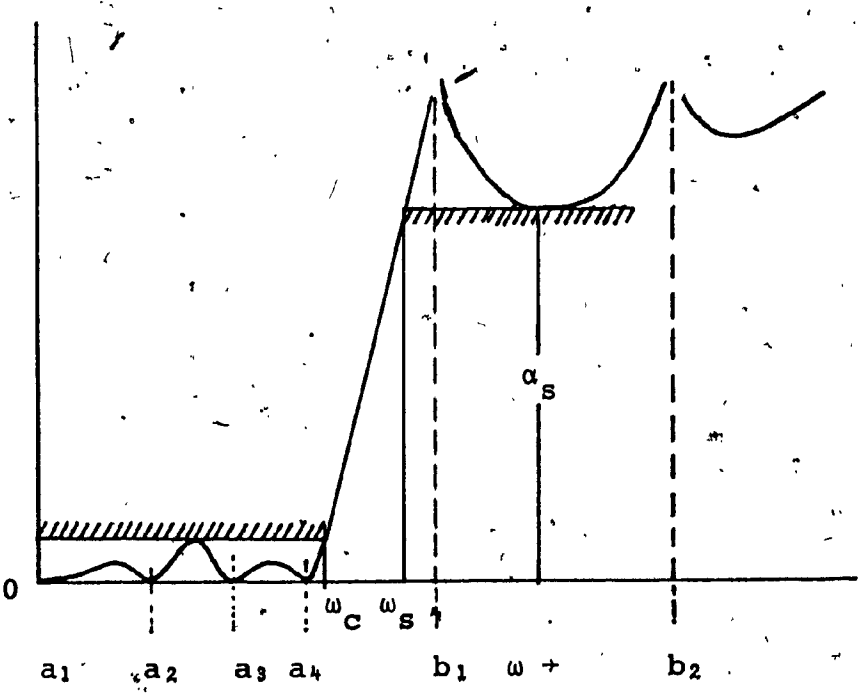

FIG.2.3 PRACTICAL LOW-PASS PROTOTYPE FILTER RESPONSE

with the following restrictions:

- All zeros of K(s) to lie on the jω-axis in the pass-band region.
- All poles of K(s) to lie on the jω-axis or real axis.

Although the quadrantal symmetry for the poles of K(s) is permitted, we shall confine the locations to jω or real axis in this thesis. This covers the requirements for most practical applications.

The characteristic function K(s) considered here, will therefore have the following forms:

$$K(s) = \frac{F(s)}{P(s)} = \frac{s(s^2+a_1^2)(s^2+a_2^2)\cdots}{(s^2\pm b_1^2)(s^2\pm b_2^2)\cdots} \qquad (2.19)$$

for odd-order networks, and

$$K(s) = \frac{F(s)}{P(s)} = \frac{(s^2+a_1^2)(s^2+a_2^2)(s^2+a_3^2)\cdots}{(s^2\pm b_1^2)(s^2\pm b_2^2)\cdots}$$

for even-order networks. The constraints on a's and b's referred to as the critical frequencies are

$$1 \leq a_1, a_2, \ldots \geq 0$$

and

$b_1, b_2, \ldots$ can have any value except between 0 and 1 inclusively.

The amplitude response is normalized such that the pass-band cut-off frequency is unity. It is to be noted that $j\omega$-axis location of the poles and zeros must occur in conjugate pairs to keep the polynomials rational. The real-axis zeros of $P(s)$ must also occur in conjugate pairs to satisfy the restriction for $P(s)$ to be pure even or odd polynomials. This also implies that zeros of $P(s)$ must have quadrantal symmetry.

To examine these polynomials with respect to reflection and transmission characteristics, we recall the relationships

$$\rho(s) = \frac{F(s)}{E(s)}$$

and

$$t(s) \quad \frac{P(s)}{E(s)}$$

and

$$E(s)\ E(-s) = F(s)\ F(-s) + P(s)\ P(-s)$$

From this, it is evident that the frequencies a_1, a_2, ... are zeros of reflection, i.e., frequencies at which all power is transmitted and none reflected. These frequencies are therefore also referred to as attenuation

zeros. Similarly, frequencies b_1, b_2, ... are zeros of transmission (if located on $j\omega$-axis), i.e., at these frequencies no power is transmitted and there is a total reflection of power. For this reason, these frequencies are more commonly termed as attenuation poles or transmission zeros. Together, a's and b's are termed as critical frequencies and they determine completely the basic response shape of a filter network.

The polynomial E(s), as stated earlier, is strictly Hurwitz, i.e., all its zeros must lie in the left-half of the s-plane. Since E(s) occurs in the denominator of t(s), the zeros of E(s) are commonly referred to as the poles of the transfer or insertion loss function.

2.4 UNIFIED DESIGN CHARTS RELATIONSHIPS

The concept of unified design charts is explained in references [24,25,26]. A brief summary giving the underlying principle and its application in filter design is provided in this section.

It has been shown in the previous sections that the characteristic function K(s) can be described by

$$\left|K(s)\right|^2_{s=j\omega} = \frac{Pr}{Pt} = \frac{\text{reflected power}}{\text{transmitted power}} \qquad (2.20)$$

If we choose ω_1 as the band-width corresponding to the maximum ripple in the pass-band and ω_3 as the bandwidth corresponding to the minimum attenuation in the stop-band, then we can write

$$\left(\frac{Pr}{Pt}\right)_{s=j\omega_1} \cdot \left(\frac{Pt}{Pr}\right)_{s=j\omega_3} = \frac{|K(s)|^2_{s=j\omega_1}}{|K(s)|^2_{s=j\omega_3}} = FF(\omega_1,\omega_3) \text{ (say)} \tag{2.21}$$

$$\therefore (R_1-A_1) + (A_3-R_3) = 10 \log FF(\omega_1,\omega_3)$$
$$= - F(\omega_1,\omega_3) \text{ (say)} \tag{2.22}$$

or

$$- (R_1+A_3) + (A_1+R_3) = F(\omega_1,\omega_3) = F \tag{2.23}$$

where

R_1, A_1 are the return loss and transmission loss in dB corresponding to the maximum ripple in the pass-band

R_3, A_3 are the return loss and transmission loss in dB corresponding to the minimum attenuation in the stop-band

F is a dimensionless quantity with dB as the units. It is termed by the author as the Characteristic Factor

F Vs (ω_3/ω_1) gives rise to the unified design charts. For most practical applications, F > 20 dB and $A_1 + R_3 \simeq 0$, and, consequently,

$$- (R_1 + A_3) \simeq F \qquad (2.24)$$

Thus, a tradeoff exists, dB for dB between the return loss in the pass-band and transmission loss in the stop-band at a pair of specified frequencies. The choice of these frequencies is arbitrary, as long as $A_1 + R_3 \simeq 0$. However, for universal and useful application of the F Vs (ω_3/ω_1) curves, ω_1 is chosen with respect to the equi-ripple peaks of return loss in pass-band if applicable, or with respect to the maximum ripple for the non-equi-ripple type of filter functions. Similarly, ω_3 is chosen with respect to an equi-ripple or maximum ripple in a stop-band as applicable. Reference [11] provides unified design chart relationships and curves for the known transmission functions. This concept is applied later for some new functions developed in the thesis.

Before concluding this section, two points need emphasis:

Firstly, the relationship $F = (R_1+A_3) + (A_1+R_3)$ is an exact relationship. Also, there are only two independent variables since the return loss and transmission loss in

dBs are related by

$$A = 10 \log \left[1-10^{R/10}\right] \qquad (2.25)$$

Secondly, unified design charts provide, at a glance, the order of filter required for a given set of amplitude constraints. In addition, they provide the trade-offs between the return loss in pass-band and attenuation in stop-band or, alternatively, between the pass-band and stop-band bandwidths for a given order of filter and the amplitude constraints.

A judicious choice of order of filter 'n', pass-band return loss R_1, and the pass-band bandwidth ω_1 using these charts invariably provides an excellent first-cut filter design.

2.5 RIPPLE FACTOR AND ITS SIGNIFICANCE IN FILTER DESIGN

In all discussions so far, we have written the characteristic function as

$$K(s) = \frac{F(s)}{P(s)} = \frac{(s^2+a_1^2)(s^2+a_2^2)\ldots}{(s^2+b_1^2)(s^2+b_2^2)\ldots}$$

and the power transmitted per unit incident (available) power is

$$Pt = \frac{1}{1 + \left|(K(s)\right|^2_{s=j\omega}} \qquad (2.26)$$

Without loss of generality, one may introduce a real constant ε referred to as the ripple factor, such that

$$K(s) = \varepsilon \frac{(s^2+a_1^2)(s^2+a_2^2)\ldots}{(s^2+b_1^2)(s^2+b_2^2)\ldots} \qquad (2.27)$$

It does not alter the position of attenuation poles or zeros and hence the basic shape of the response. However, it does affect the location of the poles of the transfer function, since

$$t(s) = \frac{P(s)}{E(s)}$$

and

$$E(s)\,E(-s) = F(s)\,F(-s) + P(s)\,P(-s)$$

where

$$F(s) = \varepsilon(s^2+a_1^2)(s^2+a_2^2)\ldots \qquad (2.28)$$

As a consequence, the filter response depends upon the choice of ε. For equi-ripple pass-bands, ε determines the magnitude of the ripple maxima. For a maximally flat pass-band or non equi-ripple pass-band, ε is normally chosen with respect to the maximum permissible ripple. In practical terms, it is determined as follows:

$$|t(j\omega)|^2 = \frac{1}{1 + \varepsilon^2 |K(s)|^2_{s=j\omega}}$$

$$= 1 - |\rho(j\omega)|^2 \qquad (2.29)$$

If ω_1 is the pass-band bandwidth corresponding to the maximum ripple of A_1 dB in the pass-band, then

$$\varepsilon = \sqrt{\frac{|t(j\omega_1)|^{-2} - 1}{|K(j\omega_1)|^2}} \qquad (2.30)$$

where

$$|t(j\omega_1)| = 10^{A_1/20}$$

If R_1 is the return loss in dB corresponding to the maximum ripple, then

$$R_1 = 10 \log [1 - 10^{A_1/10}] \text{ dB} \qquad (2.31)$$

For low-pass prototype networks, ω_1 is referred to as the cut-off frequency and is normally chosen to be unity. For Chebyshev filters,

$$|K(s)|_{s=j1} = 1$$

and

$$\varepsilon = \sqrt{10^{-A_1/10} - 1} \qquad (2.32)$$

For Cauer parameter filters with unity pass-band cutoff frequency or for other general non-equi-ripple or linear phase class of filters, ε must be determined through the relationship of Equation (2.30).

An important point will be made here regarding the unified design chart relationship as described by Equation (2.26). It is easily seen that this relationship is independent of the ripple factor ε since we deal with the ratio of K(s) at two different frequencies. The value of the characteristic factor F remains unchanged and is determined solely by the choice of attenuation zero and pole frequencies. The choice of ε on the other hand, governs the tradeoff between the return loss in the pass-band and attenuation in the stopband for a given F. More explicity, from the relationship

$$-(R_1 + A_3) + (A_1 + R_3) = F$$

and for a given F, choice of ε alters the values of $R_1(A_1)$ and $A_3(R_3)$ within the constraint of a constant F. In other words, the dB for dB tradeoff between the return loss in pass-band and attenuation in stop-band is preserved and provided by the selection of the ripple factor.

2.6. LOW-PASS PROTOTYPE CHARACTERISTICS

Practical filters are typically specified in terms of their

- Insertion Loss in decibels (dB) versus frequency response and
- Pass-band group delay or phase deviation from linearity in nano-seconds and degrees, respectively.

Insertion loss in dB is defined by

$$\alpha(j\omega) = 10 \log \frac{P_{max}}{P^2} = 10 \log 1/|t(j\omega)|^2$$

$$= 20 \log \frac{|E(s)|}{|P(s)|} \qquad (2.33)$$

The power ratio can be represented in the form [18]

$$|t(s)|^2 = \frac{P_2}{P_{max}} = \frac{|P(s)|^2}{|E(s)|^2}$$

$$= H_0^2 \frac{|(s-S_1)(s-S_3)(s-S_5) \ldots (s-S_m)|^2}{|(s-S_2)(s-S_4)(s-S_6) \ldots (S-S_n)|^2} \qquad (2.34)$$

where

H_0 is an arbitrary constant to ensure that $\frac{P_2}{P_{max}} \leq 1$.

It is to be noted that $t(s)$ represents the voltage transfer function of the filter networks as it represents the square root of the ratio of the power delivered to the load and the available power. $S_2, S_4, \ldots S_n$ are the poles of $t(s)$ and must lie in the left-half of the s-plane. $S_1, S_3, \ldots S_m$ represent zeros of the transmission function if they lie on the $j\omega$-axis, and represent a linear phase structure if they lie along the σ-axis.

The insertion loss 'α' can be written as

$$\alpha = 10 \log e \cdot \ell n \frac{1}{H_0^2} \cdot \frac{|(s-S_2)(s-S_4) \ldots (s-S_n)|^2}{|(s-S_1)(s-S_3) \ldots (s-S_m)|^2}$$

$$= 20 \log e \, [\ell n|s-S_2| + \ell n|s-S_4| + \ldots - \ell n|s-S_1| - \ell n|s-S_3| - \ldots] - 20 \log e . \ell n \, H_0 \text{ dB} \qquad (2.35)$$

At real frequencies, i.e., at $s = j\omega$, a typical term in the insertion loss is given by

$$|s-S_k|_{s=j\omega} = |s-\sigma_k-j\omega_k|_{s=j\omega}$$

$$= \sqrt{\sigma_k^2 + (\omega-\omega_k)^2} \qquad (2.36)$$

where

$S_k = \sigma_k + j\omega_k$ represents the k^{th} pole or zero of the transfer function.

The derivatives of α are given in reference [25].

The phase response for the filter network is given by

$$\beta(\omega) = \text{Arg } t(j\omega)$$

$$= \tan^{-} \frac{\text{Im } t(j\omega)}{\text{Re } t(j\omega)}$$

$$= \sum_{\text{zeros}} \tan^{-1}\left(\frac{\omega-\omega_k}{\sigma_k}\right) - \sum_{\text{poles}} \left(\frac{\omega-\omega_k}{\sigma_k}\right) \qquad (2.37)$$

The derivatives of β are given by [25]

$$\frac{d\beta}{d\omega} = \sum_{\text{zeros}} \left(\frac{\sigma_k}{\sigma_k^2 + (\omega-\omega_k)^2}\right) - \sum_{\text{poles}} \left(\frac{\sigma_k}{\sigma_k^2 + (\omega-\omega_k)^2}\right) \qquad (2.38)$$

$$\frac{d^2\beta}{d\omega^2} = \sum_{\text{zeros}} 2\tau_k^2 \tan \beta_k - \sum_{\text{poles}} 2\tau_k^2 \tan \beta_k \qquad (2.39)$$

and so on. The term τ_k is the group delay given by

$$\tau_k = -\frac{d\beta_k}{d\omega} = \frac{\sigma_k}{\sigma_k^2 + (\omega-\omega_k)^2} \qquad (2.40)$$

2.6.1 Phase Linearity

Phase linearity is defined as the deviation of phase from the linear phase versus frequency curve. The reference

frequency chosen is normally zero for low-pass prototype filters and center frequency for band-pass filters. There is no restriction on the choice of reference frequency.

Let ω_{ref} be the reference frequency. The linear phase ϕ_L is then given by

$$\phi_L = \left(\frac{d\beta}{d\omega}\right)_{\omega=\omega_{ref}} \cdot (\omega-\omega_{ref})$$

$$= \tau_{ref} \cdot (\omega-\omega_{ref}) \qquad (2.41)$$

where

τ_{ref} is the absolute group delay at the reference frequency

The phase linearity '$\Delta\phi$' at a given frequency ω is given by

$$\Delta\phi = \beta(\omega) - \phi_L \qquad (2.42)$$

If the reference frequency is zero, then

$$\Delta\phi = \beta(\omega) - \tau_0 \cdot \omega \qquad (2.43)$$

where

$$\tau_0 = \left.\frac{d\beta}{d\omega}\right|_{\omega=0}$$

2.7 FREQUENCY TRANSFORMATIONS

All the discussion on filter design throughout this thesis is based upon the lumped-element, low-pass prototype network. Practical lumped element filters or narrow-band filters using distributed elements are then derived using the frequency transformations [1,18,19]. These transformations are equally applicable for distributed circuits consisting of lumped resistors and commensurate transmission lines [26,27,28]. The equivalence between the lumped circuit elements and the TEM distributed structures is given by Richard's transformation [26]. Wenzel [27] has given a tutorial summary on the exact synthesis approach for TEM structures. The bulk of the practical applications are for narrow-band band-pass filters. The relationships that describe the amplitude and phase and their derivatives in terms of their low-pass prototype parameters for such filters are given in reference [25].

For practical filters used in the communications systems, it is most convenient to deal in units of dB, MHz, degrees and nano-seconds.

Amplitude response, as given by equation (2.39) is in dB's. The derivatives of the amplitude with respect to frequency in MHz are given by

$$\frac{d^n\alpha}{df^n} = \left[\frac{f_0}{\Delta f}\left(\frac{1}{f_0} + \frac{f_0}{f^2}\right)\right]^n \frac{d^n\alpha}{d\omega'^n} \qquad (2.44)$$

where

the frequencies f_0, f and the band-width Δf are all in MHz and

$d^n\alpha/df^n$ is in $dB/(MHz)^n$.

The phase linearity response is given by equation (2.41) and is in radians. It is straight-forward to convert it to degrees by multiplying it by $180/\pi$.

The group delay τ in nano seconds is given by

$$\tau = (10^3/2\pi)\left[\frac{f_0}{\Delta f}\left(\frac{1}{f_0} + \frac{f_0}{f^2}\right)\frac{d\beta}{d\omega'}\right] \qquad (2.45)$$

where

f_1, f_0 and Δf are all in MHz and

τ is in nanoseconds.

The derivatives of the group delay in nanoseconds/$(MHz)^n$ are given by

$$\frac{d^n\tau}{df^n} = \left[+ 2\pi\,\frac{f_0}{\Delta f}\left(\frac{1}{f_0} + \frac{f_0}{f^2}\right)\right]^{n+1} \frac{d^{n+1}\beta}{d\omega'^{n+1}} \qquad (2.46)$$

where

ω' is the normalized low-pass prototype frequency variable

2.8 CHARACTERISTIC POLYNOMIALS VERSUS RESPONSE SHAPES

In this section, we describe all the possible forms of the characteristic functions and the resulting response shapes for doubly terminated low-pass prototype networks. The only restriction imposed is that all the attenuation zeros lie on the $j\omega$ axis to ensure low loss in the pass-band.

2.8.1 All Pole Functions

Such functions are characterized by

$$t(s) = \frac{1}{E(s)} \tag{2.47}$$

with

$$P(s) \equiv 1$$

There are no finite transmission zeros and the attenuation rises monotonically beyond the pass-band. All the attenuation poles are located at infinity. The response shape is determined by the form of the polynomial $F(s)$. There are two basic forms of $F(s)$, viz.,

$$F(s) \rightarrow \varepsilon s^n$$

or

$$F(s) \rightarrow \varepsilon s^m (s^2+a_1^2)(s^2+a_2^2) \ldots \qquad (2.48)$$

The first form has all the zeros at the origin and the transmission response is characterized by a maximally flat pass-band response - known commonly as the Butterworth response.

The second form of $F(s)$ is characterized by some or all of its zeros at finite frequencies, $a_1, a_2, \ldots$. The best known response shape of this variety is the equi-ripple response (with maximum possible peaks) known commonly as the Chebyshev response.

The more general form of $F(s)$ for an all-pole function is

$$F(s) \rightarrow s^m (s^2+a_1^2)(s^2+a_2^2) \ldots \qquad (2.49)$$

with arbitrary m and a's.

Figure 2.4 describes such an arbitrary response shape and the corresponding distribution of poles and zeros.

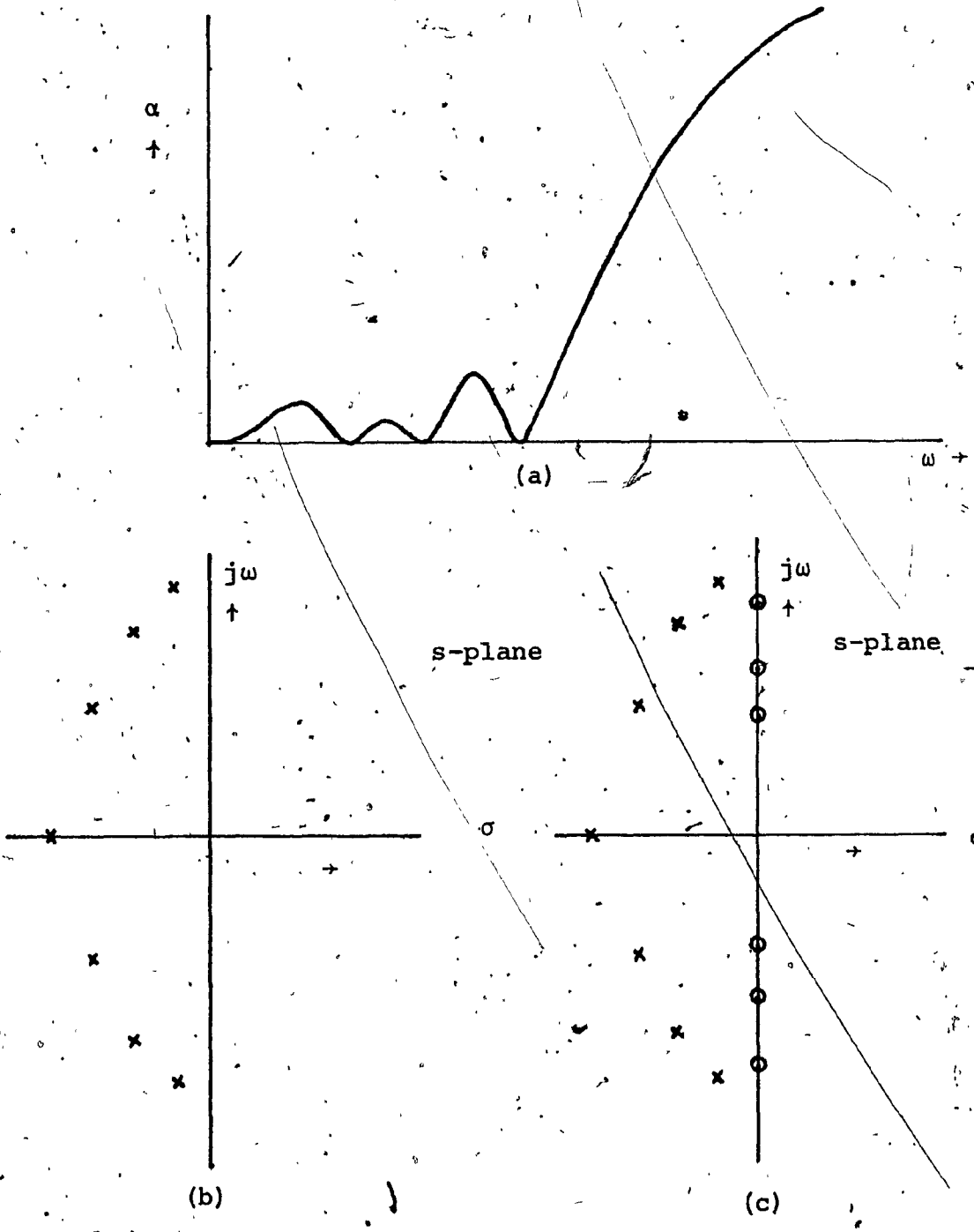

FIG. 2.4 GENERAL RESPONSE SHAPE AND POLE ZERO DISTRIBUTION OF ALL-POLE FUNCTION FILTERS, (a) GENERAL RESPONSE SHAPE, (b) POLE DISTRIBUTION OF TRANSMISSION FUNCTION, AND (c) POLE-ZERO DISTRIBUTION OF REFLECTION FUNCTION

2.8.2 Functions With Finite Transmission Zeros

Such a function is characterized by

$$t(s) = \frac{P(s)}{E(s)}$$

$$K(s) = \frac{F(s)}{P(s)}$$

$$P(s) = (s^2+b_1^2)(s^2+b_2^2) \ldots \quad (2.50)$$

and

$$F(s) = s^m(s^2+a_1^2)(s^2+a_2^2) \ldots \quad (2.51)$$

The difference between this and the all-pole functions is the introduction of transmission zeros which tend to increase the selectivity of the transmission response near the pass-band. This increased selectivity is obtained at the expense of a poorer wide-band amplitude response in the stop-band. For most practical applications, a minimum attenuation level in the range 30 to 50 dB is adequate, and consequently, the response function can be optimized by exploiting this requirement.

The response functions of the all-pole variety of the previous section can all be realized in conjunction with transmission zeros. Additional variables available here can be utilized to generate equi-ripple stop-band response

or the more general non-equi-ripple response. The different response shapes available here, along with the corresponding characteristic functions and pole-zero distribution, are itemized as follows.

2.8.3 Filters With Transmission Zeros and Maximally Flat Pass-Band

These filters are characterized by all attenuation zeros at their origin and arbitrary distribution of the attenuation poles.

The characteristic function K(s) has the form

$$K(s) = \frac{F(s)}{P(s)} = \varepsilon \frac{s^n}{(s^2+b_1^2)(s^2+b_2^2) \ldots (s^2+b_m^2)} \qquad (2.52)$$

where

n is the order of the filter and

m represents the number of transmission zeros which must be equal to or less than n

The conventional equi-ripple form of this class of filters are commonly referred to as 'inverse Chebyshev filters'. Reference [22] provides extensive data on the pole-zero configuration for such filters.

2.8.4 Equi-Ripple Elliptic Function

These filters are characterized by equi-ripple pass- and stop-bands and their characteristic polynomials have the form [21] :

$$K(s) = \varepsilon s \prod_{\nu=1}^{m} \left(\frac{s^2+a_{2\nu}^2}{s^2a_{2\nu}^2+1}\right), \quad n : \text{odd}, \; m = (n-1)/2 \qquad (2.53)$$

$$= \varepsilon \prod_{\nu=1}^{m} \left(\frac{s^2+a_{2\nu}^2}{s^2a_{2\nu}^2+1}\right), \quad n : \text{even}, \; m = n/2 \qquad (2.54)$$

Explicit formulae have been given by Cauer [29] and Darlington [30] for the critical frequencies a_ν. A review of such filters is given in [21] and their pole-zero configurations are well described in reference [22].

2.8.5 Non-Equi-Ripple Elliptic Function Filters

These filter networks are characterized by the non-equi-ripple nature of the pass and stop-bands. Further, the critical frequencies of these functions are related analytically to the elliptic functions and to the number of attenuation poles and zeroes, which are less than the Cauer parameter filters of the same order. References [13,31,32] discuss the nature, application and low-pass prototype characteristics of such filters. A more detailed

discussion of this filter type is described in Chapter V of this thesis.

2.8.6 Linear Phase Filters

These filters are characterized by a real axis or a complex quad of zeros of the transfer function. The characteristic function is given by

$$K(s) = \frac{(s^2+a_1^2)(s^2+a_2^2) \ \ldots}{(s^2-b_1^2)(s^2-p_1^2)(s^2-\bar{p}_1^2) \ \ldots} \qquad (2.55)$$

where

$b_1 > 0$ are the real axis zeros, and

$$p_1 = \sigma_1 + j\omega_1$$

and

$$\bar{p}_1 = \sigma_1 - j\omega_1$$

$p_1, \bar{p}_1, -p_1, -\bar{p}_1$ give the complex quad of zeros of the transfer function

For simplicity, we have confined our attention to the real-axis zeros for linear phase structures throughout this thesis.

The pass-band of such filters could be equi-ripple, maximally flat or non-equi-ripple.

2.8.7 All-Pass Networks

All-pass networks - as the name implies - are characterized by the constant loss (zero for ideal loss-less components) and a phase or group delay response, that can be controlled. Such networks find extensive application, all the way from 70 MHz to well into the microwave frequency spectrum. The primary reason is the independent nature of the all-pass network. It can be optimized to correct for any phase or group delay response, with a negligible effect upon the amplitude. Thus, a highly selective minimum phase-type filter function can be used in conjunction with an all-pass network to provide a sharp amplitude response in the stop-band and a relatively flat group delay response in the pass-band. It may be possible to obtain such a response with a linear phase filter. However, the order of the filter is generally higher, resulting in an increased design and realization complexity, as well as a higher pass-band insertion loss.

The transfer function of an all-pass network can be represented as:

$$Z_{12}(s) = \frac{H(-s)}{H(s)} \qquad (2.56)$$

where

H(s) is a strict Hurwitz polynomial.

In microwave terminology, all-pass sections with a real-pole are referred to as C-sections, and all-pass sections with non-real poles (or zeros) are referred to as D-sections.

CHAPTER III

EFFECT OF DISSIPATION ON FILTER AND ALL-PASS NETWORKS

CHAPTER III

EFFECT OF DISSIPATION ON FILTER AND ALL-PASS NETWORKS

3.1 INTRODUCTION

This Chapter examines the effect of dissipation on the response of filter networks designed from loss-less prototype low-pass filters. It is normal to assume non-dissipative elements in the prototype filter. In that case, closed-form formulae are available for designing a variety of low-pass prototype filters exhibiting maximally flat or equi-ripple response shapes. However, power dissipation is always present in a practical filter, and as a result, the actual insertion loss will deviate from the theoretical response of the ideal prototype. This is most evident in the pass-band where it introduces a finite insertion loss, tends to partially or completely obliterate the ripples and smooths out the edges near the cut-off region. In the stop-band, the effect is usually small. This approach has the advantage of design simplicity and the lowest possible insertion loss over the pass-band, since no mismatch loss is introduced to correct for the presence of dissipation. Its drawback is non-idealized response shape. For most practical applications - especially where distributed circuitry is employed (above 200 MHz), the reduced insertion loss far exceeds the benefits of an idealized response shape. For the computation of pass-band

loss, Cohn [33] has described an approximate formula for the computation of center-frequency loss of band-pass filters in terms of bandwidth, unloaded Q of the resonators, and the element values of the idealized low-pass prototype network. Young [34] extended this approach to compute the loss over the entire pass-band. Although the formula is simple, it requires the element values (g_k parameters) of the prototype network. This restricts it to those functions for which element values are readily available, either in tabular form [3] or as simple analytic relationships [35]. For more complicated transfer functions, this can be a severe restriction.

Moreover, the formula deals only with pass-band loss of low-pass and band-pass filters. The effect on group delay and out-of-band response due to the presence of dissipation, although small, is not determined.

In this Chapter, the problem of dissipation is tackled in terms of the displacement of poles and zeros of the idealized prototype transfer function with the sole restriction that the dissipation is uniform. This is usually the case for practical filters - especially in distributed circuitry. The same technique is applied to the case of lumped, as well as transmission-line all-pass networks. The equivalent dissipation factors for the prototype network are derived in terms

of the frequency, band-width and the uniform unloaded Q of practical low-pass, high-pass, band-pass, band-top and lumped or distributed all-pass networks. These dissipation factors are utilized to derive the relationships for the amplitude and group delay response and their first derivative in the presence of uniform dissipation. The approximate formulae for insertion loss at zero frequency for low-pass filters and at band-center for band-pass filters are derived in terms of the pole-zero configuration of the prototype network. These formulae are equivalent to those derived by Cohn [33].

It is to be emphasized here, that filter functions can be designed to have any physically-realizable response shape in the presence of dissipation. Dishal [36] and others [37,38] have treated this problem. This, however, can be done only at the expense of increased insertion loss in the pass-band. As stated earlier, for most practical applications where the distributed circuitry is employed (> 200 MHz), reduced insertion loss is preferred to an idealized response shape. Moreover, in the microwave region, unloaded Qs that are normally obtained are sufficiently high to have any significant impact on the response function except for the pass-band loss. The basic low-pass prototype transfer function, based on loss-less elements, can therefore be usefully employed to

design practical filters and all-pass networks. Response in the presence of uniform dissipation can then be calculated by determining the equivalent dissipation factors, as described in this Chapter.

3.2 EFFECT OF DISSIPATION ON TWO-PORT NETWORKS

The transfer function of a two-port network may be written as:

$$t(s) = H_0 \frac{(s-S_1)(s-S_3)\ldots}{(s-S_2)(s-S_4)\ldots} \qquad (3.1)$$

where

$t(s)$ is the transfer voltage ratio

For loss-less networks terminated in unity load and generator resistances, the power transmitted (to the load) P_t per unit incident power (available power) is given by

$$P_t = |t(j\omega)|^2$$
$$= H_0^2\left[\left|\frac{(s-S_1)(s-S_3)\ldots}{(s-S_2)(s-S_4)\ldots}\right|\right]^2 \qquad (3.2)$$

The amplitude 'α' of the network in decibels is given by

$$\alpha = 10 \log P_t$$

$$= 20 \log e[\ell n|s-S_1| - \ell n|s-S_3| + \ldots. - \ell n|s-S_2| - \ell n|s-S_4| - \ldots.] + 20 \log e.\ell n\, H_0 \qquad (3.3)$$

where

ℓn represents the natural logarithm

The constant H_0 is determined by the initial conditions. For a low-pass prototype structure with unity terminations

$$H_0^2 = \frac{|j-S_2||j-S_4|\ldots}{|j-S_1||j-S_3|\ldots} \cdot (1-|\rho|^2) \qquad (3.4)$$

where

ρ is the specified reflection coefficient at the cutoff frequency

$$\therefore \ell n\, H_0 = \sum_{\text{poles}} \ell n|S_p| - \sum_{\text{zeros}} \ell n|S_z| + \ell n(1-|\rho|^2) \qquad (3.5)$$

In the physical realization of filter networks, the finite conductivities of the materials involved introduce dissipation of energy and consequently perturb the expected response of the transfer functions based on loss-less elements. The approximate effect of incidental dissipation in an inductance is to associate with it a series resistance;

in a capacitance element it effectively produces a parallel conductance. To consider this effect on the transfer function, let us analyze the effect of changing the complex frequency variable s to $s + \delta$

where

δ is a positive quantity,

that is,

$$\begin{cases} s \rightarrow s + \delta \\ s.L_k \rightarrow s.L_k + \delta.L_k \\ s.C_k \rightarrow s.C_k + \delta.C_k \end{cases} \qquad (3.6)$$

where

k subscript denotes the $k^{\underline{th}}$ element.

This conversion then implies that each inductance has associated with it a proportionate amount of series resistance $\delta.L_k$ and each capacitance has a parallel conductance of the value $\delta.C_k$. If r and r' are the associated series resistance and shunt conductances, then

$$\delta.L_k = r \text{ or } \delta = \frac{r}{L_k} \qquad (3.7)$$

Similarly,

$$\delta = \frac{r'}{C_k}$$

This common ratio δ is referred to as the dissipation ratio or factor. The location of the poles and zeros is modified accordingly, by δ, since

$$s + \delta = S_k \quad \text{for the } k^{\underline{th}} \text{ pole or zero}$$

i.e.,

$$s = S_k - \delta \qquad (3.8)$$

Hence, all zeros and poles of the transfer function $Z(s)$ are displaced horizontally to the left, by an amount δ. This assumes that the dissipation ratios of the inductances and capacitances are identical. Thus, by subtracting δ from the real part of the poles and zeros of the transfer function, one can obtain the network response with finite unloaded Q's.

Incorporating the displacement δ into the pole/zero configuration,

$$\alpha = 20 \log e[\ell n|s+\delta-S_1| + \ell n|s+\delta-S_3| + \ldots - \ell n|s+\delta-S_2| + \ell n|s+\delta-S_4| - \ldots] + 20 \log e \; \ell n \; H_0 \qquad (3.9)$$

At $\omega = 0$, let $\alpha = \alpha_0$, and therefore

$$\alpha_0 = 20 \log e \; \ell n|\delta - S_1| + \ell n|\delta - S_3| + \ldots - \ell n|\delta - S_2| + \ell n|\delta - S_4| - \ldots] + 20 \log e \cdot \ell n H_0 \qquad (3.10)$$

A typical term in the bracket is $\ell n|\delta - S_k|$

where

$S_k = \sigma_k + j\omega_k$ is the $k^{\underline{th}}$ pole or zero

$$\therefore \quad \ell n|s - S_k| = \ell n[(\delta - \sigma_k)^2 + \omega_k^2]^{\frac{1}{2}}$$

or

$$\ell n|\delta - S_k| \cong \ell n|S_k| \pm \delta \frac{(\frac{1}{2}\delta - \sigma_k)}{|S_k|^2}$$

$$\text{if} \quad \delta << |\sigma_k| \qquad (3.11)$$

Substituting, we get

$$\alpha_0 = 20 \log e . \delta . [\sum_{\text{zero}} \frac{\frac{1}{2}\delta - \sigma_z}{|S_z|^2} - \sum_{\text{poles}} \frac{\frac{1}{2}\delta - \sigma_p}{|S_p|^2}] \qquad (3.12)$$

$$\therefore \quad \alpha_0 = 20 \log e . \delta . [\Sigma \frac{\sigma_p}{|S_p|^2} - \Sigma \frac{\sigma_z}{|S_z|^2} + \Sigma \frac{\delta/2}{|S_z|^2} - \Sigma \frac{\delta/2}{|S_p|^2}] \qquad (3.13)$$

This determines the amplitude response in the presence of dissipation. Next, we determine the phase and group delay response. If τ and β are group delay and phase respectively, then

$$\tau = -\frac{d\beta}{d\omega} \tag{3.14}$$

where the phase β is given by

$$\beta = \sum_{\text{zeros}} \tan^{-1}\left(\frac{\omega-\omega_z}{\delta-\sigma_z}\right) - \sum_{\text{poles}} \tan^{-1}\left(\frac{\omega-\omega_p}{\delta-\sigma_p}\right) \tag{3.15}$$

$$\therefore \tau = \frac{d}{d\omega}\left[\sum_{\text{poles}} \tan^{-1}\left(\frac{\omega-\omega_z}{\delta-\sigma_z}\right) - \sum_{\text{zeros}} \tan^{-1}\left(\frac{\omega-\omega_p}{\delta-\sigma_p}\right)\right] \tag{3.16}$$

At $\omega = 0$, let $\tau = \tau_0$, and therefore

$$\tau_0 = \sum \frac{\delta-\sigma_p}{(\delta-\sigma_p)^2+\omega_p^2} - \sum \frac{\delta-\sigma_z}{(\delta-\sigma_z)^2+\omega_z^2} = -\Sigma\left[\frac{\sigma_p}{(\delta-\sigma_p)^2+\omega_p^2} - \frac{\sigma_z}{(\delta-\sigma_z)^2+\omega_z^2}\right] + \delta\left[\frac{1}{(\delta-\sigma_p)^2+\omega_p^2} - \frac{1}{(\delta-\sigma_z)^2+\omega_z^2}\right] \tag{3.17}$$

If we assume $\sigma >> \delta$,

$$\tau_0 \approx -\left[\Sigma \frac{\sigma_p}{|s_p|^2} - \Sigma \frac{\sigma_z}{|s_z|^2}\right] + \delta\left[\Sigma \frac{1}{|s_p|^2} - \frac{1}{|s_z|^2}\right] \quad (3.18)$$

Substituting in the equation for α_0, we obtain

$$\alpha_0 = 20 \log e\, \delta\left[-\tau_0 + \frac{\delta}{2}\left(\Sigma\frac{1}{|s_p|^2} - \Sigma\frac{1}{|s_z|^2}\right) + \right.$$

$$\left. + \frac{\delta}{2}\left(\Sigma\frac{1}{|s_z|^2} - \Sigma\frac{1}{|s_p|^2}\right)\right] = 20 \log e\, \delta\left[-\tau_0 + \right.$$

$$\left. + \frac{\delta}{2}\left(\Sigma\frac{1}{|s_p|^2} - \Sigma\frac{1}{|s_z|^2}\right)\right] = -20 \log e.\delta.\tau_0 +$$

$$+ 10 \log e\, .\delta^2\left(\Sigma\frac{1}{|s_p|^2} - \Sigma\frac{1}{|s_z|^2}\right) \quad (3.19)$$

If $\frac{\delta}{|s_k|} \ll 1$, i.e., when dissipation is small

$$\alpha_0 \approx -20 \log e.\delta.\tau_0 \quad (3.20)$$

This shows that the insertion loss at $\omega = 0$ (or band-center for band-pass filters) is directly proportional to the absolute time delay at that frequency for small dissipation.

This result is the same as that obtained by Young [34] based on Cohn's [33] method utilizing the element values of the prototype network.

3.3 RELATIONSHIP OF DISSIPATION FACTOR δ AND QUALITY FACTOR, Q_0

Dissipation factor 'δ' represents the displacement of poles and zeros along the real (σ) axis in the complex frequency plane. It has the dimensions of radian frequency.

Unloaded Q (Q_0) represents radian frequency times the energy stored, divided by the energy dissipated per cycle, or

$$Q_0 = \omega_0 \left(\frac{\text{energy stored}}{\text{average power loss}}\right)$$

$$= 2\pi \left(\frac{\text{energy stored}}{\text{energy dissipated per cycle}}\right) \qquad (3.21)$$

where

Q_0 is a dimensionless quantity and provides an indication of the losses in the circuit

For an LCR circuit

$$Q_0 = \omega_0 \frac{\mu}{\omega_L} \qquad (3.22)$$

where

μ is the energy stored in the circuit

and

ω_L is the average power loss, i.e.,

$$\omega_L = - \frac{d\mu}{dt}$$

The energy in the circuit can be calculated when it is all in the inductance, i.e.,

$$\mu = \tfrac{1}{2} L(I_{max})^2 = L\frac{A^2}{2} \qquad (3.23)$$

where

$$I = A \cos(\omega_0 t+\phi)$$

The average power loss in resistance r is

$$\omega_R = \tfrac{1}{2} r(I_{max})^2 = r\frac{A^2}{2}$$

$$Q_0 = \omega_0 \frac{LA^2/2}{rA_2/2} \qquad (3.24)$$

$$Q_0 = \omega_0 \frac{L}{r}$$

As described in the previous section,

$$\delta = r/L$$

for an inductance. If we apply the change of variable $s = s+\delta$ implying uniform shift, then the pertinent value of δ equals $r/2L$. It implies that losses are divided equally between L and C.

$$Q_0 = \frac{\omega_0}{2} \cdot \frac{1}{\delta} \qquad (3.25)$$

As described earlier, we are concerned in this thesis with filters and the equivalent circuits that can be derived from the low-pass prototype network through the use of appropriate frequency transformations. This makes the technique very versatile and convenient. The low-pass prototype circuit assumes loss-less L and C elements.

In terms of the low-pass prototype g_k parameters [1],

$$\delta = \frac{r}{g} \qquad (3.26)$$

and

$$Q_0 = \omega' \cdot \frac{g}{r} \qquad (3.27)$$

where

g is the element value

and

ω' is the normalized frequency variable

Normalization is normally chosen with respect to 1 radian per second and therefore,

$$Q_0 = \frac{1}{\delta} \tag{3.28}$$

for the prototype network.

In the next section, we derive the equivalent value of δ for the prototype network that will give rise to the same response as the required low-pass, high-pass, band-pass or band-stop filters.

3.4 EQUIVALENT δ FOR LOW-PASS/HIGH-PASS FILTERS

Frequency transformation used for low-pass filters is

$$\omega' = \frac{\omega}{\omega_c} \tag{3.29}$$

The normalizing, or cut-off frequency of the prototype structure, $\omega' = 1$, corresponds to $\omega = \omega_c$.

$$\therefore \quad \omega' g \rightarrow \omega \frac{g}{\omega_c}$$

or

$$g \rightarrow g/\omega_c \tag{3.30}$$

$$r \rightarrow r$$

since r is an invariant

$$\therefore \quad \delta'_{Lp} = \frac{r}{g/\omega_c}$$

$$= \omega_c \cdot \delta$$

where

δ' and δ are the dissipation factors for the low-pass filter and the prototype filter, respectively

The unloaded Q for the low-pass filter is given by

$$Q_0 = \frac{\omega_c}{\delta'}$$

$$= \frac{\omega_c}{\omega_c \cdot \delta} = \frac{1}{\delta} \qquad (3.31)$$

$$\therefore \quad \delta = \frac{1}{Q_0}$$

Thus, the equivalent displacement of the pole/zero pattern of the low-pass prototype structure is simply the reciprocal of the unloaded Q of the low-pass filter determined at the cut-off frequency.

Similarly, for high-pass filters

$$\omega' = \frac{\omega_c}{\omega}$$

$$\omega' g = \frac{\omega_c}{\omega} \cdot g \qquad (3.32)$$

$$g \rightarrow g\omega_c$$

$$r \rightarrow r$$

Note that an L is converted to a C, and vice-versa.

Therefore,

$$\delta'_{HP} = rc$$

$$= r \cdot \frac{1}{g\omega_c}$$

where

c is the equivalent capacitance derived from inductance g of the prototype element value

Since $$\delta = \frac{r}{g} \qquad (3.33)$$

therefore

$$\delta'_{HP} = \frac{\delta}{\omega_c}$$

The unloaded Q of the high-pass filter is

$$Q_0 = \frac{1}{\omega_c \cdot \delta'}$$

$$= \frac{1}{\omega_c} \cdot \frac{\omega_c}{\delta} \qquad (3.34)$$

$$\therefore \quad \delta = \frac{1}{Q_0}$$

3.5 EQUIVALENT δ FOR BAND-PASS/BAND-STOP FILTERS

The frequency transformation used for a band-pass filter is

$$\omega' = \frac{\omega_0}{\Delta\omega}\left(\frac{\omega}{\omega_0} - \frac{\omega_0}{\omega}\right), \tag{3.35}$$

where

ω_0 is the band-center

and

$\Delta\omega$ is the band-width.

$$\omega' g \rightarrow \frac{g}{\Delta\omega}\cdot\omega - g\frac{\omega_0^2}{\Delta\omega}\cdot\frac{1}{\omega}$$

i.e., an inductive element value of the low-pass prototype structure gives rise to an LC tuned circuit, where the equivalent $L \rightarrow \frac{g}{\Delta\omega}$ and equivalent $C \rightarrow g\frac{\omega_0^2}{\Delta\omega}$; and

$$r \rightarrow r$$

Assuming r is associated with L only, (it is no loss of generality, since the same result is obtained by assuming equal losses for L and C),

$$\delta'_{BP} = \frac{r}{L} = \frac{r}{g/\Delta\omega} \tag{3.36}$$

and the unloaded Q at the resonance is given by

$$Q_0 = \frac{\omega_0}{\delta'_{BP}} = \frac{\omega_0}{\Delta\omega} \cdot \frac{q}{r}$$

or

$$Q_0 = \frac{\omega_0}{\Delta\omega} \cdot \frac{1}{\delta} \qquad (3.37)$$

or

$$\delta = \frac{\omega_0}{\Delta\omega} \cdot \frac{1}{Q_0} = \frac{f_0}{\Delta f} \cdot \frac{1}{Q_0}$$

where

δ is the equivalent displacement of the pole/zero pattern of the low-pass prototype structure

Similarly, it can be shown that for band-stop filters,

$$\delta = \frac{f_0}{\Delta f} \cdot \frac{1}{Q_0}$$

3.6 EFFECT OF DISSIPATION ON LUMPED ALL-PASS NETWORKS

The transfer function of an all-pass network can be represented as

$$Z_{12}(s) = \frac{H(-s)}{H(s)} \qquad (3.38)$$

where

H(s) is a strict Hurwitz polynomial

$$Z_{12}(s) = \frac{\prod_{i=1}^{\ell}(\sigma_i - s)\prod_{k=1}^{m}(s^2 - 2s\sigma_k + |p_k|^2)}{\prod_{i=1}^{\ell}(\sigma_i + s)\prod_{k=1}^{m}(s^2 + 2s\sigma_k + |p_k|^2)} \qquad (3.39)$$

From the above expression, one can identify the well-known theorem [39] on all-pass networks, viz.,

"Any all-pass network is equivalent to a number of first and second-degree all-pass networks in tandem."

Utilizing the above theorem, we shall drop the multiplicative factor $\prod_{i,k}$ thereby simplifying the analysis without any loss of generality, i.e.,

$$Z_{12}(s) = \frac{(\sigma_i - s)(s^2 - 2s\sigma_k + |p_k|^2)}{(\sigma_i + s)(s^2 + 2s\sigma_k + |p_k|^2)}$$

The total response of a multi-section all-pass network is then obtained by adding algebraically, the contributions of individual first and second-order all-pass sections.

For loss-less networks, terminated in unity load and generator resistances, the power transmitted p_t per unit incident power (available power) is given by

$$P_t = |t(j\omega)|^2 = |Z_{12}(j\omega)|^2 = H_0^2 \frac{|(\sigma_i - s)|^2}{|(\sigma_i + s)|^2} \frac{|s^2 - 2\sigma_k s + |p_k|^2|^2}{|s^2 + 2\sigma_k s + |p_k|^2|^2} \qquad (3.40)$$

where

H_0 is a multiplier constant.

For all-pass networks, it can be easily shown that $H_0 = 1$. The above expression can be put in the form

$$P_t = \left|\frac{\sigma_i - s}{\sigma_i + s}\right|^2 \cdot \left|\frac{(s-p_k)(s-p_k^*)}{(s-\bar{p}_k)(s-\bar{p}_k^*)}\right| \qquad (3.41)$$

where

$$\left.\begin{aligned} p_k &= \sigma_k + j\omega_k \\ p^*_k &= \sigma_k - j\omega_k \end{aligned}\right\} \text{ conjugate pair}$$

$$\left.\begin{aligned} \bar{p}_k &= -\sigma_k + j\omega_k \\ \bar{p}_k^* &= -\sigma_k - j\omega_k \end{aligned}\right\} \text{ conjugate pair} \qquad (3.42)$$

The amplitude 'α' of the network in decibels is given by

$$\alpha = 10 \log P_t$$

$$= 20 \log e[\ell n|\sigma_i - s| + \ell n|s-p_k| + \ell n|s-p_k^*| - \ell n|\sigma_i + s) - \ell n|s-\bar{p}_k| - \ell n|s-\bar{p}_k^*|] \qquad (3.43)$$

For lossless networks, $s = \omega j$ and it can be easily seen that $\alpha = 0$.

For dissipative networks, assuming a uniform dissipation factor δ,

$$\alpha = 20 \log e \left[\ln|\sigma_i - (s+\delta)| + \ln|s + \delta - p_k| + \ldots - \ln|\sigma_i + s + \delta| - \ldots\right] \tag{3.44}$$

Rationalizing the above, we get

$$\bar{\alpha} = 20 \log e \ln\left[\frac{(\sigma_i-\delta)^2+\omega^2}{(\sigma_i+\delta)+\omega^2}\right]^{\frac{1}{2}} \left\{\frac{(\delta-\sigma_k)^2+(\omega-\omega_k)^2}{(\delta+\omega_k)^2+(\omega-\omega_k)^2}\right\} \cdot \left\{\frac{(\delta-\sigma_k)^2+(\omega+\omega_k)^2}{(\delta+\sigma_k)^2+(\omega+\omega_k)^2}\right\}\Bigg]^{\frac{1}{2}} \tag{3.45}$$

Thus, knowing the dissipation factor, one can determine the amplitude response of all-pass networks, given their pole-zero locations.

Often, it is more convenient to use the normalized frequency variable ω/σ since, for most practical networks, ω is of the order of σ over the band of interest. Therefore, α can be written as

$$\alpha = 20 \log e . \ln\left[\frac{(1-\frac{\delta}{\sigma_i})^2+(\frac{\omega}{\sigma_i})^2}{(1\ \frac{\delta}{\sigma_i})^2+(\frac{\omega}{\sigma_i})^2}\right]^{\frac{1}{2}} \left[\frac{(1-\frac{\delta}{\sigma_k})^2+(\frac{\omega}{\sigma_k}-\frac{\omega_k}{\sigma_k})^2}{(1+\frac{\delta}{\sigma_k})^2+(\frac{\omega}{\sigma_k}-\frac{\omega_k}{\sigma_k})^2}\right] \times \times \frac{(1-\frac{\delta}{\sigma_k})^2+(\frac{\omega}{\sigma_k}+\frac{\omega_k}{\sigma_k})^2}{(1+\frac{\delta}{\sigma_k})^2+(\frac{\omega}{\sigma_k}+\frac{\omega_k}{\sigma_k})^2}\Bigg]^{\frac{1}{2}} \tag{3.46a}$$

Therefore

$$\alpha = 20 \log e . \ell n \left[\frac{(1-\delta')^2+\omega'^2}{(1+\delta')^2+\omega'^2}\right]^{\frac{1}{2}} \left[\left\{\frac{(1-\delta')^2+(\omega'-\omega_k')^2}{(1+\delta')^2+(\omega'-\omega_k')^2}\right\} \times \right.$$

$$\left. \times \left\{\frac{(1-\delta')^2+(\omega'+\omega_k')^2}{(1+\delta')^2+(\omega'+\omega_k')^2}\right\}\right]^{\frac{1}{2}} \qquad (3.46b)$$

where

$$\delta' \equiv \delta/\sigma$$

$$\omega' \equiv \omega/\sigma$$

$$\omega_k' \equiv \omega_k/\sigma_k$$

are the normalized variables.

In a similar manner, it can be shown that group delay τ in the presence of dissipation is given by

$$\tau = \frac{1}{\sigma_i} \sum_{i=1}^{\ell} \left(\frac{1-\delta'}{(1-\delta')^2+\omega'^2} + \frac{1+\delta'}{(1+\delta')^2+\omega'^2}\right) +$$

$$+ \frac{1}{\sigma_k} \sum_{k=1}^{m} \left(\frac{1-\delta'}{(1-\delta')^2+(\omega'-\omega_k')^2} + \frac{1-\delta'}{(1-\delta')^2+(\omega'+\omega_k')^2} + \right.$$

$$\left. + \frac{1+\delta'}{(1+\delta')^2+(\omega'-\omega_k')^2} + \frac{1+\delta'}{(1+\delta')^2+(\omega'+\omega_k')^2}\right). \qquad (3.47)$$

3.6.1 Dissipation Loss at Zero Frequency

(1) First-Order Sections

$$\alpha = 20 \log e.\ell n \left[\frac{(1-\delta')^2+0}{(1+\delta')^2+0}\right]^{\frac{1}{2}} = 20 \log e.\ell n \left[\frac{1-\delta'}{1+\delta'}\right]$$

$$\simeq 20 \log e.\ (-2\delta') \simeq -\ 20 \log e.\delta\left(\frac{2}{\sigma}\right) \qquad (3.47)$$

or

$$\alpha = -\ 40 \log e.\ \left(\frac{\delta}{\sigma}\right)$$

or

$$\alpha = -\ 20 \log e.\delta.\tau_0 \qquad (3.48)$$

where

τ_0 is the group delay at zero frequency and can be easily shown to be equal to $2/\sigma$.

This result is identical to the one obtained for the filter networks.

(ii) Second-Order Sections

$$\alpha = 20 \log e.\ell n \left[\frac{(1-\delta')^2+\omega_k'^2}{(1+\delta')^2+\omega_k'^2} \times \frac{(1-\delta')^2+\omega_k'^2}{(1+\delta')^2+\omega_k'^2}\right]^{\frac{1}{2}} =$$

$$= 20 \log e.\ell n \left[\frac{(1-\delta')^2+\omega_k'^2}{(1+\delta')^2+\omega_k'^2}\right] \qquad (3.49)$$

Three cases aris, viz.,

(a) If $\sigma_k >> \omega_k$, i.e., if $\omega_k' << 1$, then

$$\alpha = 20 \log e.2.(-2\delta') = -20 \log e.\delta.\left(\frac{4}{\sigma}\right) \qquad (3.50)$$

$$= -80 \log e.\left(\frac{\delta}{\sigma}\right)$$

or

$\alpha = -20 \log e.\delta.\tau_0$, τ_0: group delay at $\omega=0$

(b) If ω_k' equals unity

$$\alpha = 20 \log e.\ln\left[\frac{1+\delta'^2-2\delta'+1}{1+\delta'^2+2\delta'+1}\right] \qquad (3.51)$$

Assuming $\delta' << 1$, and therefore neglecting second-order terms:

$$\alpha = 20 \log e.\ln\left(\frac{1-\delta'}{1+\delta'}\right) = 20 \log e.(-2\delta') =$$

$$-20 \log e.\delta.\left(\frac{2}{\sigma}\right) \qquad (3.52)$$

$$\therefore \quad \alpha = -40 \log e.\frac{\delta}{\sigma}$$

or

$\alpha = -20 \log e.\delta.\ \tau_k$, τ_k: group delay at $\omega=0$ when $\omega_k=\sigma_k$.

(c) If $\omega_k' >> 1$, i.e., if $\sigma_k << \omega_k$, then

$$\alpha = 20 \log e.\ln\left[\frac{\omega_k'^2}{\omega_k'^2}\right] = 0 \qquad (3.53)$$

It is evident that the dissipation loss is proportional to the group delay.

3.6.2 Evaluation of Dissipation Factor

The unloaded Q at a given frequency ω is given by

$$Q_0 = \frac{\omega}{\delta}$$

or

$$\frac{\delta}{\omega} = \frac{1}{Q_0}$$

For typical equalizers, $\frac{\omega}{\sigma_k}$ is taken as the normalized frequency variable since σ or $|S_k|$ is of the order of ω, the frequency of interest.

Expressing $\frac{\omega}{|S_k|}$ by k where k lies typically between 1 and 10,

$$Q_0 = k \frac{|S_k|}{\delta}$$

or

$$\delta = k \frac{|S_k|}{Q_0} \qquad (3.54)$$

or

$$\frac{\delta}{\sigma_k} = \frac{k}{Q_0} \frac{|S_k|}{\sigma_k}$$

3.7 EFFECTS OF DISSIPATION ON DISTRIBUTED ALL-PASS NETWORKS

For distributed networks consisting of lumped resistors and a commensurate microwave network, the all-pass function can be expressed as [40,41]

$$Z_{12}(t) = \left(\frac{1-t}{1+t}\right)^{n/2} \frac{H(-t)}{H(t)} \qquad (3.55)$$

where

n = the effective number of unit elements

t = tanh S, $S=j\omega'$, ω' being the normalized real frequency variable

= j tan ω' for loss-less cases, and

H(t) = a strict Hurwitz polynomial

The transformation t = j tan ω' is the well-known Richards' transformation [26]. It is to be noted that ω' is the normalized frequency variable. Most frequently, the normalization is chosen such that at $\omega=\omega_0$ (center frequency), the transmission line (or equivalent wave-guide cavity) is a quarter wave, i.e.,

$$\omega' = -\frac{\pi}{2} \cdot \frac{\omega}{\omega_0}$$

$$\therefore \quad t = \Sigma + j\Omega = \tanh\left(\delta' + j\frac{\pi}{2}\cdot\frac{\omega}{\omega_0}\right) \qquad (3.56)$$

where

Σ and Ω are the real and imaginary parts of the transformed frequency variable t

and δ' represent the normalized dissipation factor for lossy structures, i.e.,

$$\delta' = \frac{\pi}{2\omega_0} \cdot \delta$$

where

δ is the true dissipation factor given by

$$\delta = \frac{\omega_0}{Q_0}$$

$$\therefore \quad \delta' = \frac{\pi}{2Q_0} \qquad (3.57)$$

Alternatively, one can look at it as

$$S \rightarrow S \rightarrow \delta$$

$$= j\omega + \delta$$

$$\therefore \quad \frac{\pi}{2\omega_0} S \rightarrow j\frac{\pi}{2} \cdot \frac{\omega}{\omega_0} + \delta \cdot \frac{\pi}{2\omega_0} = \frac{\omega_0}{Q_0} \cdot \frac{\pi}{2\omega_0} +$$

$$+ j\frac{\pi}{2} \cdot \frac{\omega}{\omega_0} = \frac{\pi}{2Q_0} + j\frac{\pi}{2} \cdot \frac{\omega}{\omega_0} \qquad (3.58)$$

and $t = \tanh\left(\frac{\pi}{2\omega_0} \cdot S\right) = \tanh\left(\frac{\pi}{2Q_0} + j\frac{\pi}{2} \cdot \frac{\omega}{\omega_0}\right)$.

From this relation, one can easily derive

$$\Sigma = \frac{\alpha_R(1+\tan^2\theta)}{1+\alpha_R^2 \tan^2\theta} = \frac{1}{\alpha_R} \quad \text{at} \quad \theta=\pi/2$$

$$\Omega = \tan\theta \frac{1-\alpha_R^2}{1+\alpha_R^2 \tan^2\theta} = 0 \text{ at } \theta=\pi/2 \qquad (3.59)$$

where

$$\alpha_R = \tanh \delta' \approx \delta' = \frac{\pi}{2} \cdot \frac{1}{Q_\phi} \quad \text{if } \delta' \ll 1 \qquad (3.60)$$

These are the general expressions for the real and imaginary parts of the frequency variable t. It is easily seen that for loss-less structures, α_R is zero and therefore

$$\Sigma = 0$$

$$\Omega = \tan\theta \qquad (3.61)$$

$$\theta = \frac{\pi}{2} \cdot \frac{\omega}{\omega_\phi}$$

Furthermore, it can be shown that

$$\frac{d\Sigma}{d\theta} = 2\alpha_R(1-\alpha_R^2) \frac{\tan\theta \sec^2\theta}{(1+\alpha_R^2 \tan^2\theta)^2} = 0 \quad \text{at } \theta=\pi/2 \qquad (3.62)$$

and

$$\frac{d\Omega}{d\theta} = (1-\alpha_R^2) \sec^2\theta \frac{(1-\alpha_R^2 \tan^2\theta)}{(1+\alpha_R^2 \tan^2\theta)^2} = 1 - \frac{1}{\alpha_R^2} \text{ at } \theta=\pi/2 \qquad (3.63)$$

For the loss-less case, it is easily seen that

$$\frac{d\Sigma}{d\theta} = 0 \quad \text{and} \quad \frac{d\Omega}{d\theta} = \sec^2\theta \qquad (3.64)$$

These relationships will be used in subsequent derivations of amplitude and group delay responses.

As shown by Cristal [40], wave-guide structures can be included by modifying the expression for θ to

$$\theta = \frac{\pi}{2} \cdot \left[\frac{F^2 - F_0^2}{1 - F_0^2}\right]^{\frac{1}{2}} \qquad (3.65)$$

where

$$F = \frac{f}{f_0} = \frac{\omega}{\omega_0}$$

$$F_0 = \frac{f_{c_0}}{f_0}$$

and f_{c_0}: Cut-off frequency of the wave-guide.

For TEM structures, $f_{c_0}=0$ and θ reduces to the familiar $\theta = \frac{\pi}{2} \cdot \frac{\omega}{\omega_0}$.

3.7.1 Dissipation Factor in Wave-Guide Structures

In dispersive media, the wave-lengths must be taken as the variable, instead of the usual frequency variable, i.e.,

$$S \rightarrow \delta' + j\frac{2\pi}{\lambda_g} \cdot L \qquad \left.\begin{array}{l}\lambda_g : \text{Guide wavelength} \\ L : \text{Commensurate line-length}\end{array}\right. \qquad (3.66)$$

Assuming that $\theta=\pi/2$ at $\omega=\omega_0$, as before, i.e., $L=\frac{\lambda_{g_0}}{4}$

$$S = \delta' + j\frac{\pi}{2} \cdot \frac{\lambda_{g_0}}{\lambda_g}$$

The equivalent dissipation factor is therefore given by $(\frac{\omega_0}{Q_0} \rightarrow \frac{1}{\lambda_0} \cdot \frac{1}{Q_0})$

$$\delta' = \frac{\pi}{2} \cdot \frac{1}{Q_0} \cdot \frac{\lambda_{g_0}}{\lambda_0} \qquad \left.\begin{array}{l}\lambda_0 : \text{free-space wavelength at } \omega=\omega_0\end{array}\right.$$

$$= \frac{\pi}{2} \cdot \frac{1}{Q_0} \cdot \frac{1}{[1-F_0^2]^{\frac{1}{2}}} \qquad (3.67)$$

where

$$F_0 = \frac{f_{c_0}}{f_0} \quad \frac{\lambda_{g_0}}{\lambda_{c_0}} \qquad \left.\begin{array}{l}\lambda_{c_0} : \text{cut-off wave-length}\end{array}\right.$$

Therefore, the factor α_R is given by

$$\alpha_R = \frac{\pi}{2Q_0} \cdot \frac{1}{[1-F^2]^{\frac{1}{2}}} \qquad (3.68)$$

3.7.2 Effect of Dissipation on Amplitude Response

For a C-section

$$H(t) = t + \sigma \tag{3.69}$$

$$\therefore \quad \alpha = 20 \log e\left[\frac{n}{2} \ln|1-t| + \ln|-t+\sigma| - \frac{n}{2} \ln|1+t| - \ln|t+\sigma|\right]$$

or

$$\alpha = 10 \log e\left[\frac{n}{2} \ln \frac{(1-\Sigma)^2+\Omega^2}{(1+\Sigma)^2+\Omega^2} + \ln \frac{(\sigma-\Sigma)^2+\Omega^2}{(\sigma+\Sigma)^2+\Omega^2}\right] dB \tag{3.70}$$

and

$$\frac{d\alpha}{df} = 10 \log e\left[\frac{n}{2}\left\{\frac{2(1-\Sigma)\frac{d\Sigma}{df}+2\Omega\frac{d\Omega}{df}}{(1-\Sigma)^2+\Omega^2} - \frac{2(1+\Sigma)\frac{d\Sigma}{df}+2\Omega\frac{d\Omega}{df}}{(1+\Sigma)^2+\Omega^2}\right\} + \right.$$

$$\left. + \frac{2(\sigma-\Sigma).2\frac{d\Sigma}{df}+2\Omega\frac{d\Omega}{df}}{(\sigma-\Sigma)^2+\Omega^2} - \frac{2(\sigma+\Sigma).2\frac{d\Sigma}{df}+2\Omega\frac{d\Omega}{df}}{(\sigma+\Sigma)^2+\Omega^2}\right] \tag{3.71}$$

For a D-section

$$H(t) = [(t+\sigma_k)+j\omega_k][(t+\sigma_k) - j\omega_k]$$

$$= \Sigma^2 - \Omega^2 + 2\sigma_k\Sigma + \sigma_k^2 + \omega_k^2 +$$

$$+ j(2\Omega\Sigma+2\sigma_k\Omega) \tag{3.72}$$

$$\text{Re } H(t) = \Sigma^2 - \Omega^2 + 2\sigma_k\Sigma + \sigma_k^2 + \omega_k^2 = A(\text{say})$$

$$\text{Im } H(t) = 2\Omega(\Sigma+\sigma_k) = B(\text{say}) \qquad (3.73)$$

In a similar manner,

$$\text{Re } H(-t) = \Sigma^2 - \Omega^2 - 2\sigma_k\Sigma + \sigma_k^2 + \omega_k^2 = C(\text{say})$$

$$\text{Im } H(-t) = 2\Omega(\Sigma-\sigma_k) = D(\text{say}) \qquad (3.74)$$

$$\therefore \quad \alpha = 10 \log e\left[\frac{n}{2} \ln\frac{(1-\Sigma)^2+\Omega^2}{(1+\Sigma)^2+\Omega^2} + \ln\frac{C^2+D^2}{A^2+B^2}\right] \text{ dB} \qquad (3.75)$$

and

$$\frac{d\alpha}{df} = 10 \log e\left[\frac{n}{2}\left\{\frac{2(1-\Sigma)\frac{d\Sigma}{df}+2\Omega\frac{d\Omega}{df}}{(1-\Sigma)^2+\Omega^2} - \frac{2(1+\Sigma)\frac{d\Sigma}{df}+2\Omega\frac{d\Omega}{df}}{(1+\Sigma)^2+\Omega^2}\right\} + \right.$$

$$\left. + \frac{2C\frac{dC}{df}+2D\frac{dD}{df}}{C^2+D^2} - \frac{2A\frac{dA}{df}+2B\frac{dB}{df}}{A^2+B^2}\right] \qquad (3.76)$$

where

$$\frac{dA}{df} = 2\Sigma\frac{d\Sigma}{df} - 2\Omega\frac{d\Omega}{df} + 2\sigma_k\frac{d\Sigma}{df}$$

$$\frac{dB}{df} = 2\Omega\frac{d\Sigma}{df} + 2\Sigma\frac{d\Omega}{df} + 2\sigma_k\frac{d\Omega}{df}$$

$$\frac{dC}{df} = 2\Sigma\frac{d\Sigma}{df} - 2\Omega\frac{d\Omega}{df} - 2\sigma_k\frac{d\Sigma}{df}$$

$$\frac{dD}{df} = 2\Omega\frac{d\Sigma}{df} + 2\Sigma\frac{d\Omega}{df} - 2\sigma_k\frac{d\Omega}{df}$$

The values of $\frac{d\Sigma}{df}$ and $\frac{d\Omega}{df}$ can be derived as

$$\frac{d\Sigma}{df} = \frac{\pi}{f_0} \cdot S(F,F_0) \cdot \alpha_R(1-\alpha_R^2)\frac{\tan\theta\sec^2\theta}{(1+\alpha_R^2\tan^2\theta)^2} \quad (3.77)$$

$$\frac{d\Omega}{df} = \frac{\pi}{2f_0} \cdot S(F,F_0) \cdot (1-\alpha_R^2)\sec^2\theta\frac{1-\alpha_R^2\tan^2\theta}{(1+\alpha_R^2\tan^2\theta)^2} \quad (3.78)$$

3.7.3 Group Delay in the Presence of Dissipation

The effect of dissipation on group delay is normally small. It acquires significance only for very lossy structures.

From the general transfer function, the phase β is given by

$$\beta=\frac{n}{2}\tan^{-1}\frac{Im(1-t)}{Re(1-t)} - \frac{n}{2}\tan^{-1}\frac{Im(1+t)}{Re(1+t)} + \\ + \tan^{-1}\frac{Im[H(-t)]}{Re[H(-t)]} - \tan^{-1}\frac{Im[H(t)]}{Re[H(t)]} \quad (3.79)$$

and the group delay is given by

$$\tau = -\frac{d\beta}{d\omega} = -\left[\frac{n}{2}\,\frac{1}{1+\left(\frac{I_1}{R_1}\right)^2}\,\frac{d}{d\omega}\left(\frac{I_1}{R_1}\right) - \frac{n}{2}\,\frac{1}{1+\left(\frac{I_2}{R_2}\right)^2}\cdot\right.$$

$$\cdot\,\frac{d}{d\omega}\left(\frac{I_2}{R_2}\right) + \frac{1}{1+\left(\frac{I_3}{R_3}\right)^2}\cdot\frac{d}{d\omega}\left(\frac{I_3}{R_3}\right) - \frac{1}{1+\left(\frac{I_4}{R_4}\right)^2}\cdot$$

$$\left.\cdot\,\frac{d}{d\omega}\left(\frac{I_4}{R_4}\right)\right] \qquad (3.80)$$

where

I and R denote the imaginary and real parts of the terms, as shown.

Typical terms are of the form

$$\frac{d}{d\omega}\left(\frac{I}{R}\right) = \frac{d}{d\theta}\left(\frac{I}{R}\right)\cdot\frac{d\theta}{dF}\cdot\frac{dF}{d\omega} =$$

$$= \frac{\pi}{2}\cdot S(F,F_0)\cdot\frac{1}{\omega_0}\cdot\frac{d}{d\theta}\left(\frac{I}{R}\right) \qquad (3.81)$$

and

$$\frac{d}{d\theta}\left(\frac{I}{R}\right) = \frac{1}{R}\,\frac{dI}{d\theta} - \frac{I}{R^2}\cdot\frac{dR}{d\theta}$$

$$\tau = -\frac{S(F,F_0)}{4f_0}\cdot\frac{n}{2}\left[F(R_1,I_1) - F(R_2,I_2)\right] -$$

$$-\frac{S(F,F_0)}{4f_0}\left[F(R_3,I_3) - F(R_4,I_4)\right] \qquad (3.82)$$

where

$$F(R,I) = \frac{R^2}{R^2+I^2}\left[\frac{I}{R}\cdot\frac{dI}{d\theta} - \frac{I}{R^2}\cdot\frac{dR}{d\theta}\right]$$

For a C-section

$$n = 1$$

$$\begin{aligned} R_1 &= 1-\Sigma, I_1 = -\Omega, & \dot{R}_1 &= -\dot{\Sigma}, & \dot{I}_1 &= -\dot{\Omega} \\ R_2 &= 1+\Sigma, I_2 = \Omega, & \dot{R}_2 &= \dot{\Sigma}, & \dot{I}_2 &= \dot{\Omega} \\ R_3 &= \sigma_k-\Sigma, I_3 = -\Omega, & \dot{R}_3 &= -\dot{\Sigma}, & \dot{I}_3 &= -\dot{\Omega} \\ R_4 &= \sigma_k+\Sigma, I_4 = \Omega, & \dot{R}_4 &= \dot{\Sigma}, & \dot{I}_4 &= \dot{\Omega} \end{aligned} \qquad (3.83)$$

Substituting these values, group delay of a C-section network is determined in the presence of dissipation.

For a D-section

$$n = 2$$

where

R_1 and R_2 are the same as for the C-section

$$R_3 = \text{Real } H(-t) = \Sigma^2 - \Omega^2 - 2\sigma_k\Sigma + \sigma_k^2 + \omega_k^2 \qquad (3.84)$$

and $$I_3 = 2\Omega(\Sigma-\sigma_k)$$

$$R_4 = \dot{\Sigma}^2 - \Omega^2 + 2\sigma_k\Sigma + \sigma_k^2 + \omega_k^2$$

$$I_4 = 2\Omega(\Sigma+\sigma_k)$$

$$\frac{dR_3}{d\theta} = 2\Sigma\frac{d\Sigma}{d\theta} - 2\Omega\frac{d\Omega}{d\theta} - 2\sigma_k\frac{d\Sigma}{d\theta}$$

$$\frac{dI_3}{d\theta} = 2\Omega\frac{d\Sigma}{d\theta} + 2\Sigma\frac{d\Omega}{d\theta} - 2\sigma_k\frac{d\Omega}{d\theta}$$

$$\frac{dR_4}{d\theta} = 2\Sigma\frac{d\Sigma}{d\theta} - 2\Omega\frac{d\Omega}{d\theta} + 2\sigma_k\frac{d\Sigma}{d\theta}$$

$$\frac{dI_4}{d\theta} = 2\Omega\frac{d\Sigma}{d\theta} + 2\Sigma\frac{d\Omega}{d\theta} + 2\sigma_k\frac{d\Omega}{d\theta}$$

Substituting these values in the general equation, group delay in the presence of dissipation is determined.

CHAPTER IV

POLE-ZERO DETERMINATION OF THE GENERAL CLASS OF DOUBLY-TERMINATED PROTOTYPE FILTER NETWORKS USING COMPUTER-AIDED OPTIMIZATION TECHNIQUES

CHAPTER IV

POLE-ZERO DETERMINATION OF THE GENERAL CLASS OF DOUBLY-TERMINATED PROTOTYPE FILTER NETWORKS USING COMPUTER-AIDED OPTIMIZATION TECHNIQUES

4.1 INTRODUCTION

Optimization problems have long been of interest to mathematicians, scientists and engineers. In the past, however, owing to computational difficulties, the available theories could be applied to a limited class of problems. Only with the advent of modern computers has the application of optimization to the field of design and operations become a reality. In the field of electrical networks, there is little doubt that the computer can be a most effective and efficient partner.

Despite the easy availability of computers, there seems to be a lack of practical applications that use computer-aided methods in microwave circuit design. One likely reason is that the available analytic techniques provide an excellent first-cut design, which, for most applications, is quite adequate. Another reason, based on available literature and the author's experience, is the gap that presently exists between the class of problems dealt with in the literature versus the practical requirements with its physical constraints.

In this chapter, we are concerned with the synthesis in terms of pole-zero configuration and optimization of doubly terminated low-pass prototype filter networks. Proper adaptation of optimization procedures for this class of problems to the needs of practising engineers is the main intent of this chapter.

4.2. FORMULATION OF THE PROBLEM

Problems of optimization are those in which maximization or minimization of a function is sought. The function may be of one or more variables and with or without constraints. Practical problems, however, invariably have certain constraints which must be satisfied by the optimum solution. Constraints may be either equality or inequality, or both. For equality constraints, the value of constraining function should be equal to zero at the optimum point, whereas for inequality constraints, it should be greater than or equal to zero, or any specified quantity.

Unfortunately, most of the techniques developed for minimizing a function are applicable to minimizing an unconstrained function only, and hence, cannot be applied directly to solve a general optimization problem. The optimization problem must be suitably transformed into an unconstrained function before any minimization technique can be used.

The transformation of the constrained optimization problem into an unconstrained function is normally accomplished by defining an artificial objective function which is a function of the objective function and the constraints. Such an artificial unconstrained objective function has its minima lying in some feasible region. However, it is also possible in the case of special types of constraints to transform the independent design variables such that constraints are automatically taken care of. Such transformations tend to be restrictive. Therefore, the more general approach of transforming the function instead of the variable is generally used.

A typical optimization problem then has the following form [42-44].

Minimize U where

$$U = U(x) \tag{4.1}$$

and

$$x = \begin{bmatrix} x_1 \\ x_2 \\ \vdots \\ x_n \end{bmatrix}$$

U is the objective function and x are the independent parameters which may have the constraints

$$x_{\ell k} \leq x_k \leq x_{\mu k}, \qquad k = 1,2,\ldots$$

where

$x_{\ell k}$ and $x_{\mu k}$ represent the lower and upper bound, respectively.

In addition, there may be a set of functions of x that must be satisfied. In practice, these constraints can be reduced to simple equality and inequality constraints. Denoting the equality constraints by Ψ and the inequality constraints by Φ, we may write

$$\psi_j = \psi_j(x_1, x_2, x_3, \ldots, x_n) = 0, \qquad j = 1,m \qquad (4.2)$$

$$\phi_k = \phi_k(x_1, x_2, x_3, \ldots, x_n) > 0, \qquad k = 1,p \qquad (4.3)$$

where

n is the number of variables

m is the number of equality constraints

p is the number of inequality constraints.

The constraints are then combined with the objective function U to form the artificial unconstrained objective function U_{art} as

$$U_{art}(x_1, x_2, \ldots, x_n, r) = U + \sum_{i=1}^{p} \lambda_i(r) \cdot G(\phi_i(x)) + \sum_{i=1}^{m} \lambda_i(r) \cdot S(\psi_i(x)) \qquad (4.4)$$

where

r = a weighting parameter, and

$\lambda_i(r)$ = weighting functions

G and S = functions of inequality constraints and equality constraints, respectively

The difference between various transformations of this type is the difference in the ways the functions G,S, and weighting functions are selected. A method generally proceeds by selecting a sequence of parameter r_t such that $r_t \geq 0$ and $r \to \infty$ as $t \to \infty$. For each value of r, the unconstrained artificial function is optimized, and t is the number of such optimizations. Functions G and S are selected such that as $t \to \infty$, the quantity

$$F = \sum_{i=1}^{p} \lambda_i(r) \cdot G(\phi_i(x)) + \sum_{i=1}^{m} \lambda_i(r) \cdot S(\psi_i(x)) \qquad (4.5)$$

tends to zero. However, parameter r_t may also be chosen such that as $t \to \infty$, $r_t \to 0$, then functions G and S are accordingly defined so that $F \to 0$ as $t \to \infty$. In either case, as $t \to \infty$, the optimum of the unconstrained artificial function converges to the optimum of the constrained optimiza-

tion problem. Thus, the constrained optimization problem is converted into an unconstrained optimization problem and solved.

A number of transformations are possible [42] depending upon the functions and constraints. The one proposed by Fiacco and McCormick [45] is applicable to the solution of any general optimization problem and is utilized in the programs developed in this thesis. It can be represented as

$$U_{art}(x,r_t) = U + r_t \sum_{\ell=1}^{k} \frac{1}{\phi_\ell(x)} + r_t^{-\frac{1}{2}} \sum_{j=1}^{m} (\psi_j(x))^2 \quad (4.6)$$

It can be analytically proven that as $t \to \infty$, the solution of this unconstrained function approaches the solution of the actual problem. In this transformation, the inequality constraints have been handled in a manner similar to the one proposed by Carroll [46]. As the term r_t/ϕ_ℓ representing the inequality constraints tends to zero, the artificial objective function tends to infinity. Because of this property, the value of the artificial unconstrained function immediately increases if the optimum tends to go near the constraint, and hence the point stays in the feasible region. This effect is more predominant in the initial stages of optimization; later on as t increases, the value of parameter r_t becomes smaller thereby making the product r_t/ϕ_ℓ approach

smaller values at $t \to \infty$. This forces the solution of the unconstrained function towards the optimum value.

For equality constraints, Fiacco and McCormick have introduced an additional term $(\psi_j)^2/\sqrt{r_t}$. Intuitively, the addition of such a term can be explained as follows. As computation proceeds, the value of r_t decreases, this would, in turn, increase the value of the function $(\psi_j)^2/\sqrt{r_t}$ and since no minimization algorithm would permit an increase in the function the magnitude of ψ_j would necessarily decrease to nullify the increase due to $1/\sqrt{r_t}$. In the limiting case as $t \to \infty$, ψ_j must tend to zero, otherwise the function $[\psi_j^2]/\sqrt{r}$ would tend to infinity. Thus, inclusion of this term forces the equality constraint equal to zero when the optimum is reached.

The prerequisite for use of these transformations is that the solution is started from a feasible point for the inequalities. Fiacco and McCormick suggest that an additional term for violated inequality constraints should be included in the transformed unconstrained function, similar to the one used for equality constraints. Addition of such a term would make violated inequality constraint equal to zero and would force a feasible solution. Another approach is to transform the constrained optimization problem into an unconstrained function in which violated constraints are

severely penalized. The unconstrained function has the following form

$$U_{art}(x_1,x_2,\ldots,x_n,r) = U + 10^{20} \sum_{j=1}^{m} |\psi_j(x)| +$$

$$+ 10^{20} \sum_{k=1}^{p} \text{ABS} \qquad (4.7)$$

(violated inequality constraint)

This type of function puts a sort of wall around the feasible region and any feasible point stays in the feasible region. This type of transformation usually stalls quickly and does not handle equality constraints well. An infeasible start is permitted. All these transformations were tried for the optimization subroutines developed for this thesis. The one finally used has basically the same form as that proposed by Fiacco and McCormick. This has been found to give satisfactory answers. Because of the high penalty, there is sometimes a tendency to stall at inequality constraints, but this at least keeps the solution feasible. The unconstrained artificial objective function used for the subroutines of this thesis is as follows:

$$U_{art}(x_1,x_2,\ldots,x_n) = U + r_t \sum_{i=1}^{p} \frac{1}{\phi_i(x)} +$$

$$+ r_t^{-\frac{1}{2}} \sum_{j=1}^{m} (\psi_j(x))^2 + 10^{20} \sum_{i=1}^{p} \text{ABS}$$

(violated inequality constraint) (4.8)

The selection of a sequence of reduction in the value of parameter r_t has been found to have significant effect upon convergence and therefore requires a careful choice.

4.3 OBJECTIVE FUNCTION AND CONSTRAINTS FOR DOUBLY TERMINATED LOW-PASS PROTOTYPE FILTER NETWORKS

As outlined in Chapter II, the transmission coefficient t(s) of a doubly terminated low pass prototype network is given by

$$|t(s)|^2_{s=j\omega} = \frac{1}{1 + \varepsilon^2 |K(s)|^2_{s=j\omega}} \qquad (4.9)$$

where

$$K(s) = \frac{F(s)}{P(s)} = \frac{(s^2+a_1^2)(s^2+a_2^2)\ldots}{(s^2+b_1^2)(s^2+b_2^2)\ldots} \qquad (4.10)$$

a's and b's are the attenuation zeros and poles respectively (referred to as the critical frequencies) and ε is the ripple factor. The number of independent variables are entirely represented by the finite critical frequencies. Attenuation zeros at origin or poles at infinity represent fixed frequencies and therefore are not independent. ε provides the trade-off between the passband and stopband response for a given characteristic factor F (defined in Section 2.4) and hence again, does not represent an independent variable. If a specific value of F is desired, it

can be taken as an equality constraint or alternatively, critical frequencies can be generated with F as a parameter by varying one of the independent variables for the same set of constraints. This is more efficient as it dispenses with the equality constraint and helps generate the unified design charts for a given response shape.

Next comes the question as to what filter performance parameters are <u>essential</u> to determine a practical design. The word essential implies the minimum number of parameters which may then be used to generate practical filter design through the use of frequency transformations and appropriate choice of ε. All practical applications require a maximum permissible ripple in the passband and a minimum isolation in the stopband. Phase or group delay response in the passband and elsewhere is uniquely related to the amplitude response for minimum phase filters through the use of Hilbert's transforms. For such filters therefore, it is sufficient to optimize the amplitude response and accept the resulting phase response. In this thesis, we are primarily concerned with minimum phase filters although the subsequent analysis is general enough to analyze and optimize non-minimum phase types of filters as well.

To constrain the amplitude ripples in the passband or stopband, one must determine the frequencies at which

these amplitude maxima and minima occur. This is accomplished by differentiating the equation for the transmission coefficient t(s) and equating it to zero, i.e.,

$$\frac{\partial}{\partial s} |t(s)|^2 = 0 \tag{4.11}$$

or

$$\frac{\partial}{\partial s} \frac{F^2(s)}{P^2(s)} = 0 \tag{4.12}$$

or

$$F(s)P(s) - F(s)P(s) = 0 \tag{4.13}$$

This determines the frequencies corresponding to the amplitude minima in the passband and maxima in the stopband. These frequencies are determined for an arbitrary choice of ϵ. Having determined these frequencies, the transmission and reflection coefficients or loss in decibels is computed as described by relationships in Section 2.6. The cut-off frequency ω_c, corresponding to the maximum ripple in the passband, is determined by solving for t(s) equal to the maximum ripple in the passband. All other frequencies can then be normalized with respect to ω_c such that $\omega_c = 1$. For practical applications, the most convenient and almost universally used parameters for specifying amplitude response are return loss in passband and transmission loss in stopband, both parameters having units of decibels (dB). Denoting

by R(i) and T(i) the return loss and transmission or insertion loss at the i^{th} attenuation maxima or minima, the objective function U can have terms of the following three types:

$$U = U_1 + U_2 + U_3 + \ldots.$$

where

$$\begin{aligned} U_1 &= \text{ABS}[\,|R(i) - R(j)| + A_{ij}] \\ U_2 &= \text{ABS}[\,|T(i) - T(j)| + B_{ij}] \\ U_3 &= \text{ABS}[\,|R(i) - T(j)| + C_{ij}] \end{aligned} \qquad (4.14)$$

A_{ij}, B_{ij} and C_{ij} represent arbitrary constants that constrain the differences in amplitudes at the attenuation maxima and minima to some arbitrary values. For equi-ripple passband, $A_{ij} = 0$, and for equi-ripple stopband, $B_{ij} = 0$. The term U_3 is representative of the characteristic factor F. As explained earlier, if need be, it is best utilized as an equality constraint. Thus, in a generalized form, the objective function U can be represented by:

$$U = \sum_{i \neq j} \text{ABS}[\,|R(i) - R(j)| - A_{ij}] + \sum_{k \neq \ell} \text{ABS}[\,|T(k) - T(\ell)| - B_{k\ell}] \qquad (4.15)$$

where the summations extend over all attenuation maxima in passband for the first term and over all attenuation minima

in stopband for the second term. Return loss and insertion loss are given by

$$T \triangleq 10 \log[|t(s)|^2_{s=j\omega}] \qquad (4.16)$$

$$R = 10 \log[1 - |t(s)|^2_{s=j\omega}] \qquad (4.17)$$

Constraints on the independent variables viz., the finite critical frequencies, are given by

$$\begin{aligned} 0 \leq a_1, a_2, \ldots &< 1 \\ b_1, b_2, \ldots &> 1 \end{aligned} \qquad (4.18)$$

These represent the essential inequality constraints for prototype filter networks.

The objective function as defined earlier and these inequality constraints completely define the problem for generating a filter response through optimization techniques.

4.4 ANALYTIC DERIVATION OF THE GRADIENTS OF THE OBJECTIVE FUNCTION FOR LOW-PASS PROTOTYPE NETWORKS

As described in the previous sections, the unconstrained artificial function U_{art} is given by

$$U_{art} = U + \frac{r}{\sum_i |\phi_i|} + \frac{\sum_k |\psi_k|^2}{\sqrt{r}} \qquad (4.19)$$

where

r is a variable of optimization to control the imposed constraints. It is a positive number. A typical range of r is between 10^{-4} and 1.

U is the unconstrained objective function

ϕ_i is the $i^{\underline{th}}$ inequality constraint

ψ_k is the $k^{\underline{th}}$ equality constraint

At the optimum value, $U_{art} = 0$. This implies that each individual term comprising U_{art} must be zero. The unconstrained function 'U' will tend to zero at the optimum value. To ensure convergence of the constraint terms to zero, r is made smaller such that

$$\frac{r}{\sum_i |\phi_i|} \to 0$$

and

$$\frac{\sum_k |\psi_k|^2}{\sqrt{r}} \to 0$$

as

$$r \to 0$$

This is done in steps to ensure smooth convergence of U_{art} to the desired level of accuracy.

The gradient of U_{art} with respect to the attenuation zeros 'a_i' is given by

$$g_i = \frac{\partial U_{art}}{\partial a_i} = \frac{\partial U}{\partial a_i} + r \frac{\partial}{\partial a_i} \sum_i |\phi_i| + \frac{1}{\sqrt{r}} \frac{\partial}{\partial a_i} \sum_k |\psi_k|^2 \quad (4.20)$$

$$= \frac{\partial U}{\partial a_i} + \Phi + \Psi \quad (4.21)$$

Each term on the right-hand side is evaluated independently as follows.

4.4.1 Evaluation of $\frac{\partial U}{\partial a_i}$

A typical form of the unconstrained function 'U' is

$$U = |R(1)-R(2)|+|R(2)-R(3)|+ \ldots +|T(4)-T(5)|+ \\ + |T(5)-T(6)|+ \ldots \quad (4.22)$$

where R(k) and T(k) are the values of return loss and transmission loss in dB at the k^{th} attenuation maxima in passband or minima in stopband.

Considering a typical term, we have

$$U_{ik} = |R(i)-R(k)| = R(i)-R(k) \quad \text{if} \quad R(i) \geq R(k)$$

$$= -(R(i)-R(k)) \quad \text{if} \quad R(i) < R(k) \tag{4.23}$$

$$\frac{\partial U_{ik}}{\partial a_i} = \pm\left[\frac{\partial R(i)}{\partial a_i} - \frac{\partial R(k)}{\partial a_i}\right] \tag{4.24}$$

The positive sign holds when $R(i) \geq R(k)$ and vice-versa.

The partial derivatives $\frac{\partial R}{\partial a_i}$ are determined by considering the transmission function

$$|t|^2 = \frac{1}{1 + |K(s)|^2} = 1 - |\rho|^2 \tag{4.25}$$

where

ρ is the reflection coefficient

The characteristic function K(s) is given by

$$K(s) = \varepsilon \cdot \frac{s(s^2+a_1^2)(s^2+a_2^2) \ldots (s^2+a_i^2) \ldots}{(s^2+b_1^2)(s^2+b_2^2) \ldots (s^2+b_i^2) \ldots} \tag{4.26}$$

for odd-order filter functions and

$$K(s) = \varepsilon \cdot \frac{(s^2+a_1^2)(s^2+a_2^2) \ldots (s^2+a_i^2) \ldots}{(s^2+b_1^2)(s^2+b_2^2) \ldots (s^2+b_i^2) \ldots} \tag{4.27}$$

for even-order filters

$$\therefore \frac{\partial|t|^2}{\partial a_i} = -\frac{1}{[1+|K(s)|^2]^2} \cdot 2\,K(s) \cdot \frac{\partial|K(s)|}{\partial a_i}$$

$$= -4\,\frac{a_i}{(s^2+a_i^2)} \cdot \frac{K^2(s)}{[1+K^2(s)]^2} \qquad (4.28)$$

The transmission loss 'T' and return loss 'R' in dB are given by

$$T = 10 \log|t|^2 \qquad (4.29)$$

and

$$R = 10 \log|\rho|^2$$

$$= 10 \log[1-|t|^2] \qquad (4.30)$$

$$\therefore \frac{\partial T}{\partial a_i} = -40 \log 'e' \cdot \frac{K^2(s)}{1+K^2(s)} \cdot \frac{a_i}{(s^2+a_i^2)}$$

$$= -40 \log 'e' \cdot |\rho|^2 \cdot \frac{a_i}{(s^2+a_i^2)} \qquad (4.31)$$

and

$$\frac{\partial R}{\partial a_i} = 40 \log \text{"e"} \cdot \frac{1}{1+K^2(s)} \cdot \frac{a_i}{(s^2+a_i^2)}$$

$$= 40 \log \text{"e"} \cdot |t|^2 \cdot \frac{a_i}{(s^2+a_i^2)} \qquad (4.32)$$

where

"e" is the natural base for logarithms.

In a similar manner, it can be shown that the gradients with respect to the attenuation poles 'b_i' are given by

$$\frac{\partial T}{\partial b_i} = 40 \log \text{"e"} \cdot |\rho|^2 \cdot \frac{b_i}{(s^2+b_i^2)} \qquad (4.33)$$

and

$$\frac{\partial R}{\partial b_i} = -40 \log \text{"e"} \cdot |t|^2 \cdot \frac{b_i}{(s^2+b_i^2)} \qquad (4.34)$$

Thus, the partial derivatives of transmission or return loss in dB at any frequency with respect to the independent variables are determined analytically and hence the gradient of the unconstrained function U.

4.4.2 Evaluation of Inequality Constraint Gradient

The inequality constraint Φ has the form

$$\Phi = \frac{r}{|\phi_1|} + \frac{r}{|\phi_2|} + \ldots \qquad (4.35)$$

where

r is a positive number

and the

ϕ terms have the typical forms

$$\phi_k = \begin{cases} a_i \\ 1 - a_i \\ a_i - 1 \\ N - a_i, \ N \text{ is a positive number greater than } 1 \end{cases} \qquad (4.36)$$

$$\frac{\partial}{\partial a_i}\frac{1}{|\phi_k|} = -\frac{1}{\phi_k^2}\frac{\partial \phi_k}{\partial a_i} \qquad \phi_k > 0$$

$$= +\frac{1}{\phi_k^2}\frac{\partial \phi_k}{\partial a_i} \qquad \phi_k < 0 \qquad (4.37)$$

a_i is the $i^{\underline{th}}$ independent variable. The gradients for the various forms of ϕ with respect to an independent variable are described in Table 4.1.

TABLE 4.1 GRADIENTS OF THE INEQUALITY CONSTRAINT ϕ

Form of ϕ	Gradient of ϕ	Constraints
a_i	$\mp \frac{1}{a_i^2}$	$a_i \gtrless 0$
$1-a_i$	$\pm \frac{1}{(1.0-a_i)^2}$	$(1.0-a_i) \gtrless 0$
a_i-1	$\mp \frac{1}{(a_i-1)^2}$	$(a_i-1) \gtrless 0$
$N-a_i$	$\pm \frac{1}{(N-a_i)^2}$	$(N-a_i) \gtrless 0$

Thus, the gradient of Φ will have the form

$$\frac{\partial \Phi}{\partial a_i} = r.[\Sigma(\mp \frac{1}{a_i^2}) + \Sigma_k \pm [\frac{1}{(1-a_i^2)}] +$$

$$+ \Sigma(\mp \frac{1}{(a_i-1)^2}) + \Sigma(\pm \frac{1}{(N-a_i^2)})] \qquad (4.38)$$

This includes inequalities associated with attenuation zeros, as well as poles.

4.4.3 Evaluation of the Equality Constraint Gradient

The gradient of the equality constraint is

$$\Psi = \frac{1}{\sqrt{r}} \frac{\partial}{\partial a_i} \Sigma |\psi_k|^2 \qquad (4.39)$$

where

ψ_k has the form

$$\psi_k = A + R(1) + T(2) - T(1) - R(2) \quad \ldots \quad (4.40)$$

A is a constant, and

R(j) or T(J) represent the return loss and transmission loss in dB at the j^{th} maxima in passband or minima in stopband.

$$\frac{\partial}{\partial a_i} |\psi_k|^2 = 2\, \psi_k \cdot \frac{\partial \psi_k}{\partial a_i} \qquad (4.41)$$

$$\Psi = \frac{2}{\sqrt{r}} \sum_k \psi_k \left[\frac{\partial R(1)}{\partial a_i} + \frac{\partial T(2)}{\partial a_i} + \frac{\partial T(1)}{\partial a_i} - \frac{\partial R(2)}{\partial a_i} + \ldots\right] \qquad (4.42)$$

The values of R(J) or T(J) and their partial derivations were determined analytically in Section 4.4.1 and thus Ψ is realized analytically.

Hence, the gradients of the unconstrained objective function U_{art} as given by Equation (4.21) are determined analytically.

4.5 OPTIMIZATION METHODS

There is extensive literature available [42-44] describing the various methods for the optimization of a given unconstrained function. Based on literature survey and some limited experience [47], three methods were selected, one of which uses the direct search technique whereas the other two are based on gradient strategies. These methods and the results obtained are described in the subsequent sections.

4.5.1 Simplex Method

A set of n+1 points in n dimensional space defines a space called simplex. The geometry of this simplex plays the key role in the optimization process.

This method was first described by Himsworth et. al. [48] and later developed by Nelder and Mead [49]. The principle of this method is that one can form a new simplex from the current one by reflecting one point in the hyperplane spanned by the remaining points. Normally, the vortex of the simplex at which the function is greatest is chosen for reflection. If the function is lower at the reflected point, then the process can be continued so as to move the simplex closer to the minimum. The basic move of reflection is made with respect to the centroid of the simplex.

Nelder and Mead introduced a more flexible approach in which the simplex can be altered both in size and in geometry. Depending upon the outcome after reflection, the new simplex can be expanded or contracted in the direction of decreasing function. This gives rise to a moving, shrinking and expanding progress of the simplex toward the minimum. This is the strategy employed in the basic package used in this thesis.

The stopping criterion suggested by Nelder and Mead is

$$\left\{\frac{1}{n}\sum_{i=1}^{n+1}\left(f(X_i) - f(X_0)\right)^2\right\}^{\frac{1}{2}} < \varepsilon \qquad (4.43)$$

where

ε is some small preset number

This method is relatively simple to use, requires no extra information (such as gradients, etc.) and is very efficient up to four variables. The progress tends to slow down when there are more than four parameters.

4.5.2 Multidimensional Gradient Methods

Methods that utilize partial derivatives to determine the direction of search fall into this category. These methods in general are more powerful than direct search methods (such as the simplex method) but require, as a minimum, the evaluation of first-order partial derivatives. Such derivatives may be obtained either analytically or by estimation. The latter approach can be readily implemented but requires extreme caution in its use. Too small a value or too large a value of perturbation can lead to inaccurate gradients and hence, the direction of search. Whenever possible, analytic gradients should be used in these methods.

The basic theory behind such methods is briefly reviewed here [42-44]. The first three terms of the multi-dimensional Taylor series for the unconstrained objective function U are given by:

$$U(x+\Delta x) = U(x) + \nabla U^T \Delta x + \tfrac{1}{2}\Delta x^T H \Delta x + \cdots \quad (4.44)$$

where

$$\Delta x = \begin{bmatrix} \Delta x_1 \\ \Delta x_2 \\ \vdots \\ \Delta x_k \end{bmatrix} \quad (4.45)$$

represent the parameter increments

$$\nabla U = \begin{bmatrix} \frac{\partial U}{\partial x_1} \\ \frac{\partial U}{\partial x_2} \\ \vdots \\ \frac{\partial U}{\partial x_k} \end{bmatrix} \quad (4.46)$$

is the gradient vector containing the first partial derivatives, and

$$H = \begin{bmatrix} \frac{\partial^2 U}{\partial x_1^2} & \frac{\partial^2 U}{\partial x_1 \partial x_2} & \cdots & \frac{\partial^2 U}{\partial x_1 \partial x_k} \\ \frac{\partial^2 U}{\partial x_2 \partial x_1} & & & \\ \vdots & & & \\ \frac{\partial^2 U}{\partial x_k \partial x_1} & \cdots & & \frac{\partial^2 U}{\partial x_k^2} \end{bmatrix} \tag{4.47}$$

is the matrix of second partial derivatives, the Hessian matrix. Assuming the first and second derivatives exist, a point is a minimum if the gradient vector is zero and the Hessian matrix is positive definite at that point.

It can readily be shown that maximum change occurs in the direction of gradient vector U. Further, by differentiating the multidimensional Taylor series in the vicinity of the minima x we have

$$\tilde{x} = x + \Delta x \tag{4.48}$$

$$0 \approx \nabla U + H\Delta x \tag{4.49}$$

neglecting higher order terms and making use of the fact that $\nabla U(\tilde{x}) = 0$. Thus

$$\Delta x \approx - H^{-1} \nabla U \tag{4.50}$$

where

H^{-1} is the inverse of the Hessian matrix

On a quadratic function, this relationship provides the parameter increments for the minimum to be reached in exactly one step. This provides a basis for iterative schemes for function minimization. Methods of Fletcher and Powell and the new Fletcher method described in the following sections and used in this thesis make use of the above fundamental considerations.

4.5.3 Fletcher-Powell Method

This is one of the more powerful minimization methods that is now available as a standard library subroutine. It is a development of Davidon's variable metric method [52]. A brief discussion of the method is as follows [50]:

The iterative scheme followed is given by

$$x^{j+1} = x^j + \alpha^j s^j \tag{4.51}$$

where

$$s^j = - H^j \nabla U^j \tag{4.52}$$

H^j is the $j^{\underline{th}}$ approximation to the inverse of the Hessian matrix which is assumed as a positive definite matrix

The initial approximation to H is usually the unit matrix. This results in the first step being in the direction of the steepest descent.

α^j is a positive scale factor chosen to minimize U^{j+1}

H is continually updated such that

$$x^{j+1} - x^j = H^{j+1}[\nabla U^{j+1} - \nabla U^j] \qquad (4.53)$$

Thus, only first derivatives are required to update H.

In practice, the algorithm that is followed to compute H^{j+1} is given by [44,50,51]

$$H^{j+1} = H^j + \frac{\delta\delta^T}{\delta^T\gamma} - \frac{H^j\gamma\gamma^T H^j}{\gamma^T H^j\gamma} \qquad (4.54)$$

where

$$\delta = x^{j+1} - x^j = \alpha^j s^j =$$

$$= -\alpha^j H^j \nabla U^j \qquad (4.55)$$

and

$$\gamma = \nabla U^{j+1} - \nabla U^j \qquad (4.56)$$

4.5.4 New Fletcher Method

In the previously described Fletcher and Powell Method, at each iteration U^{j+1} is minimized by choosing an appropriate α^j involving linear search. This is usually done by evaluating the function $U(x+\lambda s)$ and gradient for a number of different values of λ and interpolating according to some strategy until a sufficiently accurate minimum is obtained. This requires considerable computing effort. It suffers from further disadvantage if constraints are present, as the minimum along the line may not be feasible even though no constraints limit the position of the ultimate solution.

Fletcher [51] has presented a new approach to variable metric algorithms in which the linear search subprogram is no longer necessary.

The updating formula (4.54) forces the relationship $H^{j+1}\gamma = \delta$ to hold. If Γ^j is defined as $[H^j]^{-1}$ then Γ^j and Γ^{j+1} corresponding to H^j and H^{j+1} of (4.54) would be related by

$$\Gamma^{j+1} = \left(I - \frac{\gamma\delta^T}{\delta^T\gamma}\right)\Gamma^j\left(I - \frac{\delta\gamma^T}{\delta^T\gamma}\right) + \frac{\gamma\gamma^T}{\delta^T\gamma} \qquad (4.57)$$

a relationship that forces $\Gamma^{j+1}\delta = \gamma$. Thus, a way is obtained of forcing δ into γ. Carrying out the interchange $\delta \leftrightarrow \gamma$

in the above relationship, a formula would be obtained which mapped γ into δ and this could be used to update H^j. Thus

$$H^{j+1} = (1 - \frac{\delta\gamma^T}{\delta^T\gamma})H^j(1 - \frac{\gamma\delta^T}{\delta^T\gamma}) + \frac{\delta\delta^T}{\delta^T\gamma}$$

$$= H^j - \frac{\delta\gamma^T H}{\delta^T\gamma} - \frac{H^j\gamma\delta^T}{\delta^T\gamma} +$$

$$+ (1 + \frac{\gamma^T H^j\gamma}{\delta^T\gamma})\frac{\delta\delta^T}{\delta^T\gamma} \qquad (4.58)$$

A new formula is thus obtained where linear search is no longer necessary. If H^j is updated by the above relationship, then the corresponding updating formula for Γ^j is obtained by performing the interchange $\gamma \leftrightarrow \delta$ in (4.54) to give

$$\Gamma = \Gamma + \frac{\gamma\gamma^T}{\delta^T\gamma} - \frac{\Gamma\delta\delta^T\Gamma}{\delta^T\Gamma\delta} \qquad (4.59)$$

Formulae (4.56), (4.57), (4.58) and (4.59) may be considered dual in this sense.

The treatment here is entirely based on reference [51]. The subroutine that uses this algorithm is available from Fletcher [51]. A computer program was written that utilizes the objective function and its evaluation as described earlier in this Chapter and Chapter II; analytic gradients as derived in this Chapter, and the optimization

subroutine of Fletcher. Results obtained from this program, in my view, represent an advance in the state-of-the-art for computer-aided filter design.

4.6 OPTIMIZATION PROGRAMS AND APPLICATION TO FILTER DESIGN

Based on the foregoing analysis, optimization programs were developed that use:

. Simplex Method

.. New Fletcher Algorithm

The second method of optimization requires first-order derivatives, i.e., the gradients of the unconstrained objective functions. The analytic relationships derived for the derivatives are incorporated in this programs. For the sake of comparison and as an additional check, option to compute gradients numerically is also included.

To demonstrate the usefulness and efficiency of these computer programs, the known classes of filter functions are treated first. Starting from an arbitrary set of values, the critical frequencies are computed using these programs and the results compared with the analytic values. This provides a valuable check for the computer programs and sheds some light on their relative efficiencies.

The objective functions, constraints and choice of independent variables for any arbitrary low pass prototype filter are then considered and used to generate new designs.

4.6.1 Chebyshev Function Filters

This function is characterized by equi-ripple response in the passband and a monotonically rising stopband. The objective function and constraints are therefore given by

$$U = |R(1) - R(2)| + |R(2) - R(3)| + \ldots. \quad (4.60)$$

$$1 < a_1, a_2, \ldots > 0 \quad (4.61)$$

where R(k) is the return loss at the $k^{\underline{th}}$ attenuation maxima and a's are the critical frequencies.

As an example, a sixth-order filter was analyzed. Table 4.2 describes the computed results and compares them with the analytic values. The objective function used is

$$U = |R(1) - R(2)| + |R(2) - R(3)| + |R(3) - R(4)| \quad (4.62)$$

where

R(4) is characterized by s = j1, as shown in Table 4.2. This term is necessary only if normalization with

TABLE 4.2 COMPUTED CRITICAL FREQUENCIES FOR A SIX-POLE CHEBYSHEV FILTER USING OPTIMIZATION TECHNIQUES

$$K(s) = (s^2+a_1^2)(s^2+a_2^2)(s^2+a_3^2)$$

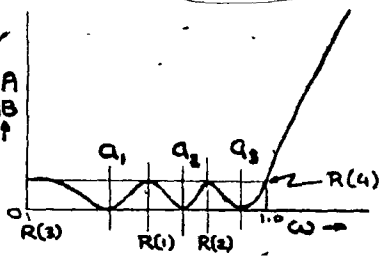

Starting Values: $a_1 = .2, a_2 = .4, a_3 = .6$
Objective Function: $|R(1)-R(2)| + |R(2)-R(3)| + |R(3)-R(4)|$
Constraints: $0 < a_1, a_2, a_3 < 1$

OPTIMIZATION METHODS	COMPUTED CRITICAL FREQUENCIES a_1	a_2	a_3	CPU TIME SECONDS
SIMPLEX	.2589	.7070	.9659	91.3
NEW FLETCHER ALGORITHM	.2588	.7071	.9659	1.59
ANALYTIC VALUES	.2588	.7071	.9659	-

respect to unity cutoff is required. Alternatively, one may compute the critical frequencies with an arbitrary cutoff frequency which could then be computed numerically by analyzing the response with respect to attenuation maxima.

As shown in the table, the results tally closely with analytic values. Fletcher's method shows a very significant improvement over the Simplex method in the CPU time.

4.6.2 Inverse Chebyshev filter response functions

These filters are characterized by monotonically increasing passband (maximally flat) and an equi-ripple stopband. The objective function and constraints are therefore evaluated as:

$$U = |T(1) - T(2)| + |T(2) - T(3)| + \ldots \quad (4.63)$$

$$b_1, b_2, \ldots > 1 \quad (4.64)$$

where

T(k) is the transmission loss at the k^{th} attenuation minima.

and the

b's are the critical frequencies.

TABLE 4.3 COMPUTED CRITICAL FREQUENCIES FOR A SIX-POLE INVERSE CHEBYSHEV FILTER USING OPTIMIZATION TECHNIQUES

$$K(s) = \frac{s^6}{(s^2+b_1^2)(s^2+b_2^2)}$$

Starting Values: $b_1 = 1.5, b_2 = 3.0$.
Objective Function: $|T(1)-T(2)| + |T(2)-T(3)| + |T(3)-T(1)|$
Constraints: $1 < b_1, b_2 < 15$

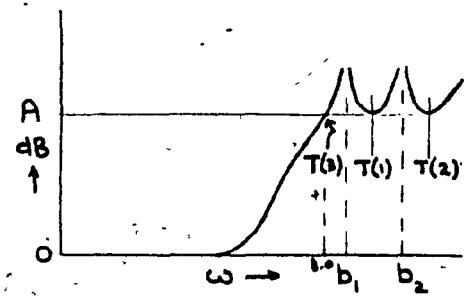

OPTIMIZATION METHODS	COMPUTED CRITICAL FREQUENCIES b_1	b_2	CPU TIME SECONDS
SIMPLEX	1.0379	1.4679	28.8
NEW FLETCHER ALGORITHM	1.0379	1.4679	1.22
ANALYTIC VALUES	1.0379	1.4679	-

Choosing the specific example of a 6-pole filter normalized to unity cutoff with respect to equi-ripple stopbands, as shown in table 4.3,

$$U = |T(1) - (T(2)| + |T(2) - T(3)| + |T(3) - T(1)| \quad (4.65)$$

$$b_1, b_2, > 1 \quad (4.66)$$

Starting from an arbitrary set of values, Table 4.3 describes the optimized values of the critical frequencies and compares them with the analytic values. The results tally to within .01% for a computation time of 1.2 seconds, using the new Fletcher algorithm.

4.6.3 Elliptic response functions

These filters are characterized by equi-ripple pass-band - and equi-ripple stopband. The objective function and constraints are therefore evaluated as

$$U = |R(1) - R(2)| + |R(2) - R(3)| + ... +$$

$$+ |T(1) - T(2)| + |T(2) - T(3)| + ... \quad (4.67)$$

$$1 < a_1, a_2, a_3, ... > 0 \quad (4.68)$$

$$b_1, b_2, ... > 1 \quad (4.69)$$

where

R(k) and T(k) are the return loss and transmission loss at the $k^{\underline{th}}$ attenuation maxima or minima

and

a's and b's are the critical frequencies.

Choosing the specific example of a 6-pole filter with two attenuation poles, as shown in Table 4.4, we have

$$U = |R(1) - R(2)| + |R(2) - R(5)| + |T(3) - T(4)| \quad (4.70)$$

$$1 < a_1, a_2, a_3 > 0 \quad (4.71)$$

$$b_1, b_2 > 0 \quad (4.72)$$

R(5) is characterized by s = j1 to incorporate the unity cutoff frequency. The Simplex method could not determine the optimum value even after removing the constraint of unity cutoff. Using Fletcher's algorithm, it takes 5.07 seconds of CPU time to determine the critical frequencies with better than .03% accuracy.

For practical filters with non-monotonic passband or stopband, it is necessary to impose some constraint on the characteristic factor F which for the example under consideration will have the form

TABLE 4.4 COMPUTED CRITICAL FREQUENCIES FOR A SIX-POLE ELLIPTIC FILTER USING OPTIMIZATION TECHNIQUES

$$K(s) = \frac{s^2(s^2+a_1^2)(s^2+a_2^2)}{(s^2+b_1^2)(s^2+b_2^2)}$$

$b_1 = 1.2995$

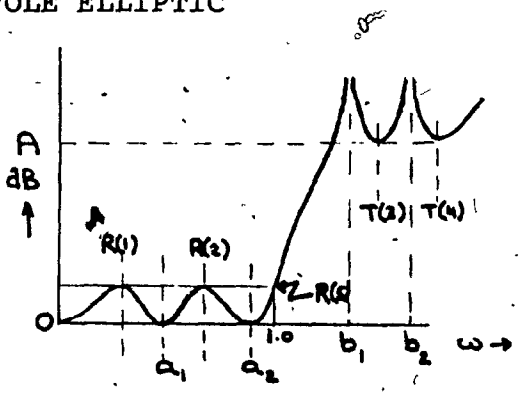

Starting Values: $a_1 = .4, a_2 = .8, b_2 = 2.0$
Objective Function: $|R(1)-R(2)| + |R(2)-R(5)| + |T(3)-T(4)|$
Constraints: $0 < a_1, a_2 < 1$
$1 < b_2 < 15$

OPTIMIZATION METHODS	COMPUTED CRITICAL FREQUENCIES a_1	a_2	b_2	CPU TIME SECONDS
SIMPLEX	.4631	.6342	1.7775	143*
NEW FLETCHER ALGORITHM	.7583	.9768	1.6740	4.75
ANALYTIC VALUES	.7583	.9768	1.6741	-

* Optimum value could not be found after 200 seconds of CPU time.

$$F = -|R(3) + T(4)| + |T(3) - R(4)|$$

$$= A \text{ (say)} \qquad (4.73)$$

As an equality constraint, this will have the form

$$PSI(1) = A + |R(3) + T(4)| - |T(3) - R(4)| \qquad (4.74)$$

Equality constraints in general increase the computation time significantly. One way to bypass this equality constraint and at the same time decrease the number of independent variables by one, is to fix one of the attenuation pole frequencies. This automatically constraints F. From a practical standpoint, this is most useful since one generates tradeoffs by choosing the pole frequencies in the neighbourhood where high isolation is specified. Using this approach, the computed critical frequencies, by choosing $b_1 = 1.2995$, are described in Table 4.4. As can be seen, there is a 10% improvement in computation efficiency.

For a larger number of variables, an increase in efficiency will likely be higher.

4.6.4 Generation of new classes of filter functions

Having demonstrated the generation of classical filter functions, we shall now consider an unconventional

eighth-order filter having the characteristic polynomial

$$K(s) = \frac{s^4(s^2+a_1^2)(s^2+a_2^2)}{(s^2+b_1^2)(s^2+b_2^2)} \qquad (4.75)$$

This function is characterized by a pair of attenuation poles, a double zero at the origin and two other non-origin zeros. We shall consider the following three cases for optimization:

4.6.5 Equi-Ripple Case

Assuming a fixed attenuation pole $b_1 = 1.25$, the objective function and constraints are given by

$$U = |R(1) - R(2)| + |T(3) - T(4)| + |R(2) - R(5)| \qquad (4.76)$$

$$1 < a_1, a_2 > 0 \qquad (4.77)$$

$$b_2 > 1 \qquad (4.78)$$

Computed critical frequencies using the new Fletcher algorithm are described in Table 4.5.

R(5) fixes the cutoff frequency as unity.

4.6.6 Non-equi-ripple stopband with ascending minima

Here, we consider an equi-ripple passband and a non-equi-ripple stopband such that the isolation provided by the second attenuation minima is higher than the first one by an arbitrary amount δ.

The objective function and constraints are given by:

$$U = |R(1) - R(2)| + |R(2) - R(5)| + |T(3) - T(4) - \delta| \qquad (4.79)$$

$$1 < a_1, a_2 \geq 0$$

$$b_2 > 1$$

For an arbitrary value of $\delta = 10$ dB, the computed critical frequencies using the new Fletcher's algorithm are described in Table 4.5.

4.6.7 Non-equi-ripple stopband with descending order

This case is similar to Case (b) except that the isolation of the first minima is higher than the second one. The objective function for this case is therefore

$$U = |R(1) - R(2)| + |R(2) - R(5)| + |T(4) - T(3) - \delta| \qquad (4.80)$$

TABLE 4.5 COMPUTED CRITICAL FREQUENCIES FOR A NEW TYPE OF 8-POLE FILTER WITH TWO ATTENUATION POLES AND A DOUBLE ATTENUATION ZERO AT ORIGIN

$$K(s) = \frac{s^4(s^2+a_1^2)(s^2+a_2^2)}{(s^2+b_1^2)(s^2+b_2^2)}$$

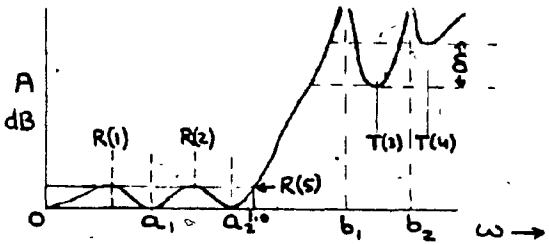

$b_1 = 1.25$

Objective Function: $|R(1)-R(2)| \quad |R(2)-R(5)| \quad |R(5)-R(1)|$
$|\pm T(3) \mp T(4) - \delta|$

δ: represents the difference in dB between the two attenuation minima in stopband

δ dB	COMPUTED a_1	CRITICAL a_2	FREQUENCIES b_2	CHARACTERISTIC FACTOR 'F' dB	CPU TIME SECONDS
0	.8388	.9845	1.4671	67.4	4.66
10	.8340	.9839	1.6211	63.1	6.37
-10	.8636	.9878	1.1541	63.25	4.46

For δ = 10 dB, computed critical frequencies are described in Table 4.5.

As a cross check for the computed critical frequencies for these new classes of filter functions, return loss and transmission loss at frequencies of attenuation minima and maxima were computed for the case of δ = ∞ 10 dB for an arbitrary ripple factor. Results are described in Table 4.6. As can be seen, there is a correlation to within .05% with respect to the specified response shape. For practical purposes, a 1% accuracy is more than adequate and this can be used to decrease the computation time.

TABLE 4.6 COMPUTED RESPONSE AT FREQUENCIES OF ATTENUATION MINIMA AND MAXIMA FOR THE NEW CLASS OF 8-POLE MINIMUM PHASE FILTER

$$K(s) = \frac{S^4 (s^2+a_1^2)(s^2+a_2^2)}{(s^2+b_1^2)(s^2+b_2^2)}$$

Critical Frequencies rad/sec	Minima/Maxima Frequencies rad/sec	Return Loss dB	Insertion Loss dB
.8636	.7064	29.615	.005
.9878	.9470	29.609	.005
1.1541	1.1897	.002	33.634
1.25	1.5464	.019	23.639
Return Loss at cut-off (1.0) : 29.631 dB			

CHAPTER V

PROTOTYPE CHARACTERISTICS OF SOME SPECIAL CLASSES OF FILTER FUNCTIONS

CHAPTER V

PROTOTYPE CHARACTERISTICS OF SOME SPECIAL CLASSES OF FILTER FUNCTIONS

5.1 INTRODUCTION

This chapter is devoted to the determination of critical frequencies for new response functions which may be of interest to filter designers. It includes the following:

- Clear description of the analytical relationships for the non-equi-ripple quazi-elliptic response functions. Such filters are of interest owing to their application in satellite multiplexers. Critical frequencies and unified design charts for such type of filters of practical interest are included.
- A brief description of the use of Bennett's transformation [53] for the determination of equi-ripple passband filters with maximum possible peaks in the passband for a given set of transmission or real-axis zeros. Included are tables of critical frequencies and unified design charts for selected filters which are or likely to be of practical interest.

The determination of critical frequencies for filter response functions for which no analytical or quazi-analytical (e.g. Bennett's transformation) relationship exists and which may have practical application. This is achieved using optimization techniques such as those described in the previous chapter.

All quantitative data supplied in this chapter is new. It is expected to be of interest and use to filter designers.

5.2 PROTOTYPE CHARACTERISTICS OF NON-EQUI-RIPPLE QUAZI-ELLIPTIC RESPONSE FILTERS

The synthesis and realization of filters exhibiting equi-ripple characteristics in both passband and stopband is well established for lumped circuitry and coupled structures. However, the realization of such filters in waveguide structures has been relatively recent. The primary reason for this was the difficulty in realizing negative coupling in coupled waveguide structures. This development also helped evolve the functions that exhibit non-equi-ripple characteristics in both passband and stopband in the realization of higher order ($\geq$ fourth order) filters in waveguides. Such non-equi-ripple functions can be realized

by exciting two orthogonal modes in a waveguide cavity or the so-called dual-mode configuration. Such filters generally yield superior response as compared to the presently used filters with Chebyshev response.

Wanselow [19] has provided some prototype characteristics of sixth and eighth-order filters with non-equi-ripple response. The normalization chosen for these characteristics is with respect to an amplitude value that lies on the transition region between the passband and stopband. This makes the usage of these characteristics most inconvenient for practical applications. Filters are normally aligned with respect to the ripples in the passband, since they are easily identified.

In this section, the prototype characteristics of the non-equi-ripple quazi-elliptic function filters are presented in a generalized form. The normalization chosen is with respect to the maximum ripple in the passband. This normalizing frequency,or the cut-off frequency, is computed by numeric techniques. An application of such a filter is discussed and compared to conventional designs, with respect to the requirements of a typical communications satellite channel by Kudsia and Swamy [32].

The characteristic function of filters exhibiting equi-ripple response in both passband and stopband is given by reference [21].

$$K(s) = \frac{F(s)}{P(s)}$$

$$= \varepsilon s \prod_{\mu=1}^{m} \left(\frac{s^2 + a_2^2\mu}{s^2 a_2^2 \mu + 1}\right), \quad \text{for } n \text{ odd and } m = \frac{n-1}{2} \tag{5.1}$$

$$= \varepsilon s^2 \prod_{\mu=2}^{m} \left(\frac{s^2 + c_2^2\mu - 1}{s^2 c_2^2 \mu - 1 + 1}\right), \quad \text{for } n \text{ even and } m = \frac{n}{2} \tag{5.2}$$

The critical frequencies a_ν and c_ν are given by

$$c_\nu = \sqrt{a_{\nu-1} \cdot a_{\nu+1}} \tag{5.3}$$

$$a_\nu = \sqrt{\sin\theta}.\mathrm{sn}\left(\frac{\nu}{n} \cdot K, \theta\right), \nu = 1, 2, \ldots \tag{5.4}$$

where

$\mathrm{sn}(\frac{\nu}{n} \cdot K, \theta)$ is the Jacobian elliptic function

K is the complete integral of the first kind with modulus $\sin\theta$,

n is the order of the filter

ε is the ripple factor,

and

s is the complex frequency variable.

Letting $a_{2m} = 0$ for odd n or $c_{2m-1} = 0$ for even n reduces the number of transmission zeros by 1. The order of the numerator polynomial of K(s) is unaffected and hence, that of the filter network. However, the passband, as well as the stopband of the response, is rendered non-equi-ripple. Thus, by letting one or more of the critical frequencies to be zero, a new class of filters, sometimes referred to as quasi-elliptic filters, is obtained. The generalized form of the analytic relationships for these filters is described in Tables 5.1 and 5.2. p is an integer that determines the depletion of the transmission zeros from the equi-ripple case, giving rise to the new class of elliptic function filters. Our preferred classification is shown in Table 5. 3.

Figure 5.1 describes the lowpass prototype response of an eighth-order, Class 1 elliptic filter. The cutoff frequency, with respect to the maximum ripple in the passband, is determined by numeric technique. Normalization of the frequencies corresponding to the attenuation minima in the stopband is with respect to this cutoff frequency.

Figures 5.2 and 5.3 describe the unified design charts for Class 1, non-equi-ripple elliptic filters. Tables A.1 to A.5 provide the unified design chart data for non-equi-ripple elliptic function (Class 1) filters in Appendix A.

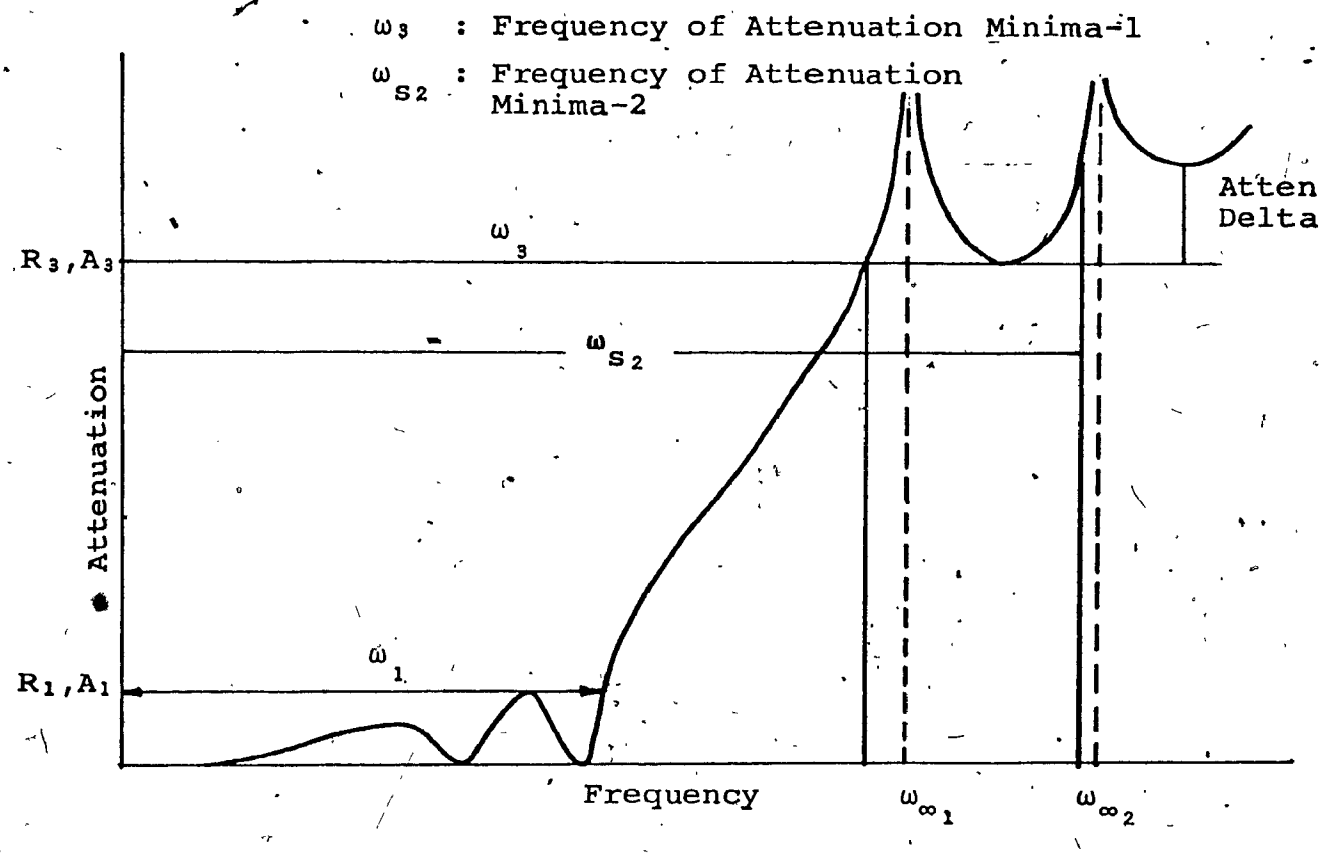

FIG.5.1 LOW-PASS PROTOTYPE RESPONSE OF AN EIGHTH-ORDER CLASS I ELLIPTIC FILTER

TABLE 5.1

ODD ORDER NON EQUI-RIPPLE ELLIPTIC FUNCTION FILTERS

n = Order of Filters
m = (n-1)/2
p = m-1 - number of transmission zeros for the lp prototype filter

Normalization is with respect to maximum ripple in the passband

$$K(s) = \varepsilon_q s^{(1+2p)} \prod_{\nu=1}^{m-p} \frac{(s^2+a_{\nu q}^2)}{(s^2+b_{\nu q}^2)}$$

$$a_{\nu q} = \frac{g_{2\nu}}{g_c}$$

$$b_{\nu q} = \frac{(1/a_{\nu q})}{g_c^2}$$

g_c = the cutoff frequency with respect to the maximum ripple in the passband

$$g_\nu = \sqrt{\sin\theta} \cdot \sin\left(\frac{\nu}{n-2p} \cdot K;\theta\right)$$

θ = the modular angle

K = the complete elliptic integral of the first kind

$sn(\ )$ = the Jacobian elliptic function of the first kind

TABLE 5.2

EVEN ORDER NON EQUI-RIPPLE ELLIPTIC FUNCTION FILTERS

n = Order of Filter
m = n/2
p = m-1 - number of transmission zeros for the lp prototype filter

Normalization is with respect to maximum ripple in the passband

$$K(s) = \varepsilon_q s^{2(1+p)} \prod_{\nu=2}^{m-p} \frac{(s^2+a_{\nu q}^2)}{(s^2+b_{\nu q}^2)}$$

$$a_{\nu q} = \sqrt{g_{2\nu-2} \cdot \frac{g_{2\nu}}{g_c}}$$

$$b_{\nu q} = \frac{(1/a_{\nu q})}{g_c^2}$$

g_c = the cutoff frequency with respect to the maximum ripple in the passband

$$g_\nu = \sqrt{\sin\theta} \cdot sn\left(\frac{\nu K}{n-2P}; \theta\right)$$

θ = the modular angle

K = the complete elliptic integral of the first kind

$sn(\ )$ = the Jacobian elliptic function of the first kind

TABLE 5.3

CLASSIFICATION OF ELLIPTIC FUNCTION FILTERS

Depletion From Maximum Transmission Zeros p	Number of Transmission Zeros		Classification of the Filter
	Odd n	Even n	
0	$\frac{n-1}{2}$	$\frac{n}{2} - 1$	Class 0, Elliptic-filter (equi-ripple)
1	$\frac{n-1}{2} - 1$	$\frac{n}{2} - 2$	Class I, Elliptic-filter (non-equi-ripple)
2	$\frac{n-1}{2} - 2$	$\frac{n}{2} - 3$	Class II, Elliptic-filter (non-equi-ripple)
and so on			

NOTE: For $p = \frac{n-1}{2}$ for n odd and $p = \frac{n}{2} - 1$ for even n, the characteristic function degenerates, giving rise to a Butterworth type of filter response.

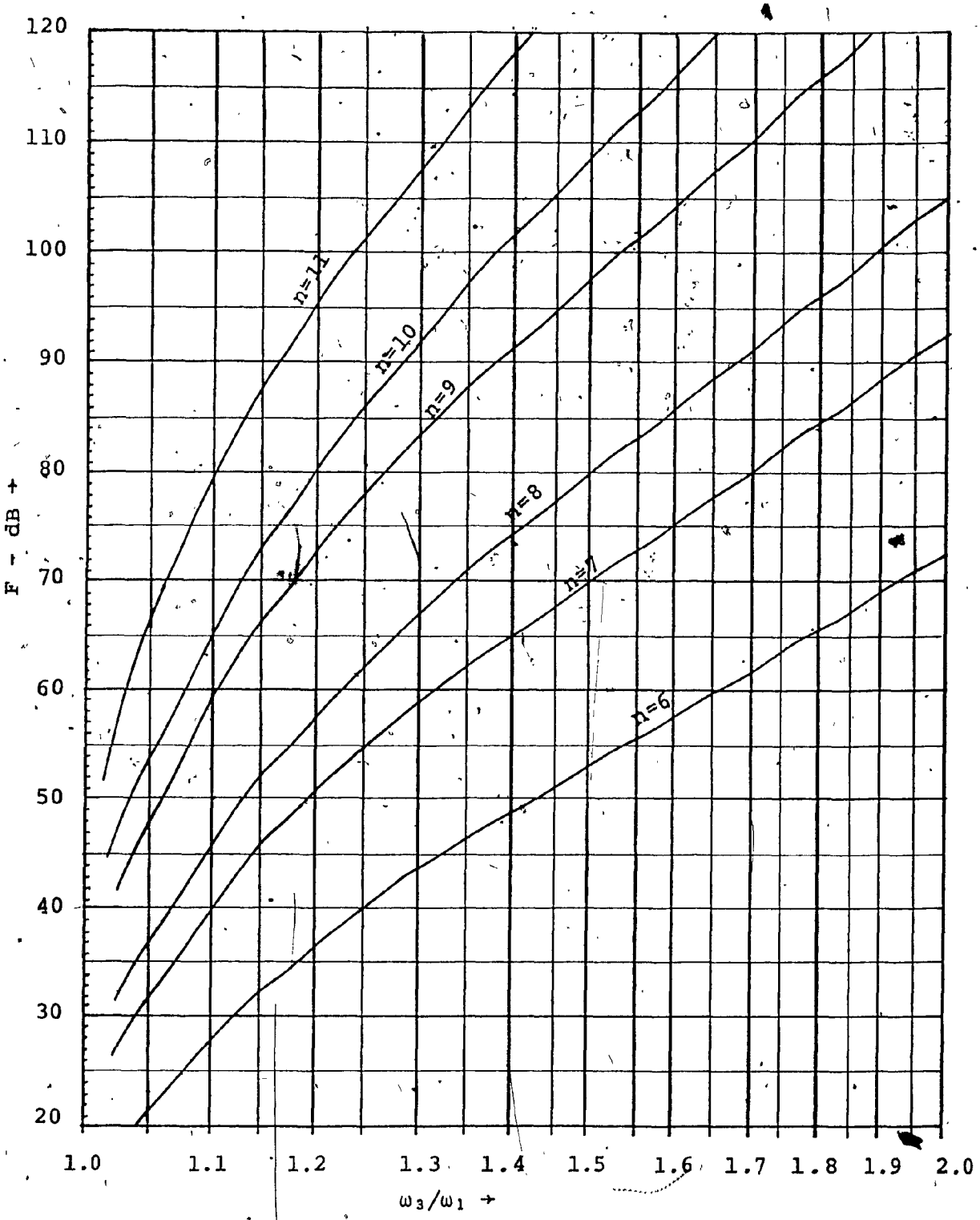

FIG.5.2 UNIFIED DESIGN CHART FOR CLASS-1 ELLIPTIC FUNCTION RESPONSE

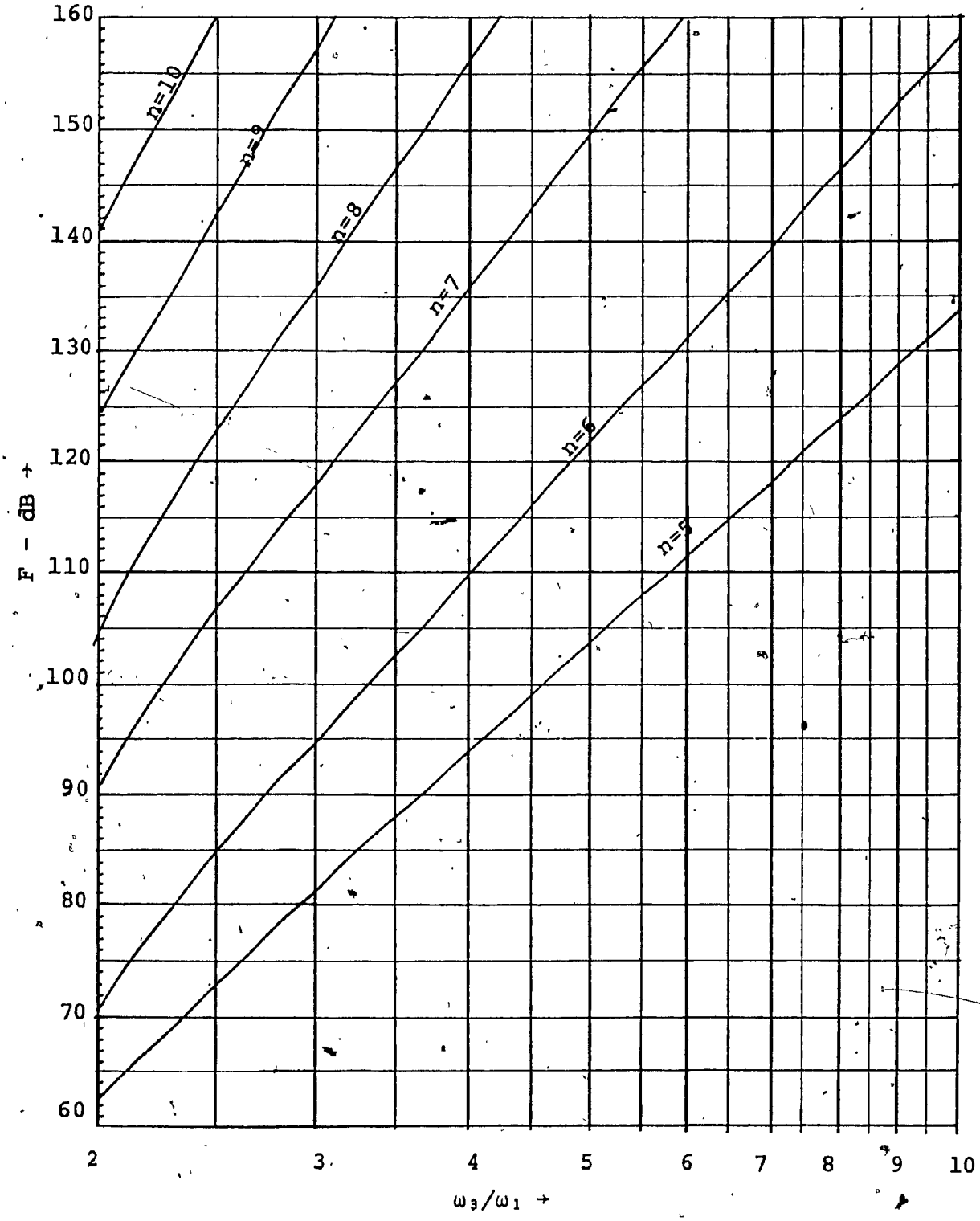

FIG. 5.3 UNIFIED DESIGN CHART FOR CLASS-1 ELLIPTIC FUNCTION RESPONSE

5.3 EQUI-RIPPLE PASSBAND FILTERS USING BENNETT'S TRANSFORMATION

It has been the author's experience that design engineers at large are not acquainted with the Bennett transformation [53] for filter design. The likely reason is that closed form analytical relationships are available for most filter response functions of practical interest. Recent advances in the realization of response functions exhibiting transmission zeros or real-axis zeros or both in coupled waveguide structures has lent fresh interest in Bennett's transformation. It can be used to determine prototype characteristics of filter networks for which no analytical relationships exist, or if they exist, they are in an incomprehensible form for practicing engineers.

The basic form of this transformation is given by [23]

$$Z^2 = 1 + \frac{1}{s^2} \quad ; \text{Re } (Z) \geq 0 \qquad (5.5)$$

where

Z is a new complex variable, and

s is the usual complex frequency variable

This transforms the passband ($s = j\omega, |\omega| < 1$) onto the imaginary axis (jy-axis) of the Z-plane and the stopband ($s=j\omega, |\omega| > 1$) onto the $0 < x < 1$ portion of the real x-axis.

If Z_i represents the transmission zeros (loss poles) at $\pm j\omega_i$ or real-axis zeros at $\pm \sigma_i$, then we may write

$$V(Z^2) + Z\,Q(Z^2) = \prod_{i=1}^{n} (Z + Z_i) \qquad (5.6)$$

where

V and Q are even polynomials, V is even and ZQ is an odd part of the overall expression.

Transmission zeros at infinity are represented by $Z = \pm 1$. The characteristic function $K(s)$ in the transformed variable can then be written in the form

$$K(Z) = \frac{1}{1 - (\frac{ZQ}{V})^2} \qquad (5.7)$$

In the transformed passband, i.e., on the jy-axis, ZQ/V behaves as a reactance since ZQ and V are the odd and even parts, respectively, of the Hurwitz polynomial V + ZQ. Consequently, $1 - (\frac{ZQ}{V})^2$ varies between 1 (when $y\,Q/V = 0$) and ∞ (when $y\,Q/V \to \infty$); and therefore $|K|^2$ oscillates between 0 and 1 (or an arbitrary constant ε). $|K|^2$ has therefore the required poles and an equi-ripple passband. By substituting back $Z^2 = 1 + s^{-2}$, the s-plane characteristic function can be obtained. In essence, therefore,

$$|K(s)|^2 = |K(Z)|^2_{Z^2 = 1+\bar{s}^{-2}} = \left[\frac{V}{V^2 - (ZQ)^2}\right]_{Z^2 = 1+\bar{s}^{-2}}$$

$$\equiv \frac{|F(s)|^2}{|P(s)|^2} \qquad (5.8)$$

where the polynomial F(s) contains the attenuation zeros and P(s) the attenuation poles (or real-axis zeros) as described in Chapter II. Since we start by assuming a given location of loss poles or real-axis zeros, all we have to determine are the roots of

$$V^2\Big|_{Z^2 = 1+\bar{s}^{-2}} = 0 \qquad (5.9)$$

which yields the attenuation zeros of the overall transfer function.

A simple algorithm to determine the attenuation zeros is

$$V(Z) = a_0 + a_1 Z^2 + a_2 Z^4 + \ldots . \qquad (5.10)$$

substituting $Z^2 = 1+\bar{s}^{-2}$

$$V(s) = a_0 + a_1(1+\bar{s}^{-2}) + a^2) + (1+\bar{s}^{-2})^2 + \ldots$$

$$= b_0 + b_1\bar{s}^{-2} + b_2\bar{s}^{-4} + \ldots . \qquad (5.11)$$

where

$$b_0 = a_0 + a_1 + a_2 + \ldots$$

$$b_1 = a_1 + a_2{}^2C_1 + a_3{}^3C_1 + \ldots$$

$$b_2 = a_2 + a_3{}^3C_2 + a_4{}^4C_2 + \ldots$$

$$b_n = a_n$$

n is the last coefficient of polynomial V.

This algorithm has been implemented on a digital computer with efficient results. This program is used to generate the critical frequencies and the unified design charts for those classes of filter functions which are of current interest or have potential application for communications systems of the future. These include:

- Filter response functions exhibiting maximum permissible equi-ripple peaks in the passband and a single transmission zero in the stopband.
- Linear Phase Filter functions with a single or double pair of real-axis zeros with or without a transmission zero in the stopband.

Tables B.1 to B.9 provide the critical frequencies and the unified design chart data for filters of practical interest in Appendix B.

Figure 5.4 describes the unified design chart for filters with a single transmission zero.

Figures 5.5 to 5.8 describe the unified design charts for linear phase filters with one and two pairs of real-axis zeros.

5.4 RESPONSE FUNCTIONS USING OPTIMIZATION TECHNIQUES

Three different filter types of practical interest are identified for the use of optimization techniques to generate the critical frequencies and the unified design chart relationships. These are:

- Eighth order filter with two transmission zeros in the stopband exhibiting equi-ripple response in the passband, as well as stopband.
- Eighth order filter with two transmission zeros in the stopband exhibiting maximum permissible equi-ripple peaks in passband and a 10 dB difference in the attenuation minima in the stopband.
- Eighth order filter with two transmission zeros in the stopband, a double attenuation zero at origin and equi-ripple pass and stopbands.

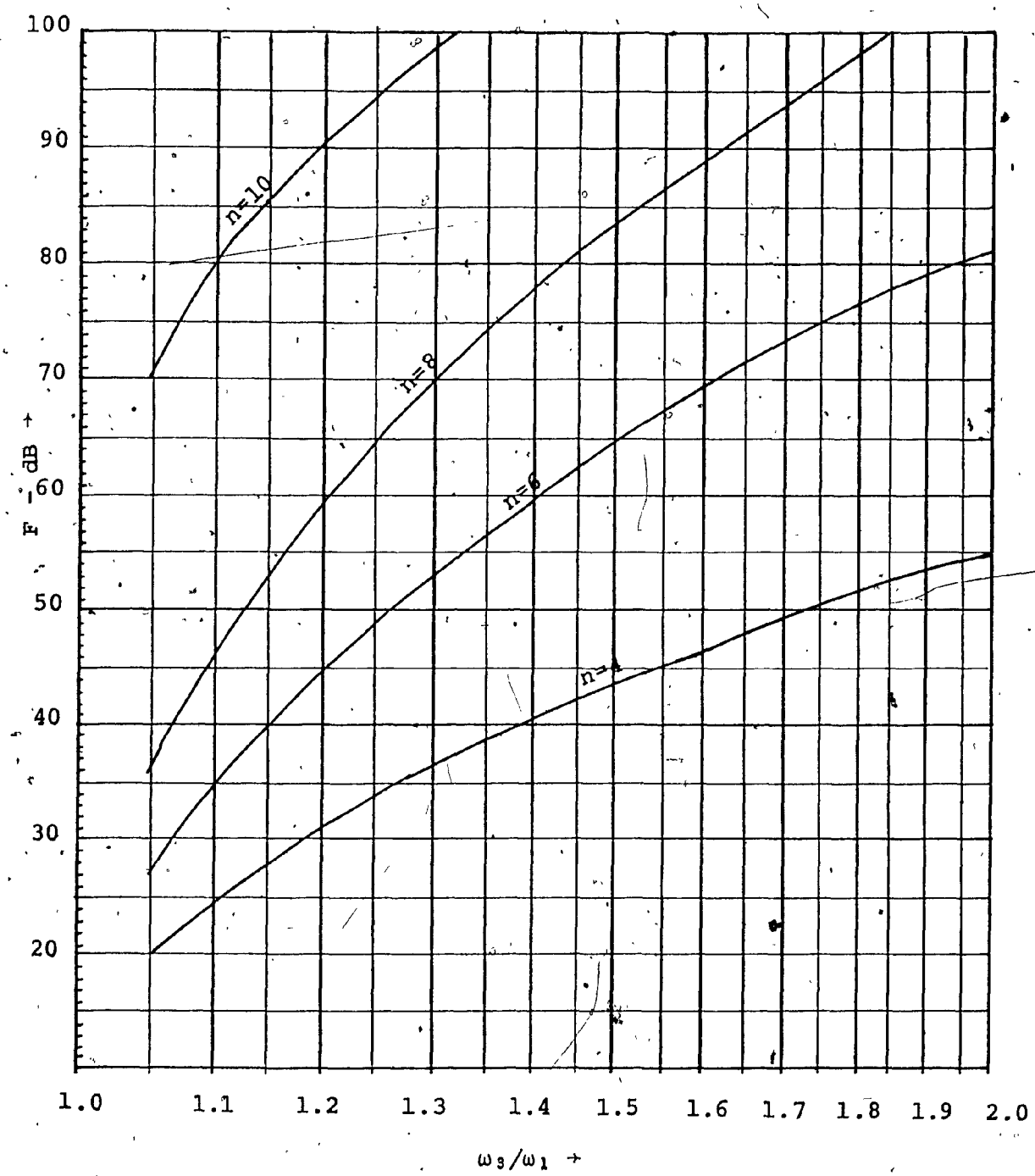

FIG. 5.4 UNIFIED DESIGN CHART FOR FILTERS WITH MAXIMUM EQUI-RIPPLE PEAKS IN PASS-BAND AND A SINGLE PAIR OF TRANSMISSION ZEROS

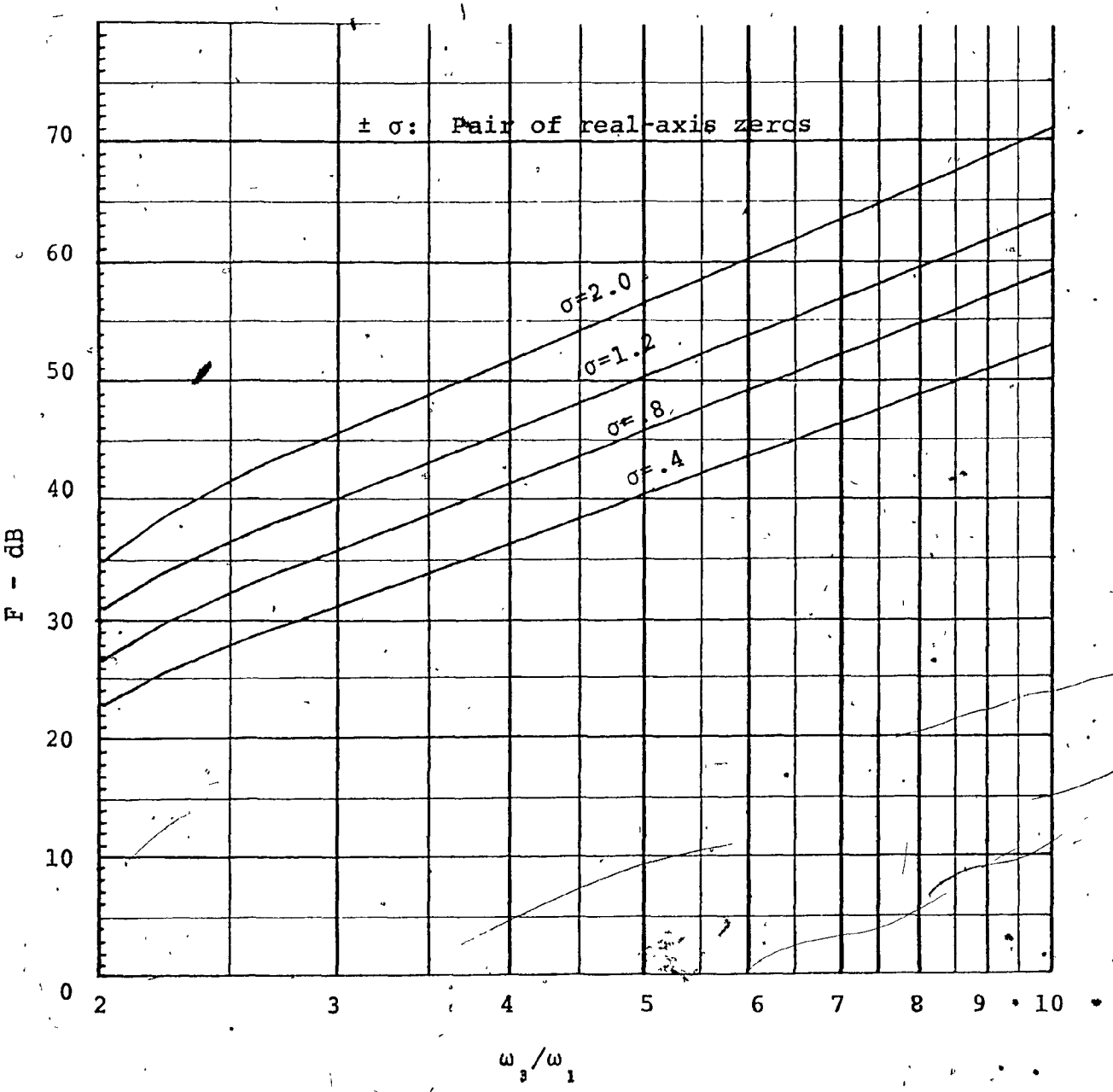

FIG. 5.5 UNIFIED DESIGN CHART FOR A 4-POLE FILTER WITH FOUR EQUI-RIPPLE PEAKS IN PASS-BAND AND A SINGLE PAIR OF REAL-AXIS ZEROS

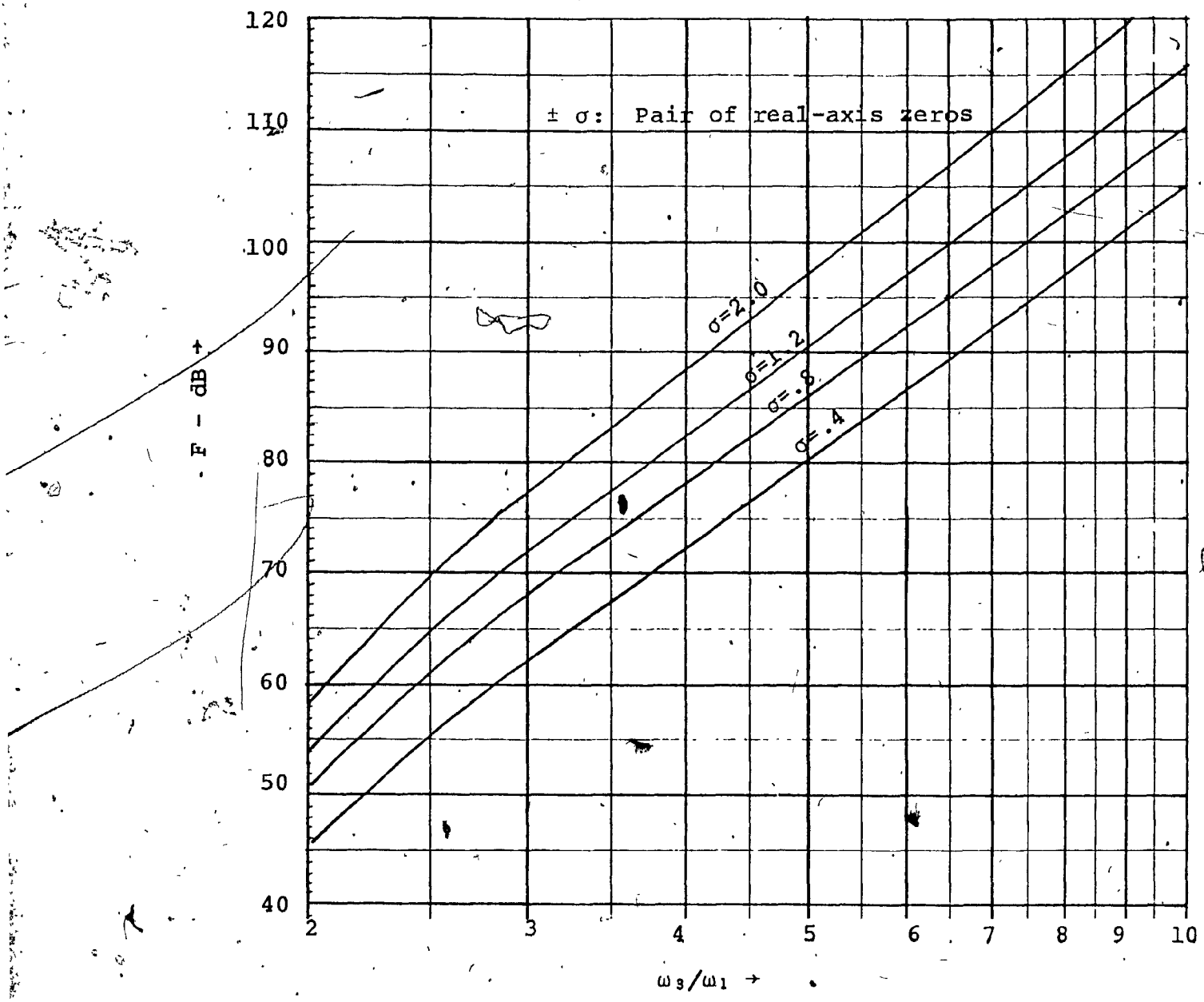

FIG.5.6 UNIFIED DESIGN CHART FOR A 6-POLE FILTER WITH SIX EQUI-RIPPLE PEAKS IN PASS-BAND AND A SINGLE PAIR OF REAL-AXIS ZEROS

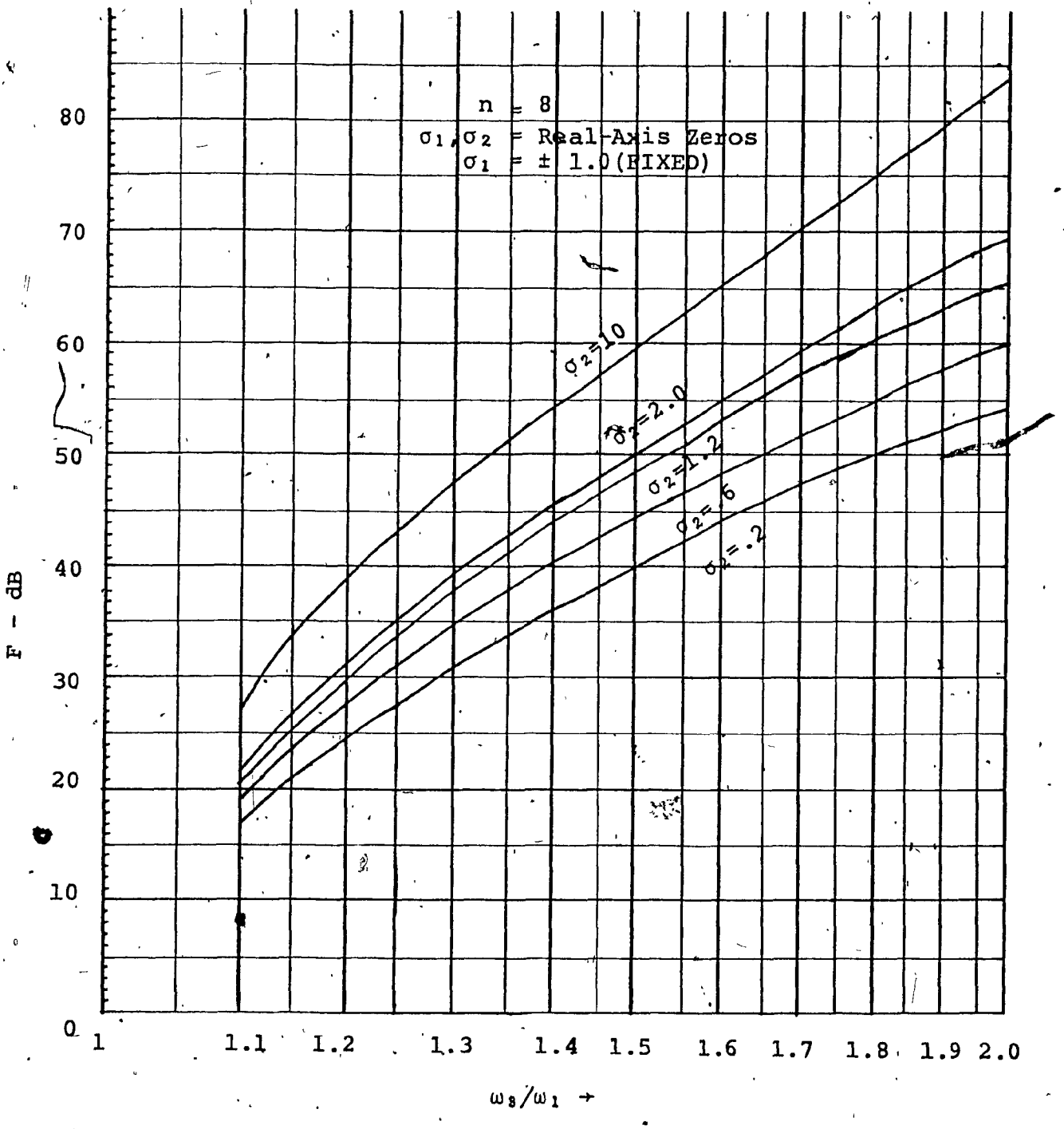

FIG.5.7(a) UNIFIED DESIGN CHARTS FOR AN 8-POLE FILTER WITH EIGHT EQUI-RIPPLE PEAKS IN PASS-BAND AND TWO PAIRS OF REAL-AXIS ZEROS

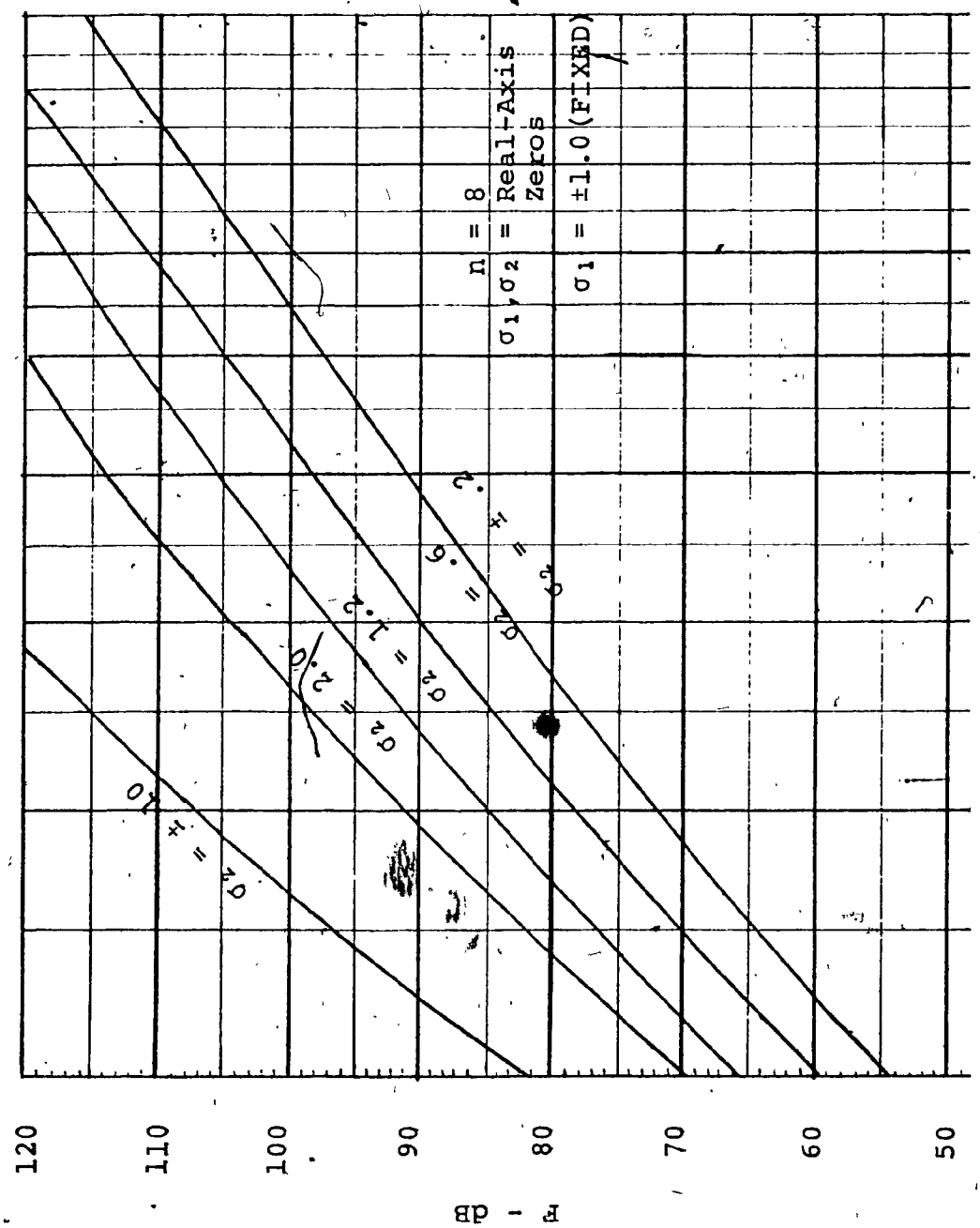

FIG. 5.7(b) UNIFIED DESIGN CHARTS FOR AN 8-POLE FILTER WITH EIGHT EQUI-RIPPLE PEAKS IN PASS-BAND AND TWO PAIRS OF REAL-AXIS ZEROS

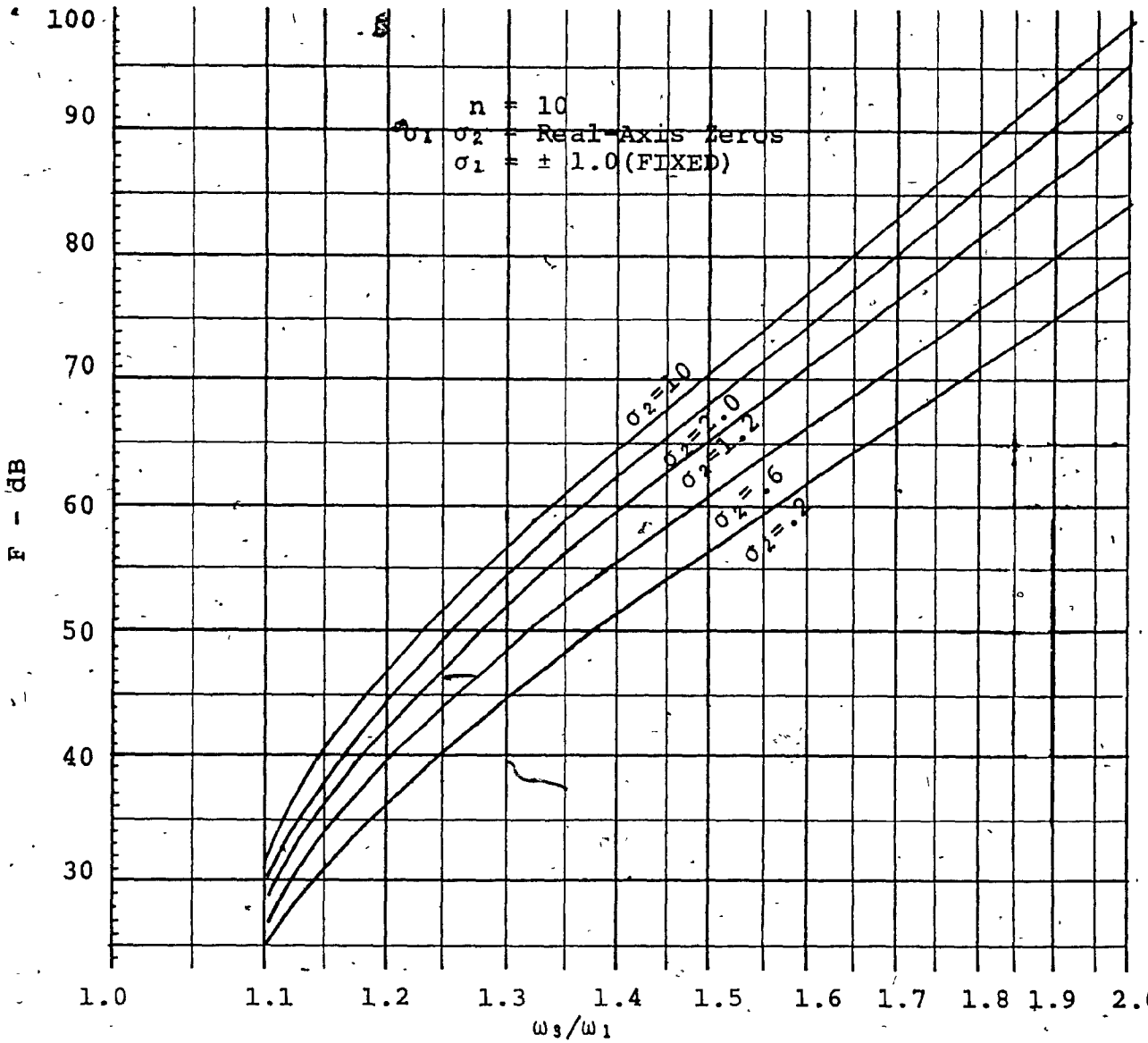

FIG. 5.8 UNIFIED DESIGN CHARTS FOR A 10-POLE FILTER WITH TEN EQUI-RIPPLE PEAKS IN PASS-BAND AND TWO PARIS OF REAL-AXIS ZEROS

This data is of practical interest for dual-mode realization of microwave filters and gives a measure of the efficiency and flexibility of the optimization program.

Tables 5.4 to 5.6 provide the critical frequencies and the unified design chart data. A similar procedure can be used to generate critical frequencies for filters of any order and arbitrary amplitude response shape, as described in this and the last chapter.

5.5 CONCLUSION

From the design data of some new types of filters provided in this chapter, it can be seen that filters with maximum permissible equi-ripple peaks in the pass-band and an equi-ripple stop-band provide the sharpest cut-off characteristics. Making the stop-band non-equi-ripple improves the pass-band performance at the expense of decreased selectivity. Introducing attenuation zeros at the origin further improves the pass-band at the expense of still decreased selectivity. Thus, for a given order of filters, one can derive practical performance trade-offs by manipulating the response function in an arbitrary manner. This is exemplified in Figures 5.9 and 5.10, which show the computed amplitude and group delay response for a 0.5% band-width 8-pole band-pass filter at 12 GHz for the three alternative response functions with one

TABLE 5.4 CRITICAL FREQUENCIES AND UNIFIED DESIGN CHART DATA FOR AN 8-POLE FILTER WITH TWO TRANSMISSION ZEROS AND EQUI-RIPPLE PASS AND STOP-BANDS

$$K(s) = \frac{(s^2+a_1^2)(s^2+a_2^2)(s^2+a_3^2)(s^2+a_4^2)}{(s^2+b_1^2)(s^2+b_2^2)}$$

a_1	a_2	a_3	a_4	b_1	b_2	b_S	F
.2901	.7414	.9433	.9956	1.0302	1.0971	1.0255	40
.2790	.7203	.9322	.9943	1.0466	1.1299	1.0404	45
.2690	.7013	.9218	.9931	1.0675	1.1678	1.0596	50
.2599	.6838	.9119	.9919	1.0938	1.2123	1.0840	55
.2518	.6683	.9028	.9907	1.1251	1.2624	1.1135	60
.2445	.6541	.8943	.9896	1.1634	1.3209	1.1497	65
.2382	.6417	.8868	.9886	1.2068	1.3850	1.1911	70
.2277	.6212	.8741	.9868	1.3123	1.5946	1.2921	80
.2196	.6050	.8638	.9854	1.4487	1.7209	1.4235	90
.2135	.5930	.8561	.9843	1.6128	1.9394	1.5822	100

F : Characteristic Factor in dB

TABLE 5.5 CRITICAL FREQUENCIES AND UNIFIED DESIGN CHARTS DATA FOR AN 8-POLE FILTER HAVING TWO TRANSMISSION ZEROS WITH 10 dB DIFFERENCE IN ATTENUATION MINIMA AND AN EQUI-RIPPLE PASS-BAND

$$K(s) = \frac{(s^2+a_1^2)(s^2+a_2^2)(s^2+a_3^2)(s^2+a_4^2)}{(s^2+b_1^2)(s^2+b_2^2)}$$

a_1	a_2	a_3	a_4	b_1	b_2	b_s	F
.2072	.7049	.9255	.9938	1.0460	1.2070	1.0384	40
.2618	.6885	.9159	.9925	1.0664	1.2514	1.0568	45
.2539	.6732	.9067	.9913	1.0914	1.3037	1.0802	50
.2403	.6464	.8903	.9891	1.1601	1.4321	1.1437	60
.2295	.6250	.8768	.9873	1.2520	1.5911	1.2306	70
.2210	.6081	.8660	.9857	1.3719	1.7876	1.3449	80
.2147	.5954	.8577	.9846	1.5192	2.0186	1.4860	90
.2099	.5857	.8514	.9837	1.6972	2.2901	1.6572	100

F : Characteristic Factor in dB

TABLE 5.6 CRITICAL FREQUENCIES AND UNIFIED DESIGN CHART DATA FOR AN 8-POLE FILTER WITH A DOUBLE ZERO AT THE ORIGIN, TWO TRANSMISSION ZEROS AND EQUI-RIPPLE PASS AND STOP-BANDS

$$K(s) = \frac{S^4 (s^2+a_1^2)(s^2+a_2^2)}{(s^2+b_1^2)(s^2+b_2^2)}$$

a_1	a_2	b_1	b_2	F
.9012	.9926	1.0501	1.1566	40
.8871	.9909	1.0734	1.1990	45
.8742	.9893	1.1023	1.2473	50
.8628	.9878	1.1364	1.3011	55
.8522	.9863	1.1774	1.3626	60
.8429	.9851	1.2249	1.4315	65
.8347	.9839	1.2788	1.5074	70
.8213	.9820	1.4057	1.6807	80
.8109	.9804	1.5640	1.8911	90
.8029	.9793	1.7571	2.1430	100

F : Characteristic Factor in dB

pair of transmission zeros and having 8,7 and 5 equi-ripple peaks in the pass-band.

In conclusion, then, we claim that by using the analytic expression for gradients and optimization techniques described in this and the last chapter, filters with completely arbitrary response shape can be derived most efficiently. This provides a powerful tool to filter designers and system engineers involved in the optimization of communication channels.

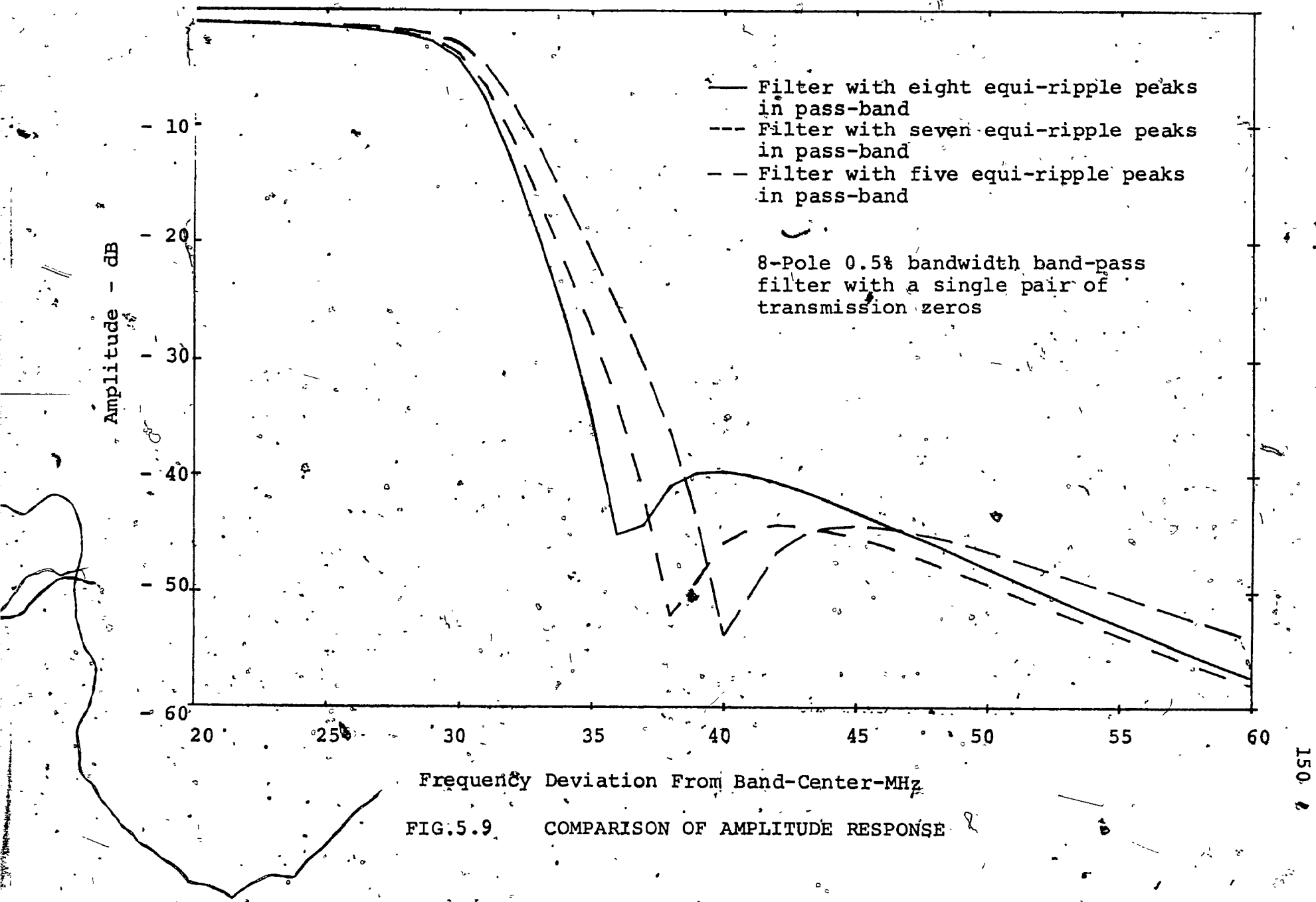

FIG.5.9 COMPARISON OF AMPLITUDE RESPONSE

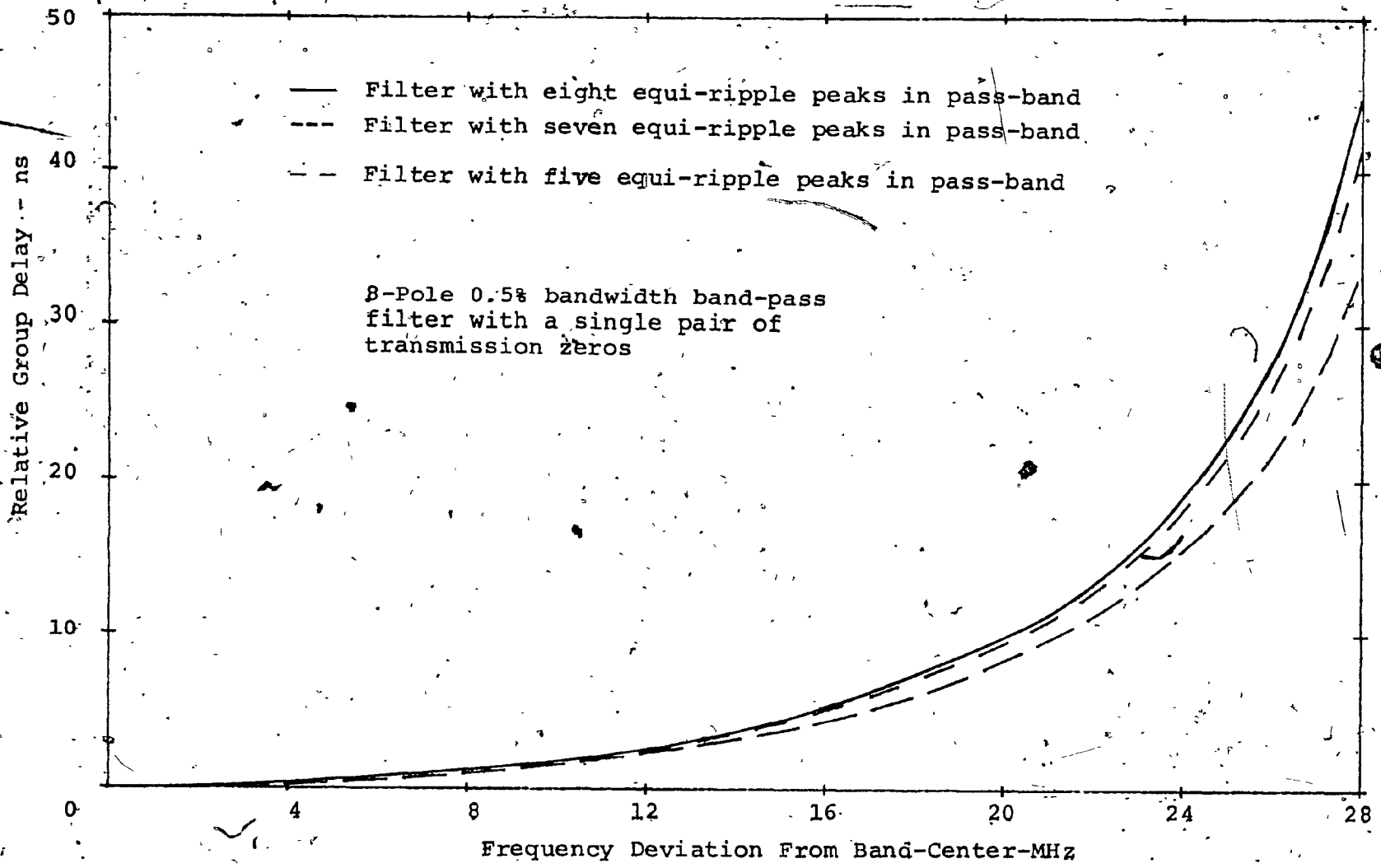

FIG.5.10 COMPARISON OF GROUP DELAY RESPONSE

CHAPTER VI

COUPLED-CAVITY SYNTHESIS OF SYMMETRICAL BAND-PASS FILTERS

CHAPTER VI

COUPLED-CAVITY SYNTHESIS OF SYMMETRICAL BAND-PASS FILTERS

6.1 INTRODUCTION

In this chapter, we shall describe the synthesis of waveguide band-pass filter networks at microwave frequencies from their low-pass prototype network in a dual-mode configuration. It includes:

- A brief description of the relationship between the pole-zero frequencies of the low-pass prototype network and the eigenvalues of the generalized coupling matrix of a coupled-cavity structure excited in orthogonal modes.
- A new technique to determine and optimize the available mutual couplings from these eigenvalues to realize the desired response function.
- A brief description of the relationships between the mutual-couplings and the physical dimensions of the dual-mode waveguide band-pass filters.

.. Measured versus computed response for the following filters:

.. Sixth-order filter with six equi-ripple peaks in pass-band and a transmission zero located symmetrically on either side of the pass-band in the 11 GHz frequency band.

.. Eighth-order filter with eight equi-ripple peaks in pass-band, a single pair of transmission zeros located symmetrically on either side of the pass-band followed by a two-pole all-pass network in the 11 GHz frequency band.

.. Tenth-order linear phase filter with ten equi-ripple peaks in pass-band and having two pairs of real-axis zeros for linearization of phase.

All filters are realized in a dual-mode configuration..

6.2 EIGENVALUES OF A NARROW-BAND COUPLED-CAVITY FILTER NETWORK

More than two decades ago, Cohn [1] in his classic paper, described the realization of half-wave direct-coupled cavity waveguide filters from the conventional minimum phase

low-pass prototype network. The basic concept introduced in this paper was the close relationship between an ideal immittance inverter and a shunt inductive iris embedded in a small negative length of waveguide. In the physical realization, the negative length associated with the coupling iris is taken care of by the equivalent shortening of the resonant waveguide cavity. Cohn has demonstrated that the fractional bandwidths of up to 20% could be readily obtained in the synchronously tuned filter. This procedure is still the basis in realizing the more general filter characteristics.

For a simple cascade of coupled cavities [1] where only the adjacent cavities are coupled to each other, only all-pole insertion loss functions can be realized. For more general characteristics, the coupling between the non-adjacent cavities is required. Kurzrok [10] was the first to describe how extra coupling between the first and last cavity of a directly-coupled 4 coaxial-cavity structure produces a zero of transmission. Easter and Powell [54] have described similar filters in the rectangular waveguide. Saito [55] has presented a synthesis procedure for general coupled-resonator transmission networks. It involves a large number of couplings and therefore, is not very practical. Rhodes [47] has described a synthesis

procedure for generalized inter-digital networks and direct-coupled cavity linear phase filters. More recently, Atia et al. [13,14,56] have described a synthesis procedure for synchronously tuned coupled cavities with multiple couplings in a non-cascaded form. This procedure is being widely used for the realization of microwave filters in a dual-mode configuration, and is followed, in part, in this thesis. The following is a brief description of the determination of eigenvalues for the generalized symmetric coupling matrix, as described in Reference [56].

Figure 6.1 shows the n-loop equivalent circuit for a multiply-coupled structure of synchronously tuned cavities. The cavities are assumed identical, all tuned to the normalized center frequency $\omega_0 = 1/\sqrt{LC} = 1$, with a normalized characteristic impedance $Z_o = \sqrt{L/C} = 1$. Further, upon using the narrow-band approximation, the cavities are represented by their lumped element representation. The $n \times n$ symmetric coupling impedance matrix jM has zero diagonal entries and arbitrary signs on other entries. It is purely imaginary and frequency independent for frequencies near ω_0. The coupling coefficient between the $i^{\underline{th}}$ and $j^{\underline{th}}$ cavities is denoted by M_{ij} which are real numbers and assumed independent of frequency. Further, we will denote the source and load impedances by R_S and R_L which are assumed purely resistive.

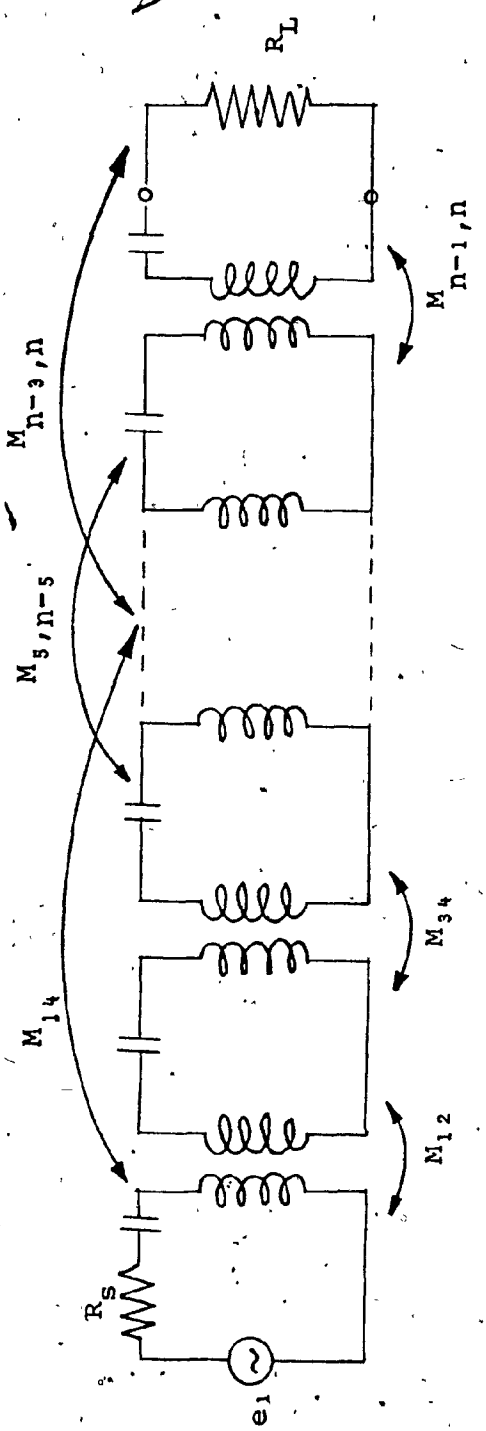

FIG.6.1 EQUIVALENT CIRCUIT OF COUPLED-CAVITY BAND-PASS FILTER

The loop equations can be written as:

$$[R_s \delta_{1i} + R_L \delta_{ni} + S] I_i + j \sum_{\substack{k=1 \\ k \neq 1}}^{n} M_{ik} I_k = e_1 \delta_{1i} \qquad (6.1)$$

$$i = 1, 2, 3, \ldots n$$

where

δ_{ij} is the Kronecker delta

e_1 is the input voltage, and

S is the band-pass frequency variable given by $S = s + 1/s$, $s = j\omega$

Equation (6.1) can be put into the matrix form

$$[-jSI - jR + M] \begin{bmatrix} I_1 \\ I_2 \\ \vdots \\ I_n \end{bmatrix} = -je_1 \begin{bmatrix} 1 \\ 0 \\ 0 \\ \vdots \\ 0 \end{bmatrix} \qquad (6.2)$$

where

I is the identity matrix and

$$R = \begin{bmatrix} R_s & 0 & 0 & . & . & . \\ 0 & 0 & . & . & . & . \\ 0 & 0 & . & . & . & . \\ . & . & . & . & . & R_L \end{bmatrix} \qquad (6.3)$$

$$M = \begin{bmatrix} 0 & M_{12} & 0 & M_{14} & \cdots & M_{1n} \\ M_{21} & 0 & M_{23} & 0 & \cdots & 0 \\ & & \vdots & & & \\ M_{n1} & 0 & M_{n3} & 0 & \cdots & 0 \end{bmatrix} \quad (6.4)$$

M is a real symmetric matrix with $M_{ij} = M_{ji}$. The transfer voltage ratio $I_n R_L/e_1$ can be determined by solving the system of equations given by equation (6.2). It is the quotient of polynomials in S with denominator as the $n^{\underline{th}}$ order Hurwitz polynomial equal to the determinant of the matrix $(-jSI - jR + M)$.

In terms of the two-port short-circuit admittance parameters 'y' [19,30] as shown in Figure 6.2

$$\begin{aligned} I_1 &= y_{11}V_1 + y_{21}V_2 \\ I_2 &= y_{21}V_1 + y_{22}V_2 \end{aligned} \quad (6.5)$$

and y's can be deduced as

$$y_{11}(S) = -j[(-jSI + M)^{-1}]_{11} \quad (6.6)$$

and

$$y_{21}(S) = -j[(-jSI + M)^{-1}]_{21} \quad (6.7)$$

by solving (6.2) with $R_s = R_L = 0$ and $e_1 = 1$.

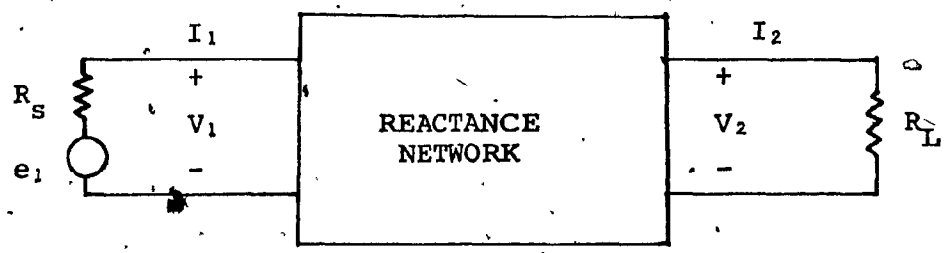

FIG. 6.2 TWO PORT EQUIVALENT CIRCUIT FOR DOUBLY-TERMINATED FILTER NETWORKS

These equations reveal that the denominator of both y_{11} and y_{21} is the characteristic polynomial of the matrix, -M. Since M is real symmetric, all its eigenvalues are real and it can be reduced to a diagonal matrix of the eigenvalues.

A two-port network can have four alternative representations [19,57], two on the impedance basis and the other two on the admittance basis. Choosing the latter, the short-circuit admittance parameters are related to the characteristic polynomials by

$$y_{11} = \frac{E_o - F_o}{E_e + F_e} \tag{6.8}$$

and

$$y_{21} = \frac{jP}{E_e + F_e} \tag{6.9}$$

where the subscripts o and e stand for the odd and even parts respectively, of the indicated polynomial. Thus, the eigenvalues of the symmetric coupling matrix M are given by

$$E_e + F_e = 0 \tag{6.10}$$

and are of the form

$$j\lambda_i \quad i = 1,2,3, \ldots$$

Atia and Williams [13] have shown that the symmetric coupling matrix 'M' can be represented in a reduced form without loss of generality. This compact form takes advantage of the

symmetry and is defined as the even-mode coupling matrix M_e given by

$$-M_e = \begin{bmatrix} M_{1,n} & M_{1,2} & M_{1,n-2} & M_{1,4} & M_{1,n-4} & \cdots & M_{1,n/2} \\ M_{1,2} & M_{2,n-1} & M_{2,3} & \vdots & \vdots & & \vdots \\ M_{1,n-2} & M_{2,3} & M_{3,n-2} & \vdots & \vdots & & \vdots \\ \vdots & \vdots & \vdots & \vdots & \vdots & & \vdots \\ M_{1,n/2} & & & & & & M_{n/2,(n/2)+1} \end{bmatrix} \quad (6.11)$$

The corresponding even-mode driving point admittance y_e is given by [13]

$$Y_e = \frac{1}{2}[y_{11}+y_{21}] \quad (6.12)$$

The even-mode input admittance may then be expanded in the form

$$y_e(s) = \frac{C_1}{S-j\lambda_1} + \frac{C_2}{S+j\lambda_2} + \frac{C_3}{S-j\lambda_3} + \cdots \quad (6.13)$$

where

$C_1, C_2, C_3, \ldots$ are the residues at the respective eigenvalues.

6.3 CLOSED-FORM RELATIONSHIPS FOR MUTUAL COUPLINGS FROM EIGENVALUES

Atia et al. [14] synthesize the coupling network by first generating a coupling matrix containing all possible couplings from the eigenvalues using the Gram-Schmidt orthonormalization process. Then, they use the reverse process of similarity reduction based on Jacobi's or Given's [68] methods to reduce the undesired couplings to zero. Thus, a symmetric coupling matrix is obtained containing only the available couplings for a given filter structure. It is to be noted that, in general, the coupling matrix to realize a given transfer function is not unique and the available couplings exceed the number of independent variables, as determined by the order of the filter or the eigenvalues of the coupling matrix. This leads to an infinity of solutions for transfer functions with finite zero locations.

The method of Atia et al. [14] involves considerable matrix manipulations and restricts the relationships between the mutual couplings to the criteria used in Jacobi or Given's method of similarity reduction in conjunction with the choice of element values of the orthogonal transformation matrix 'T' in the equation to generate the general coupling matrix. The method described in this section alleviates the above drawbacks but suffers from lack of complete generality. Closed-form relationships for mutual-couplings are derived for 4,6

and 8-pole filters in a dual-mode configuration. This, in the author's view, fulfills the performance requirements of most of the communication systems -- especially the ones involving communications satellites. The method can be extended to odd and higher-order (> $8^{\underline{th}}$ order) filters or to canonical realization [59] of dual-mode networks. This is left as an area for future investigation.

Before deriving these relationships, we shall briefly describe the operation of dual-mode filters.

6.3.1 Dual-Mode Filter Structure

The dual-mode filter is depicted in Figure 6.3. It employs a cascade of waveguide cavities, each of which resonates, synchronously, in two orthogonal modes. These cavities are either square or cylindrical. The modes of propagation that are employed are TE_{110} or TE_{11N} for the square and cylindrical cavities, respectively.

The coupling between the orthogonal modes within the cavities is provided by a structural discontinuity, such as a probe or a screw. This screw is located at an E field anti-node (maximum) and is oriented at a 45^{o} angle between the orthogonal E field vectors, as shown in Figure 6.3.

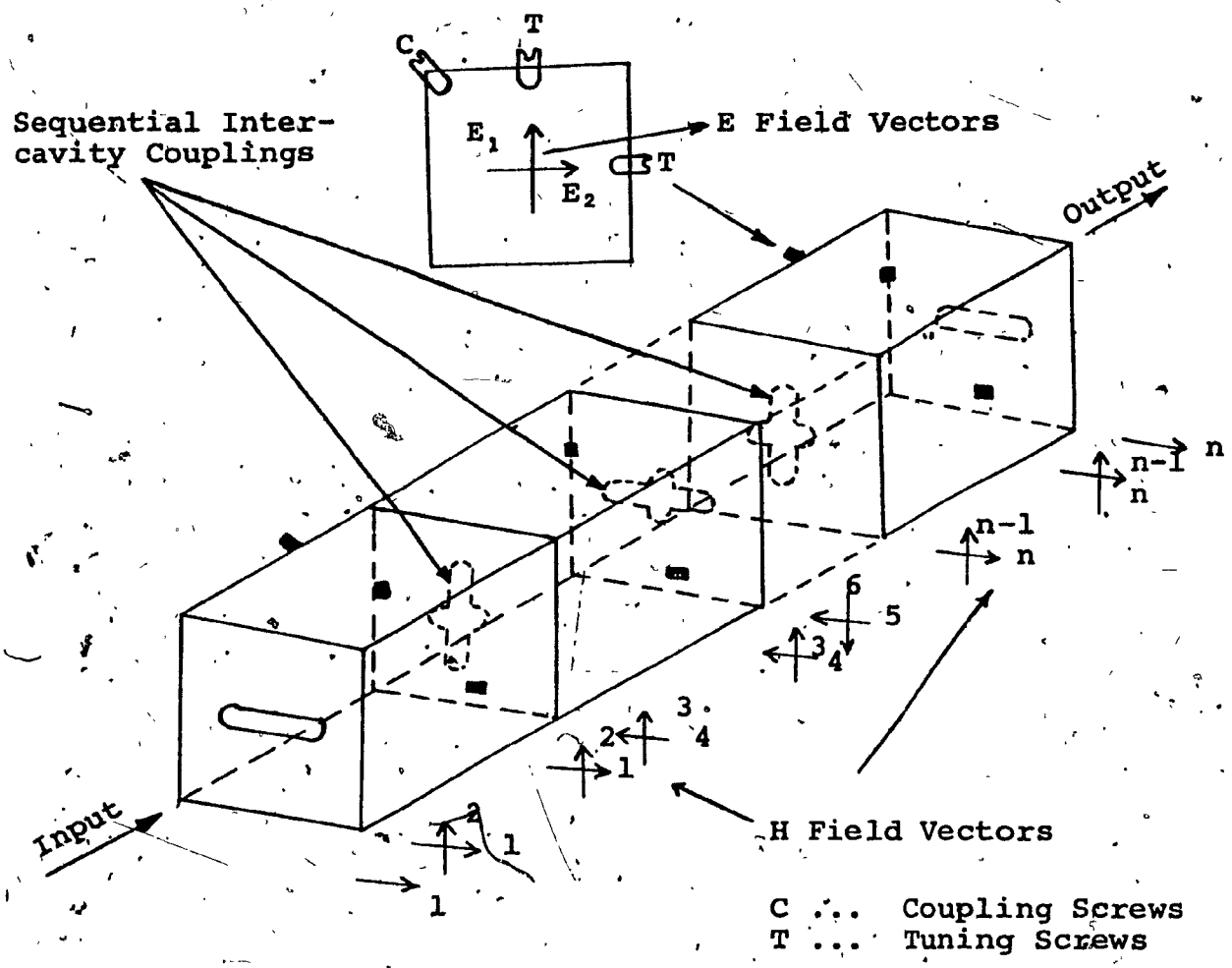

FIG.6.3(a) THE LONGITUDINAL DUAL-MODE STRUCTURE WITH SQUARE CAVITIES

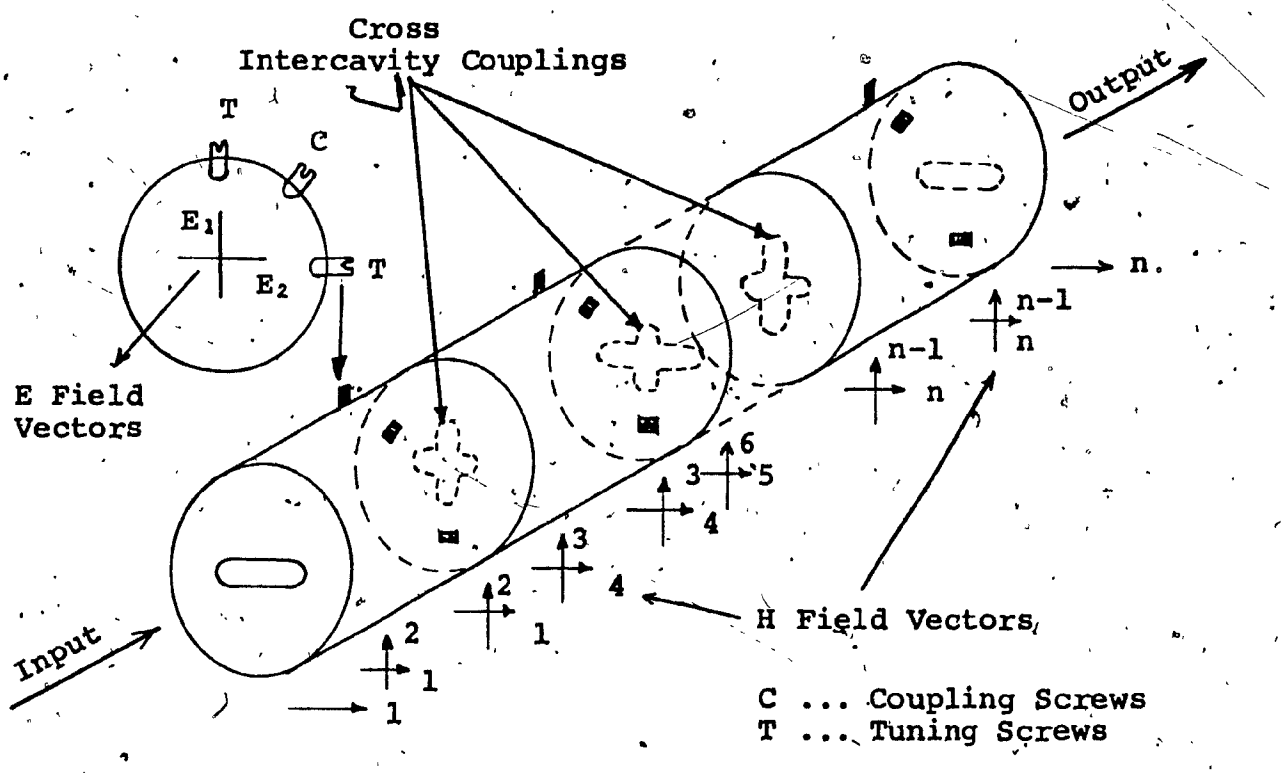

FIG.6.3(b) THE LONGITUDINAL DUAL-MODE STRUCTURE WITH CIRCULAR CAVITIES

Such coupling is called "intracavity" coupling; it is capacitive and couples the E field vectors (1,2), (3,4), (5,6) ... (n-1,n).

Direct coupling between the physical cavities is provided by polarization apertures located at the common walls between the cavities. This coupling is called "intercavity" coupling, and is inductive since it couples the H field vectors of the adjacent cavities. There are two types of intercavity couplings: the "sequential" ones, which couple the H vectors (2,3), (4,5), (6,7), ... (n-2),(n-1), and the "cross" couplings which couple the H vectors (1,4), (3,6), (5,8), ... (n-3,n).

In addition to the 45^{o} coupling screw which provides the intracavity coupling, each cavity is provided with tuning screws, as shown in Figure 6.3. These project into the cavity parallel to each E field vector, and control the frequency of each resonant mode by varying its electrical length.

The filter has n resonances in n/2 physical cavities and hence, the name dual-mode. When the input and output ports of the filter are in line, as shown in Figure 6.3, it is called a longitudinal dual-mode filter. It provides the simplest physical configuration. The relative orientation of its ports depends upon the number of physical cavities

employed. These ports are in phase if the filter has an even number of cavities, and are rotated at a 90^{o} angle, with respect to each other, if the number of cavities is odd.

The all-pole dual-mode filter is realized using the sequential couplings only. Transmission zeros or real-axis zeros require cross-couplings in addition to the sequential couplings. Transmission zeros are normally realized when the H field vectors are 180^{o} out of phase. Such couplings are called 'negative'. These are realized by coupling screws oriented to have 90^{o} phase difference between each other, as shown in Figure 6.3. On the other hand, when the coupling screws are in phase, they create real-axis zeros resulting in linear phase filters.

The longitudinal dual-mode filter, as defined herein, have input and output ports located at the physically first and last cavities. It provides the simplest physical structure. The permissible couplings are:

Sequential Couplings	$M_{12}, M_{23}, M_{34}, \cdots M_{n-1,n}$
Cross Couplings	$M_{14}, M_{36}, M_{58}, \cdots M_{k,k+3}, \cdots M_{n-3,n}$

The available number and type of cross-couplings determine the number of permissible zero locations - be it transmission zeros or real-axis zeros. Table 6.1 enumerates the available cross-couplings and zero locations for even-order dual-mode filters.

6.3.2 Canonical Dual-Mode Filters

Recently, Atia and Williams [59] and Pfitzenmaier [60] described independently the realization of a six-pole elliptic function filter exhibiting two paris of transmission zeros in a dual-mode configuration. This realization is referred to as the canonical dual-mode realization, as it involves the least number of cross-couplings for a given number of zeros of the transfer function. This realization involves a set of couplings different from that of the longitudinal structure, and does not have the input and output ports located at the first and last physical cavity. This makes the configuration more complicated than the longitudinal structure, but offers the realization of the maximum number of zeros, which can be of significant advantage, depending upon the performance requirements of a given system. For even-order filters, the maximum permissible zeros are (n-2) where n is the order of the filter.

TABLE 6.1

NUMBER OF POLES, CROSS COUPLINGS, AND TRANSMISSION ZEROS OF IN-LINE LONGITUDINAL DUAL-MODE FILTERS

Number of Physical Cavities	2	3	4	5	6	7
Number of Poles (n) or Order of Filter	4	6	8	10	12	14
Number of Available Cross Couplings	1	2	3	4	5	6
Number of Independent Cross-Couplings For a Symmetrical Structure	1	1	2	2	3	3
Number of Transmission Zeros for Bandpass Configuration	2	2	4	4	6	6

6.3.3 Closed-Form Relationships of Coupling Parameters for 4,6 and 8-Pole Dual-Mode Filters

(a) Coupling matrix for a 4^{th} order filter.

The symmetric even-mode coupling matrix for a 4-pole dual-mode filter is given by [13]

$$-M_e = \begin{bmatrix} M_{14} & M_{12} \\ M_{12} & M_{23} \end{bmatrix} \qquad (6.14)$$

The characteristic equation of this symmetric matrix is given by

$$[-M_e - \lambda I] = \begin{bmatrix} M_{14}-\lambda & M_{12} \\ M_{12} & M_{23}-\lambda \end{bmatrix} \qquad (6.15)$$

Expanding the determinant, the characteristic polynomial 'P' is obtained as:

$$P = (-M_e - \lambda I)$$

$$= k_0 + k_1\lambda + k_2\lambda^2 \qquad (6.16)$$

where the coefficients k are given by

$$k_0 = M_{14} \cdot M_{23} - M_{12}^2$$

$$k_1 = M_{14} + M_{23} \tag{6.17}$$

On the other hand, if λ_1 and λ_2 are the two eigenvalues of the symmetric even-mode coupling matrix - M_e, then

$$P = (\lambda-\lambda_1)(\lambda-\lambda_2)$$

$$= \lambda^2 - \lambda(\lambda_1+\lambda_2) + \lambda_1\lambda_2 \tag{6.18}$$

Thus, equating the coefficients of λ, we obtain

$$k_0 = \lambda_1\lambda_2 = M_{14}M_{23} - M_{12}^2$$

$$k_1 = -(\lambda_1+\lambda_2) = M_{14} + M_{23} \tag{6.19}$$

There are three available couplings but only two independent variables. This necessitates the determination of any two of the mutual couplings as a function of the remaining one and implies an infinity of solutions. If we assume M_{14} as a variable parameter, then

$$M_{23} = k_1 - M_{14}$$

$$= -(\lambda_1+\lambda_2) - M_{14} \tag{6.20}$$

and

$$M_{12} = \pm \sqrt{M_{14}\, M_{23} - k_0}$$

$$= \pm \sqrt{M_{14}\, M_{23} - \lambda_1 \lambda_2} \qquad (6.21)$$

Thus, the couplings M_{12} and M_{23} are determined, in closed-form, with M_{14} as a parameter. Varying M_{14} so that all couplings values are within the bounds of physical realizability, an infinity of practically realizable solutions can be derived. This also, therefore, provides the basis for optimizing the coupling values so as to obtain the least sensitive network. The coefficients 'k' are referred to by the author as 'characteristic coefficients'.

For all-pole functions

$$M_{14} = 0$$

and hence

$$M_{12} = \pm \sqrt{-k_0} = \pm \sqrt{-\lambda_1 \lambda_2}$$

$$M_{23} = k_1 = -(\lambda_1 + \lambda_2) \qquad (6.22)$$

The couplings are uniquely determined - a result that is identical to the classical synthesis techniques. This also provides an alternative design procedure to the classical techniques of Cohn [1] and others.

(b) Coupling Matrix For Sixth-Order Filters

The generalized even-mode coupling matrix for a symmetrical structure is given by

$$-M_e = \begin{bmatrix} M_{16} & M_{12} & M_{14} \\ M_{12} & M_{25} & M_{23} \\ M_{14} & M_{23} & M_{34} \end{bmatrix} \qquad (6.23)$$

In a manner similar to the one described in the previous section, the characteristic polynomial for this matrix is given by

$$P = |-M_e - \lambda I|$$

$$= k_0 + k_1\lambda + k_2\lambda^2 + k_3\lambda^3 \qquad (6.24)$$

where the characteristic factors k are given by

$$\begin{aligned} k_0 &= M_{16}.M_{25}.M_{34} + 2M_{12}.M_{14}.M_{23} - M_{16}M_{23}^2 - \\ &\quad M_{12}^2M_{34} - M_{14}^2M_{25} \\ k_1 &= M_{12}^2 + M_{23}^2 + M_{14}^2 - M_{16}M_{25} - M_{16}M_{34} - M_{25}M_{34} \\ k_2 &= M_{16} + M_{25} + M_{34} \\ k_3 &= -1 \end{aligned} \qquad (6.25)$$

If λ_1, λ_2 and λ_3 are the three distinct eigenvalues of the symmetric even-mode matrix - M_e, then

$$- P = - (\lambda-\lambda_1)(\lambda-\lambda_2)(\lambda-\lambda_3)$$

$$= - (k_0+k_1\lambda+k_2\lambda^2+k_3\lambda^3) \qquad (6.26)$$

where

$$\begin{aligned} k_0 &= +\lambda_1\lambda_2\lambda_3 \\ k_1 &= -(\lambda_1\lambda_2 + \lambda_2\lambda_3+\lambda_3\lambda_1) \\ k_2 &= +(\lambda_1 + \lambda_2 + \lambda_3) \\ k_3 &= - 1 \end{aligned} \qquad (6.27)$$

There are six distinct couplings and only three independent variables, i.e., distinct eigenvalues. Thus, a general solution is obtained by assuming any three couplings as variable parameters and evaluating the remaining couplings in terms of these parameters. There are three cases of particular interest.

(i) . Filter Structure With No Cross-Couplings

This implies all-pole functions and that

$$M_{16} = M_{25} = M_{14} = 0$$

Therefore,

$$k_2 = M_{34} = \lambda_1 + \lambda_2 + \lambda_3$$
$$k_1 = M_{23}^2 + M_{12}^2 + M_{14}^2 = -(\lambda_1\lambda_2 + \lambda_2\lambda_3 + \lambda_3\lambda_1) \quad (6.28)$$
$$K_0 = 2M_{12}M_{14}M_{23} - M_{12}^2 M_{34} = \lambda_1\lambda_2\lambda_3$$

Couplings are determined uniquely as expected.

(ii) Filter Structure With One Cross-Coupling

For this configuration, we shall assume a longitudinal dual-mode configuration for which

$$M_{16} = M_{25} = 0$$

and therefore

$$k_2 = M_{34}$$
$$k_1 = M_{23}^2 + M_{12}^2 + M_{14}^2 \quad (6.29)$$
$$k_0 = 2M_{12}M_{14}M_{23} - M_{12}^2 M_{34}$$

There are four available couplings and only three independent variables. Assuming $M_{12}=Y$ (say) as a variable parameter, other couplings are determined as

$$M_{34} = k_2$$
$$M_{23} = \frac{1}{2}\left(\pm\sqrt{B+2A} \pm \sqrt{B-2A}\right)$$
$$M_{14} = \frac{1}{2}\left(\pm\sqrt{B+2A} \pm \sqrt{B-2A}\right)$$

where

$$A = \frac{k_0+Y^2.k_2}{2Y}$$

$$B = k_1 - Y^2$$

The choice of a single cross-coupling gives rise to a single pair of zeros of the transfer function. This is an important consideration for the realizability of general transfer functions.

(iii) Filter Structures With Two Cross-Couplings

For this configuration, we shall assume M_{16} and M_{25} as available couplings, and

$$M_{14} = 0$$

Since there are five couplings and three independent variables, we shall assume, arbitrarily, $M_{16}=a$ and $M_{34}=Y$ as variable parameters. Then,

$$M_{25} = k_2-a-Y$$

$$M_{23} = \pm\sqrt{\frac{C_1-C_2}{1-a/Y}} \qquad (6.31)$$

$$M_{12} = \pm\sqrt{C_1 - \frac{C_1-C_2}{1-a/Y}}$$

where

$$C_1 = k_1 + aY + (a+y)(k_2-a-Y)$$

$$C_2 = a(k_2-a-Y) - k_0/Y$$

The choice of two cross-couplings gives rise to two pairs of zeros of the transfer function. Atia and Williams [59] have realized such cross-couplings in a dual-mode configuration. The response function has two transmission zeros and is being referred to as the canonical realization.

(c) Coupling Matrix for Eighth-Order Filters

If λ_1 λ_2 λ_3 and λ_4 are the four distinct 'Eigenvalues' of the transfer function for the symmetrical structure, then

$$\begin{aligned} k_0 &= \lambda_1\lambda_2\lambda_3\lambda_4 \\ k_1 &= -\lambda_1\lambda_2(\lambda_3+\lambda_4) - \lambda_3\lambda_4(\lambda_1+\lambda_2) \\ k_2 &= \lambda_1(\lambda_2+\lambda_3+\lambda_4) + \lambda_2(\lambda_3+\lambda_4) + \lambda_3\lambda_4 \\ k_3 &= +(\lambda_1+\lambda_2+\lambda_3+\lambda_4) \\ k_4 &= +1 \end{aligned} \qquad (6.32)$$

The generalized even-mode coupling matrix for a symmetric structure is given by

$$-M_e = \begin{bmatrix} M_{18} & M_{12} & M_{16} & M_{14} \\ M_{12} & M_{27} & M_{23} & M_{25} \\ M_{16} & M_{23} & M_{36} & M_{34} \\ M_{14} & M_{25} & M_{34} & M_{45} \end{bmatrix} \tag{6.33}$$

The characteristic coefficients for this general coupling matrix can be determined as described in the previous sections. We shall describe here, the solution for dual-mode longitudinal realization of a filter network.

For longitudinal dual-mode configuration,

$$M_{18} = M_{16} = M_{27} = M_{25} = 0$$

and the realizable, symmetric coupling matrix is given by

$$-M_e = \begin{bmatrix} 0 & M_{12} & 0 & M_{14} \\ M_{12} & 0 & M_{23} & 0 \\ 0 & M_{23} & M_{36} & M_{34} \\ M_{14} & 0 & M_{34} & M_{45} \end{bmatrix} \tag{6.34}$$

There are six available couplings and four degrees of freedom - identified by the distinct eigenvalues. Assuming arbitrarily

$$M_{36} = y_1$$

$$M_{14} = y_2$$

as variable parameters, the remaining couplings are given by

$$M_{45} = -M_{36} - k_3$$

$$M_{12} = \pm \sqrt{\frac{k_1 - y_1 y_2 + M_{23}^2 (y_1 + k_3)}{-k_3}} \qquad (6.35)$$

$$M_{34} = \pm \sqrt{-[M_{12}^2 + M_{23}^2 + y_2^2 + k_2 + y_1 (y_1 + k_3)]}$$

M_{23} is evaluated as a root of the $8^{\underline{th}}$ order equation

$$M_{23}^8 + M_{23}^6 (2d_1 - b_0 b_1 d_2^2) + M_{23}^4 (d_1^2 + 2d_0 - a_0 b_1 d_2^2 - a_1 b_0 d_2^2) +$$

$$+ M_{23}^2 (2d_0 d_1 - a_0 a_1 d_2^2) + d_0^2 = 0 \qquad (6.36)$$

The eighth-order polynomial yields 8 roots of which only the roots with zero imaginary parts are acceptable for physical realization.

The various terms in the above equations are given by

$$d_1 = \frac{a_0}{b_0} + \frac{a_1}{b_1} + \frac{y_1^2 + y_1 k_3}{b_1} + \frac{y_2^2}{b_0 b_1}$$

$$d_2 = -\frac{2y_2}{(b_0 b_1)}$$

$$d_0 = \frac{(a_0 a_1 + a_0 y_1^2 + a_0 y_1 k_3 - k_0)}{b_0 b_1}$$

$$a_0 = -\frac{k_1}{k_3} + \frac{y_1 y_2^2}{k_3}$$

$$b_0 = -\left(\frac{1+y_1}{k_3}\right)$$

$$a_1 = c_1 - a_0$$

$$b_1 = -(1+b_0)$$

$$c_1 = -y_1(y_1+k_3) - y_2^2 - k_2$$

The signs of M_{23}, M_{12} and M_{34} may be selected arbitrarily but within the constraint of the relationship

$$M_{23}.M_{12}.M_{34} = \frac{M_{12}^2 M_{34}^2 + y_2 M_{23}^2 - M_{12}^2 y_1 M_{45} - k_0}{2y_2} \qquad (6.38)$$

It is evident from this relationship that there will be a choice of four solutions, whether the RHS of the equation above is positive or negative.

The procedure described in this section can be extended to filters of orders higher than eight. However, beyond the tenth-order, the number of equations will be too many. For such cases, it will be easier to use the procedure given by Atia et al. [14]. From a practical standpoint, it is the author's view that filters with general characteristics and up to the tenth-order, cover the requirements of at least 90% of the communications systems. These closed-form relation-

ships should therefore aid the filter designers.

6.4 MUTUAL COUPLINGS VERSUS PHYSICAL DIMENSIONS IN WAVEGUIDE STRUCTURES

There are two basic types of couplings involved in the realization of band-pass filters in waveguide structures. These are:

(a) Input and output couplings

(b) Inter-cavity couplings

The input and output coupling apertures represent the interface between the waveguide or coax interfaces. Here, we are concerned only with filters that are realized in non-standard waveguides to achieve a low-loss or dual-mode realization, or both. A transducer is therefore required to provide the transition between the non-standard guide to a standard waveguide flange or coax interface.

The couplings between the synchronously tuned electrical cavities are referred to as the inter-cavity coupling. These can be provided by:

- Inductive or capacitive irises, or
- Appropriately placed structural discontinuities such as a screw placed at 45° between two orthogonal modes in a dual-mode realization.

For filters in standard waveguides, Cohn [1] has described the relationships between the normalized susceptance of irises in terms of the coupling coefficients between the electrical cavities for all-pole response functions.

For dual-mode filters, operating in the dominant mode, Williams [12] has described the relationships between normalized susceptances and mutual-couplings - based upon the works of Bethe [61] and others [17,62]. For all-pole dual-mode filters operating in TE_{11N} or TE_{10N} propagation mode, Kallianteris [63] has described similar relationships, based on references [17,61,62].

In this section, we shall describe the relationships between the mutual-couplings and physical dimensions of symmetric filter with the general characteristics operating in the dominant or higher order TE_{10N} or TE_{11N} propagation modes. The details of the derivations are not included, as these can be found in references [17,61,62].

6.4.1 Input and Output Coupling Apertures

The normalized susceptance B/Y_0 of a coupling aperture connecting two rectangular wave-guides of different cross-sections, or connecting a circular guide to a rectangular guide are given by:

$$\left[\frac{B}{Y_0}\right]_{TE_{10N}} = -\sqrt{\frac{N^2 Q_e \lambda_0^2 \lambda_{g_0} a b}{4\pi \ell^3 a_1 b_1}} \qquad (6.39)$$

and

$$\left[\frac{B}{Y_0}\right]_{TE_{11N}} = -\sqrt{\frac{N^2 Q_e \lambda_0^2 \lambda_{g_0} a b}{\pi^2 \ell^3 D^2}}$$

where

N is the third index of the TE waveguide modes

Q_e is the external Q [17] of the prototype network

λ_0 is the free space wavelength at the band-center

λ_{g_0} is the guide wavelength at the band-center

a,b are the inside dimensions of the interfacing (standard) rectangular waveguide.

ℓ is the length of the waveguide cavities

a_1,b_1 are the inside dimensions of the rectangular waveguide used for the realization of the filter

D is the inside diameter of the circular waveguide used for the realization of the filter

For half-wave direct-coupled waveguide structures

$$\ell = \frac{\lambda_{g_0}}{2} \cdot N \qquad (6.41)$$

The external Q (Q_e) is given by the reciprocal of R, where

$$R = \frac{(R_S+R_L)}{2} \qquad (6.42)$$

and

R_S and R_L are the source and load resistors of the prototype network

and their sum is extracted as the coefficient of S^{n-1} in the Hurwitz polynomial, E(S) of the transfer function [56].

Making use of the above relationships, the end aperture susceptances can be simplified to

$$\left[\frac{B}{Y_0}\right]_{TE_{10N}} = -\sqrt{\frac{2}{N\pi R} \cdot \left(\frac{\lambda_0}{\lambda_{g_0}}\right)^2 \frac{ab}{a_1 b_1}} \qquad (6.43)$$

$$\left[\frac{B}{Y_0}\right]_{TE_{11N}} = -\sqrt{\frac{8}{N\pi^2 R} \cdot \left(\frac{\lambda_0}{\lambda_{g_0}}\right)^2 \frac{ab}{D^2}} \qquad (6.44)$$

6.4.2 Inter-Cavity Coupling Apertures

These couplings are provided by either an inductive or capacitive iris or a tuning screw placed at 45° between two orthogonal modes for dual-mode filters. In either case, the normalized susceptances $\frac{B}{Y_0}$ of the apertures coupling two electrical cavities are given by

$$\left[\frac{B}{Y}\right]_{TE_{10N}} = \frac{N^2 \lambda_0^2 \lambda_{g_0}}{4\pi \ell^3 M_{j,j+1}} \qquad (6.45)$$

$$\left[\frac{B}{Y_0}\right]_{TE_{11N}} = \frac{3N^2 \lambda_0^2 \lambda_{g_0}}{4\pi^2 \ell^3 M_{j,j+1}} \qquad (6.46)$$

where

$M_{j,j+1}$ are the normalized coupling coefficients of the symmetric even-mode coupling matrix, M_e

Again, for half-wave resonant structures, these relationships can be simplified to

$$\left[\frac{B}{Y_0}\right]_{TE_{10N}} = \frac{2}{N\pi M_{j,j+1}} \cdot \left(\frac{\lambda_0}{\lambda_{g_0}}\right)^2 \qquad (6.47)$$

and

$$\left[\frac{B}{Y_0}\right]_{TE_{11N}} = \frac{6}{N\pi^2 M_{j,j+1}} \cdot \left(\frac{\lambda_0}{\lambda_{g_0}}\right)^2 \qquad (6.48)$$

From the normalized end-aperture or inter-cavity susceptances, the actual susceptance can be obtained as

$$\frac{B}{Y} = \left[\frac{B}{Y_0}\right] \cdot \frac{f_0}{\Delta f} \qquad (6.49)$$

where

f_0 is the center frequency

and

Δf is the filter bandwidth

From the above relations, it can be seen that in higher order mode filters, the end and intercavity susceptances are related to the corresponding susceptances of dominant mode filters by $\frac{1}{\sqrt{N}}$ and $\frac{1}{N}$ respectively. Since lower susceptance values correspond to larger apertures, the above factors make the TE_{10N} and TE_{11N} filters less sensitive to aperture dimensions.

6.4.3 Cavity Length

The nominal length 'ℓ' of the half-wave direct-coupled waveguide filters is given by

$$\ell = N \cdot \frac{\lambda_{g_0}}{2} \qquad (6.50)$$

where

N is the third index of TE propagation modes

and

λ_{g_0} is the guide wavelength at the band-center

For practical structures, the adjacent coupling apertures load the cavity, thereby increasing its effective length. This can be compensated by amending the relationship

to

$$\ell = [N\pi - \frac{1}{2}(\tan^{-1}\frac{2Y_0}{B_1} + \tan^{-1}\frac{2Y_0}{B_2})]\frac{\lambda_{g_0}}{2\pi} \quad (6.51)$$

This amended length may be used to refine the values of normalized susceptances, as given by equations (6.45) and (6.46).

6.4.4 Physical Dimensions of Coupling Apertures

The normalized susceptances $\frac{B}{Y_0}$ can be computed in terms of slot or post dimensions of coupling irises [17]. These computations assume infinitely thin irises and the approximate small diffraction theory of Bethe [61]. For narrow-band microwave band-pass filters, these computed dimensions require significant empirical adjustments to account for the underlying assumptions. For this reason, practical designers resort to a measurement of $\frac{B}{Y_0}$ versus slot dimensions of an iris of a given thickness. The normalized aperture susceptance may be obtained by measuring either the VSWR or the transmission loss of the slot and use the relationship [35]

$$\left|\frac{B}{Y_0}\right| = \frac{VSWR-1}{\sqrt{VSWR}} = 2\sqrt{10^{A/10}-1} \quad (6.52)$$

where

A is the transmission loss in dB.

This measurement is effected by placing coupling disks with slots of constant width and variable length between two square or circular guides which carry dominant modes. For filters with fractional bandwidths less than 1%, large values of susceptances are required. For such cases, the transmission loss measurements provide a greater accuracy, as it is difficult to measure accurately large VSWR values.

In the design of higher order mode filters, the measured susceptances are scaled by $\frac{1}{\sqrt{N}}$ for the end apertures and by $\frac{1}{N}$ for the intercavity apertures.

6.5 EXPERIMENTAL FILTERS AND MEASURED RESULTS

The work done during the course of this thesis found immediate and very useful application in the analysis, trade-offs, optimization and eventual experimental verification for the designs of the input and output multiplexing networks for the upcoming Canadian Domestic Satellite (ANIK-C) dedicated to the 14/12 GHz frequency band. This work has been reported by Kudsia et al. [64,65] at the 7th European Microwave Conference in Copenhagen, and at the 1978 International Microwave Symposium. In this section, we will describe the details of this work. It includes the design and measured versus computed response for the following filter types in the 12 GHz frequency band:

Sixth-order filter with six equi-ripple peaks in the passband and a single pair of transmission zeros. The filter is realized in a dual-mode configuration with TE_{103} as the mode of propagation. This filter type is intended for the output multiplexing network for the ANIK-C satellite.

Eighth-order filter with eight equi-ripple peaks in pass-band and a single pair of transmission zeros followed by a two-pole all-pass network in the 11 GHz frequency band. Both networks are realized in a dual-mode configuration with TE_{103} as the mode of propagation. This is a candidate design for the input multiplexing network for the ANIK-C satellite.

Tenth-order linear phase filter with ten equi-ripple peaks in pass-band and having two pairs of real-axis zeros for the linearization of phase. This unit is realized in a dual-mode configuration with TE_{103} as the mode of propagation. This is a competing design for the input multiplexing network for the ANIK-C satellite.

6.5.1 Sixth-Order Dual-Mode TE_{103} Filter With a Single-Pair of Transmission Zeros

This unit was designed to check out experimentally

and theoretically the longitudinal dual-mode class of filters exhibiting a single pair of transmission zeros. A sixth-order filter was designed to exhibit the following characteristics:

Center Frequency	:	11900 MHz
Equi-Ripple Pass-Band Band-width	:	38 MHz
Return Loss in Pass-Band	:	-26.5 dB
Minimum Attenuation/Notch Level/in Stop-Band	:	46.5 dB
Average Unloaded Q of Waveguide Cavities	:	$\geq$ 9000

The characteristic function for such a filter can be written as

$$K(s) = \frac{F(s)}{P(s)} = \frac{(s^2+a_1^2)(s^2+a_2^2)(s^2+a_3^2)}{(s^2+b_1^2)} \qquad (6.53)$$

where

s is the complex frequency variable

a_1, a_2, a_3 are the frequencies of attenuation zeros

b_1 is the frequency of the attenuation pole

The critical frequencies a_1, a_2, a_3 and b_1 are determined using the optimization program that makes use of the new Fletcher's algorithm, as described in Chapter V.

A computer output for this is shown in Table 6.2. Alternatively, one may use Fletcher's algorithm in conjunction with Bennett's transformation, as also described in Chapter V, for this particular example under consideration. Another alternative is to use Bennett's transformation alone to generate the critical frequencies and the resulting characteristic factor F for a range of locations of the transmission zero - as shown in Table 5.8. By inspection, one can select the set of critical frequencies that yield the F nearest to the desired value. From a practical standpoint, this is adequate and most efficient.

As shown in Table 6.2, the computed critical frequencies for the equivalent low-pass prototype network are:

$$a_1 = .2731$$

$$a_2 = .7284$$

$$a_3 = .9700$$

$$b_1 = 1.7941$$

The poles and zeros of the transfer function are computed as:

TABLE 6.2(1) COMPUTATION OF CRITICAL FREQUENCIES USING THE GENERALIZED OPTIMIZATION PROGRAM WITH NEW FLETCHER'S ALGORITHM

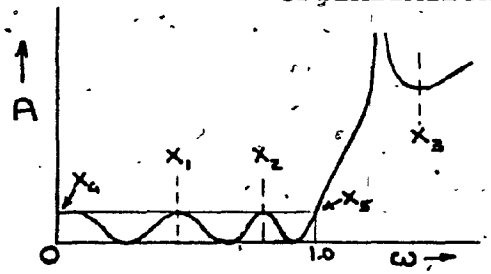

$$K(s) = \frac{(s^2+a_1^2)(s^2+a_2^2)(s^2+a_3^2)}{(s^2+b_1^2)}$$

GRADIENT CHECKING			
Variable	Analytic Gradients	Numerical Gradients	Percentage Error
.4	-2.7845E+02	-2.7846E+02	4.250E-03
.65	-8.6213E+02	-8.6220E+02	8.949E-03
.9	-3.7369E+03	-3.7383E+03	3.641E-02
1.5	-2.3720E+03	-2.3714E+03	2.628E-02

Equality Constraint: $PSI(1)=72.5+R(x_2)+T(x_3)-T(x_2)-R(x_3)$

Inequality Constraints: $0<a_1,a_2,a_3<1$

Objective Function U: $|R(x_1)-R(x_2)|+|R(x_2-x_4)|+|R(x_4-x_5)|$

Starting Values Chosen: $a_1=.4, a_2=.65, a_3=.9, b_1=1.5$

(continued)

TABLE 6.2(2) OPTIMIZATION BY NEW FLETCHER METHOD

$$K(s) = \frac{(s^2+a_1^2)(s^2+a_2^2)(s^2+a_3^2)}{(s^2+b_1^2)}$$

Iteration Number	Function Evaluations	Time Elapsed (seconds)	Objective Function	Variable Vectors
20	36	2.67	1.33E+00	.2892;.7312;.9702;1.7846
40	65	4.86	1.91E-01	.2715;.7286;.9704;1.7919
60	92	6.89	4.37E-02	.2732;.7287;.9699;1.7898

IEXIT=5 Function value less than minimum estimated has been detected

Results at Last Iteration: U=8.49E-03
X(1)=.2731
X(2)=.7284
X(3)=.9700
X(4)=1.7941

Number of Function Evaluations: 109

Execution Time in Seconds: 8.28

Poles	Zeros
- .6865 ± j .3498	± j1.7941
- .4448 ± j .8989	-
- .1398 ± j1.1419	-

The even-mode coupling matrix and the resulting susceptance matrix are computed, as described in Section 6.3. Table 6.3 is the computer output for the general synthesis program. It includes the computation of eigenvalues, characteristic coefficients, coupling matrix and the susceptance matrix. The physical dimensions for this are included in Table 6.4. Calculated and measured response of the filter are shown in Figures 6.4 and 6.5. Measured response agrees closely with the calculated response. Figure 6.6 shows the dual-mode configuration and the photograph of the prototype unit.

6.5.2 Linear Phase Versus Externally Equalized Longitudinal Dual-Mode Filters for Space Application

The linear phase and externally equalized dual-mode filters are examined, with respect to the input multiplexing requirements for the ANIK-C spacecraft. This section describes the trade-offs for two competing designs and draws conclusions for typical satellite requirements. Optimized designs are realized in a longitudinal dual-mode configura-

TABLE 6.3 TYPICAL COMPUTER OUTPUT FOR THE COUPLING AND SUSCEPTANCE MATRICES FOR THE NEW CLASS OF SIX-POLE FILTER

GENERAL COUPLED CAVITY SYNTHESIS-NEW CLASS

CENTER FREQUENCY	11900.00	MHZ	
BANDWIDTH	38.00	MHZ	
RETURN LOSS	-26.00	DB	
MODE OF PROPAGATION	TE103		
WAVEGUIDE SIZE	.91	INCHES	
INTERFACE	WR 75		

EIGEN VALUES	-.4324	1.1267	-1.2850
CHARAC COEFFS	.6260	1.3794	-.5907

EVEN MODE COUPLING MATRIX

NORM SUSCEP FACTOR 46.59

READ M12 AS Y12

50.

0.0000	.9317	-.0855
.9317	0.0000	.7099
-.0855	.7099	.5907

SUSCEPTANCE MATRIX.

0.00	50.00	-544.58
50.00	0.00	65.63
-544.58	65.63	78.87

END APERTURE SUSCEPTANCE 3.772
NOM LENGTH OF CAVITIES 1.777

CORRECTED LENGTH OF CAVITIES 1.694 1.764

TABLE 6.4 DIMENSIONS FOR THE NEW CLASS OF TE_{103} DUAL-MODE FILTER

Waveguide used Filter Realization	:	0.9 inch square waveguide
Interfacing Waveguide	:	Standard WR75
Thickness of Coupling Irises	:	.025 inch
Type of Coupling Screws Used	:	6-32 (.135" DIA)

INTERCAVITY COUPLINGS

Coupling Type	Normalized Susceptance	Coupling Coefficient	Length of Apertures (Longitudinal)	Length of Cross-Slot	Length of Coupling Screw	Cavity Length
M_{12}	50	.0030	-	-	.112	1.694
M_{23}	65.6	.0023	.254	-	-	1.764
M_{34}	78.9	.0019	-	-	.051	-
M_{14}	-545	-.0003	-	.093	-	1.694

END APERTURE COUPLINGS

End Aperture Susceptance	:	3.8
Length of coupling aperture	:	.384 inch
Thickness of End Irises	:	.025 inch

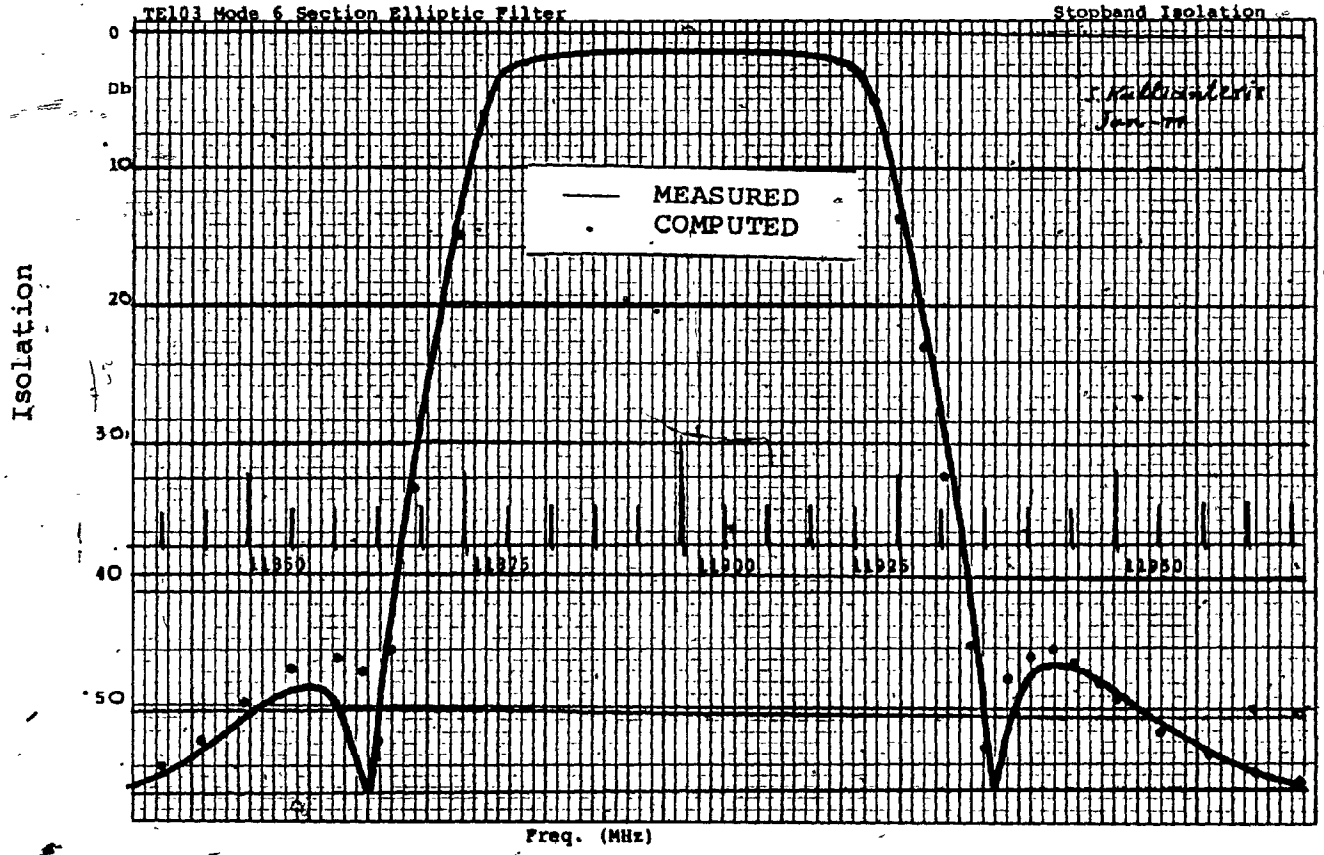

(a)

FIG.6.4 MEASURED VERSUS COMPUTED ISOLATION FOR THE NEW CLASS OF 6-POLE DUAL-MODE FILTER OPERATING IN TE_{103} PROPAGATION MODE

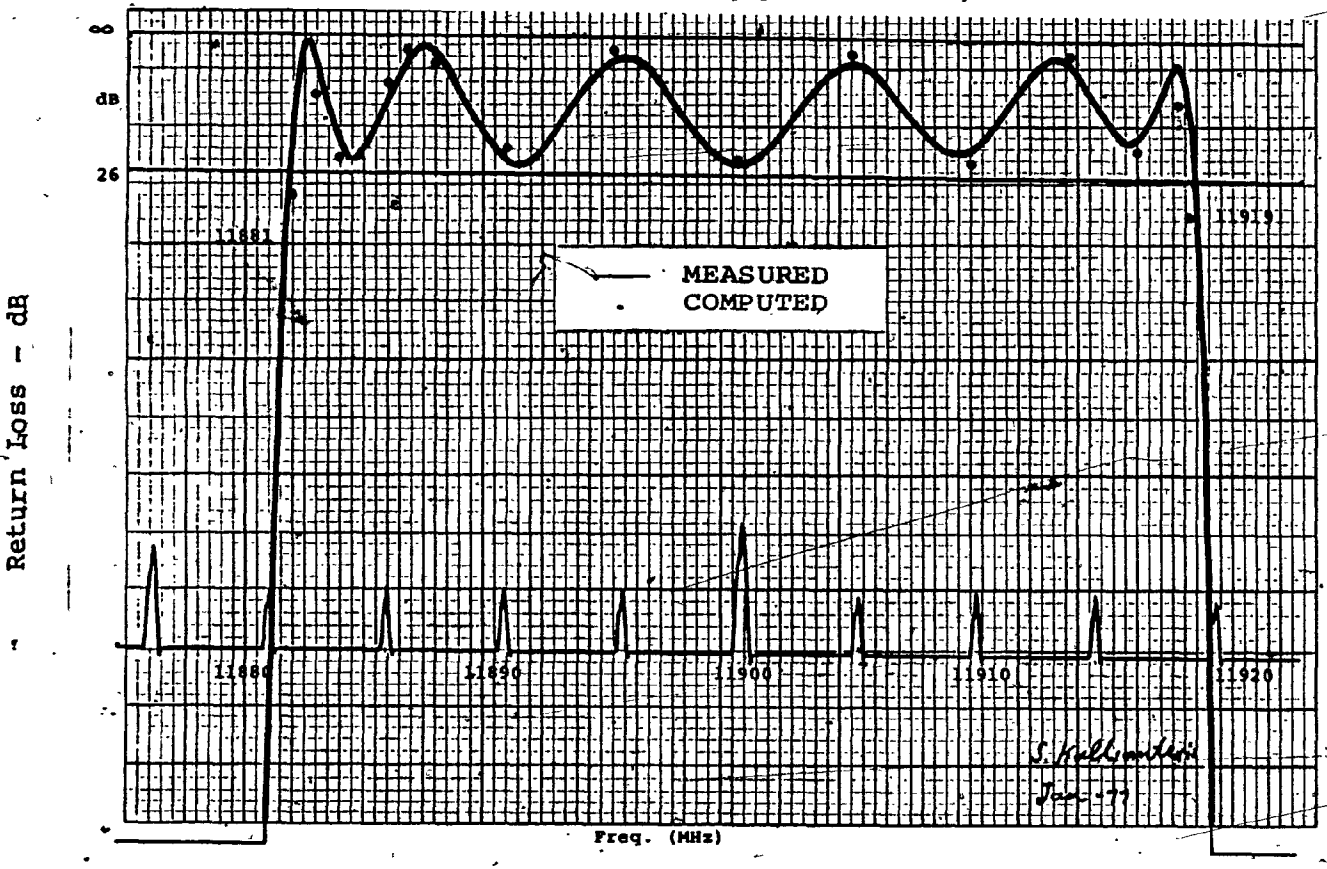

FIG.6.4 (b) MEASURED AND COMPUTED RETURN LOSS

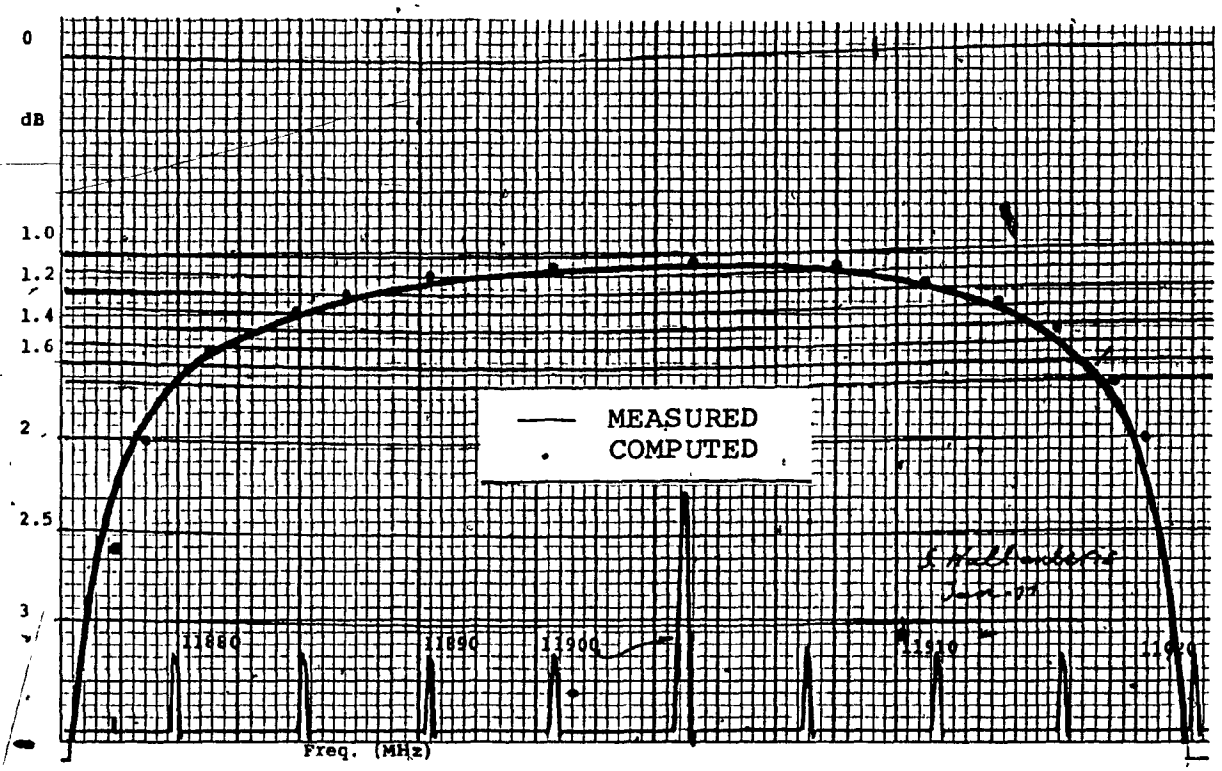

(a)

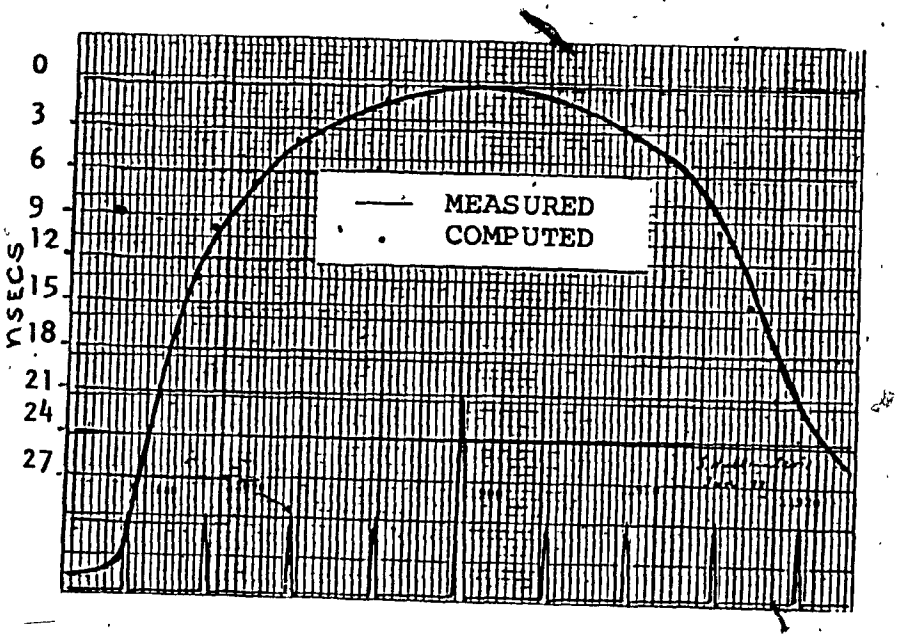

(b)

FIG. 6.5 MEASURED VERSUS COMPUTED RESPONSE FOR THE NEW CLASS OF SIX-POLE DUAL-MODE FILTER (a) INSERTION LOSS AND (b) GROUP DELAY

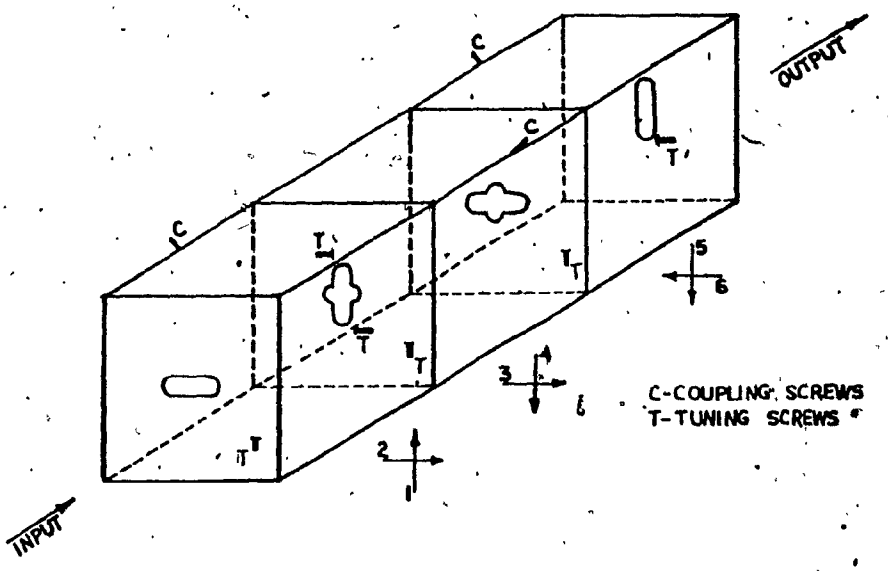

(a)

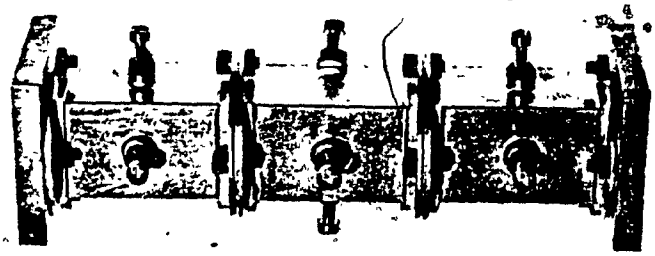

(b)

FIG.6.6 THE NEW CLASS OF DUAL-MODE SIX-POLE FILTER,
(a) FILTER-CONFIGURATION, AND
(b) PHOTOGRAPH OF THE PROTOTYPE UNIT.

tion with close correlation between the measured and predicted responses.

6.5.2.1 Design onsiderations

For space application, the requirements for optimum performance, maximum reliability and minimum weight are often in contradiction of each other. For these reasons, the following guidelines were established.

- Invar is chosen as the preferred material for the realization of the narrow-band multiplex filters.

  The primary reason for this choice is the thermal stability of this material coupled with its long history of flight experience. Graphite filter epoxy composite (GFEC) material is capable of similar thermal stability with a significant improvement in weight. Data on the GFEC filters and multiplexers at 12 GHz, in terms of such parameters as achievable unloaded Q, mechanical tolerances, short and long-term creep effects are not available, and it was not considered as candidate material.

- An allowance of ± 1 MHz for the equivalent linear frequency drift ELFD is incorporated in the tradeoff calculations.

- TE_{103} and TE_{113} are chosen as the preferred modes of propagation.

  This ensures the realization of a minimum unloaded Q of 9,000 and provides the mechanical structure less sensitive to tolerance than a dominant dual-mode design.

- Longitudinal dual-mode realizations are considered for filter networks. This represents the simplest dual-mode realization.

- For externally equalized filters, the quazi-elliptic response with the maximum possible number of equi-ripple peaks in the passband and a single pair of transmission zeros is examined.

An analysis shows the minimal difference in the performance between this response and that which exhibits a non-equi-ripple pass-band with two pairs of transmission zeros. Realization and tuning with a single transmission zero is simpler and it has been chosen for this reason.

- For the self-equalized structures, all permissible combinations of the transmission zeros and real-axis zeros with equi-ripple pass-bands are analysed. The

purpose here is to generate trade-offs with respect to all theoretically possible equi-ripple response functions for even-order filter networks. These functions can be realized in a dual-mode configuration with varying degree of complexity.

6.5.2.2 Trade-offs and Optimization of Filter Response

For equi-ripple pass-band response with the maximum possible number of peaks, it is most convenient to utilize Bennett's transformation [53] to determine the characteristic polynominal containing attenuation zeros for a given location of attenuation poles or real-axis zeros, or both. Real-axis zeros tend to linearize the phase response. This transformation is used extensively to generate the unified design charts (UDCs) for the alternative response functions, in Chapter V. UDCs for linear phase filters, are generated in a parametric form with the available zero locations as the parameters. By inspection of these design charts, one can choose the near optimal values of zero-locations to achieve the lowest group delay for a given isolation response. If necessary, further refinement can be obtained by computing the filter response with minor variations of these zero locations. This procedure, although less elegant than a formal optimization program, is significantly simpler and is best suited to generate performance

trade-offs. A similar procedure is followed for filters with transmission, as well as real-axis zeros.

The range of interest of real-axis zero locations is in the vicinity of unity. This ensures the group delay ripple to lie within one or two nanoseconds.

For configurations with external equalization, the group delay response of minimum phase filters is optimized using all-pass networks as described in reference [66]. Based on these techniques, and the computer programs developed in Chapters I to V, optimized filter trade-offs were generated with respect to the ANIK-C satellite. Tables 6.6 and 6.7 describe the optimized critical frequencies and resulting performance trade-offs, respectively.

The trade-offs are carried out so that the resulting filters may be realized as longitudinal dual-mode structures. This is the simplest dual-mode realization, but somewhat restrictive in terms of the available couplings and hence, the response shape. For such a realization, the permissible number of zeros available for 8-or 10-pole filters is two. There are two possible configurations for the linear phase filter, as described in Table 6.7. One has both zeros on the real-axis, whereas the other has one real-axis and one transmission zero. The first one yields superior in-band response but poor isolation characteristics, whereas the second one has

TABLE 6.5 OPTIMIZED CRITICAL FREQUENCIES FOR THE LINEAR-PHASE AND EXTERNALLY EQUALIZED FILTERS FOR ANIK-C SATELLITE

	Linear Phase Filter	Externally Equalized Filter
Attenuation Zeros	.1373 .4088 .6629 .8681 .9847	.2138 .5955 .8599 .9851
Attenuation Poles	-	1.30
Real-Axis Zeros	1.0 1.2	
Zero Location of Micro-Wave All-Pass Network (D-Section)	-	225 ± 125

TABLE 6.6 INPUT MULTIPLEXER FILTER TRADE-OFFS FOR ANIK-C SATELLITE

CRITICAL PERFORMANCE REQUIREMENTS*

Frequency Band	:	11.7 to 12.2 GHz
Usable Channel Bandwidth	:	f_0 ± 27 MHz
Insertion Loss Variation	:	<1.4 dB over f_0 ± 27 MHz
Isolation	:	>25 dB at f_0 ± 36 MHz, > 45 dB at f_0 ± 50 and beyond
Amplitude Slope	:	≤.01 dB/MHz over f_0 ± 13 MHz
Group Delay	:	≤2 nsec at f_0 ± 18 MHz, ≤ 5 nsec at f_0 ± 21 MHz ≤1.5 nsec ripple

Filter Configuration	Isolation at f_0±36 dB	Loss Variation over f_0±27 dB	Gain-Slope over f_0±13 dB/MHz	Group Delay - nanoseconds f_0±18	f_0±21	Ripple
10-pole linear phase filter with two pairs of real-axis zeros	15	0.8	.007	1	3	.5
	20	1.0	.009	1	4.0	1.0
	25	1.7	.016	1.8	5.5	1.0
10-pole linear phase filter with one pair of transmission zeros and one pair of real-axis zeros	20	.95	.013	3.5	8	0
	25	1.25	.02	7	11	0
	30	1.5	.02	7	12.5	0

(continued)

(continued)

Filter Configuration	Isolation at $f_0 \pm 36$ dB	Loss Variation over $f_0 \pm 27$ dB	Gain-Slope over $f_0 \pm 13$ dB/MHz	Group Delay - nanoseconds		
				$f_0 \pm 18$	$f_0 \pm 21$	Ripple
8-pole filter with one-pair of transmission zeros and 2-pole all-pass equalizer	25	0.9	.004	.7	3	.5

* These requirements are for the whole transponder prior to the TWTAs.

better isolation but very poor group delay response. The externally equalized structure of the same combined degree yields the best compromise and fulfills the specification requirements.

6.5.2.3 Experimental Results Versus Computed Response

From the optimized critical frequencies, the even-mode coupling and susceptance matrices are computed as described in Section 6.3. The reactance network for the all-pass network is developed, as described in reference [66].

The computed and measured response for the two designs, realized in the longitudinal dual-mode configuration with TE_{103} as the mode of propagation, is described in Figures 6.7 and 6.8. There is close correlation between the predicted response and measured results. Figures 6.9 and 6.10 are the photographs of the prototype units.

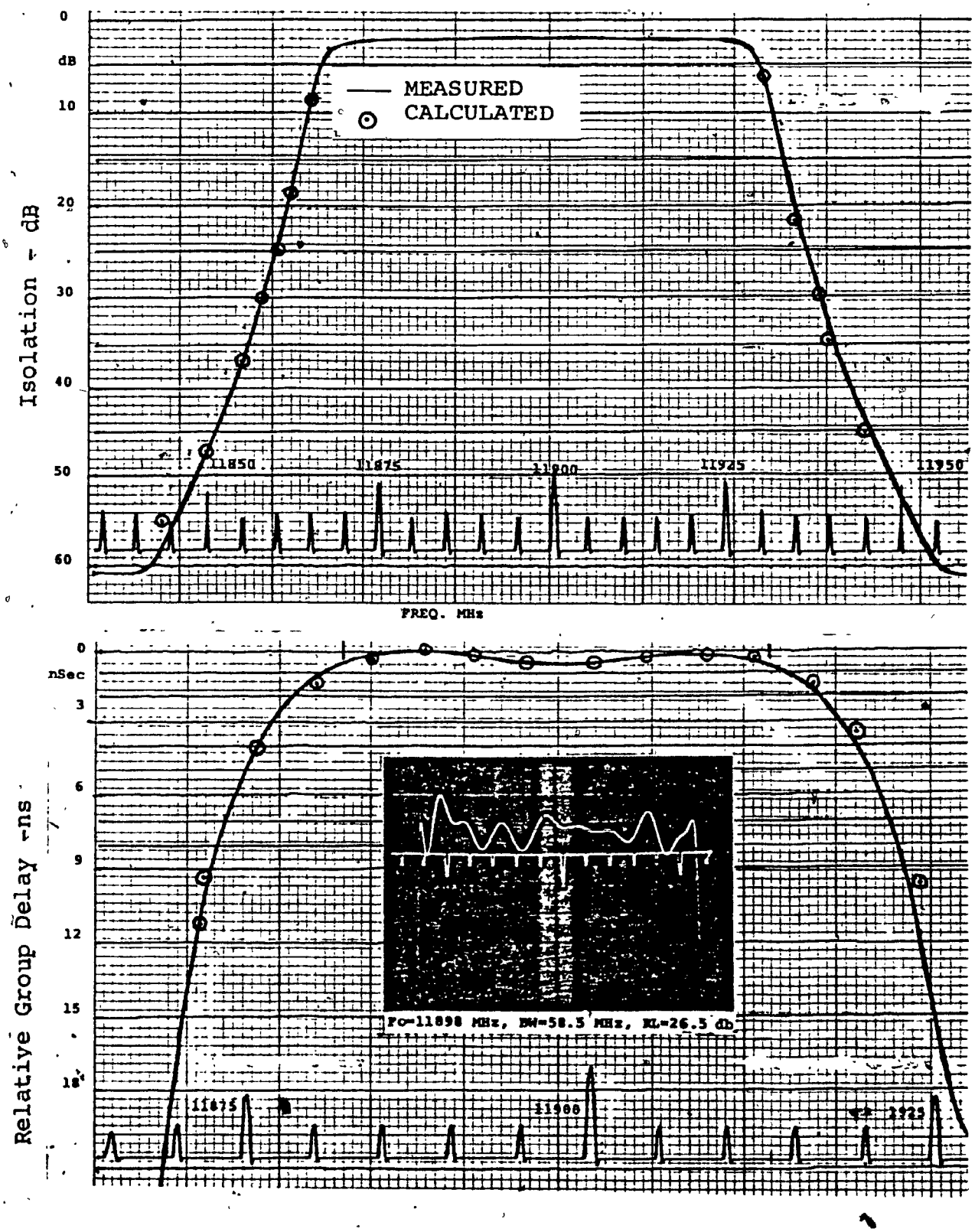

FIG. 6.7 MEASURED VERSUS COMPUTED RESPONSE OF THE LINEAR PHASE FILTER
(a) AMPLITUDE RESPONSE AND
(b) GROUP DELAY RESPONSE

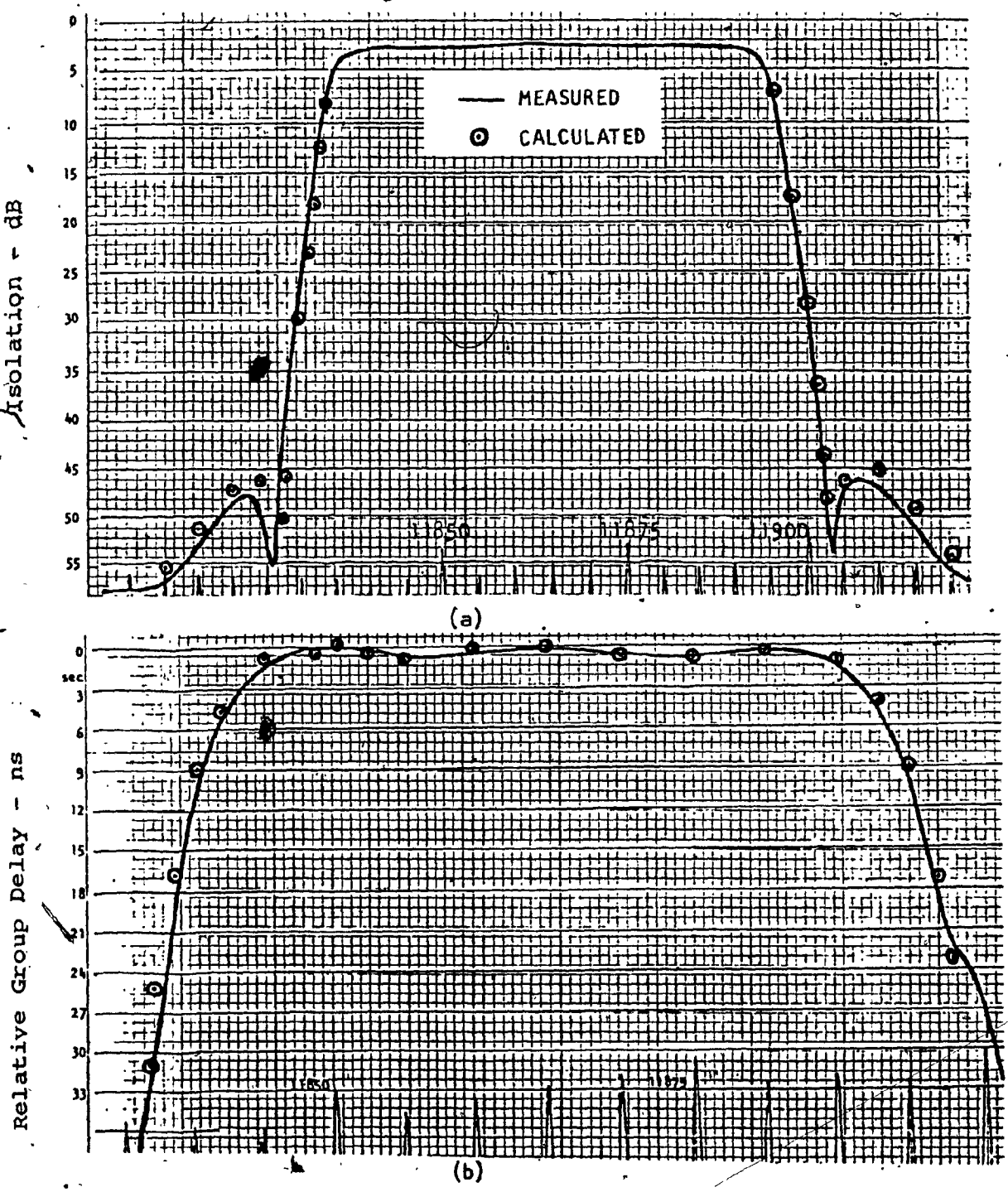

FIG.6.8 MEASURED VERSUS COMPUTED RESPONSE OF THE EXTERNALLY EQUALIZED FILTER

(a) AMPLITUDE RESPONSE AND
(b) GROUP DELAY RESPONSE

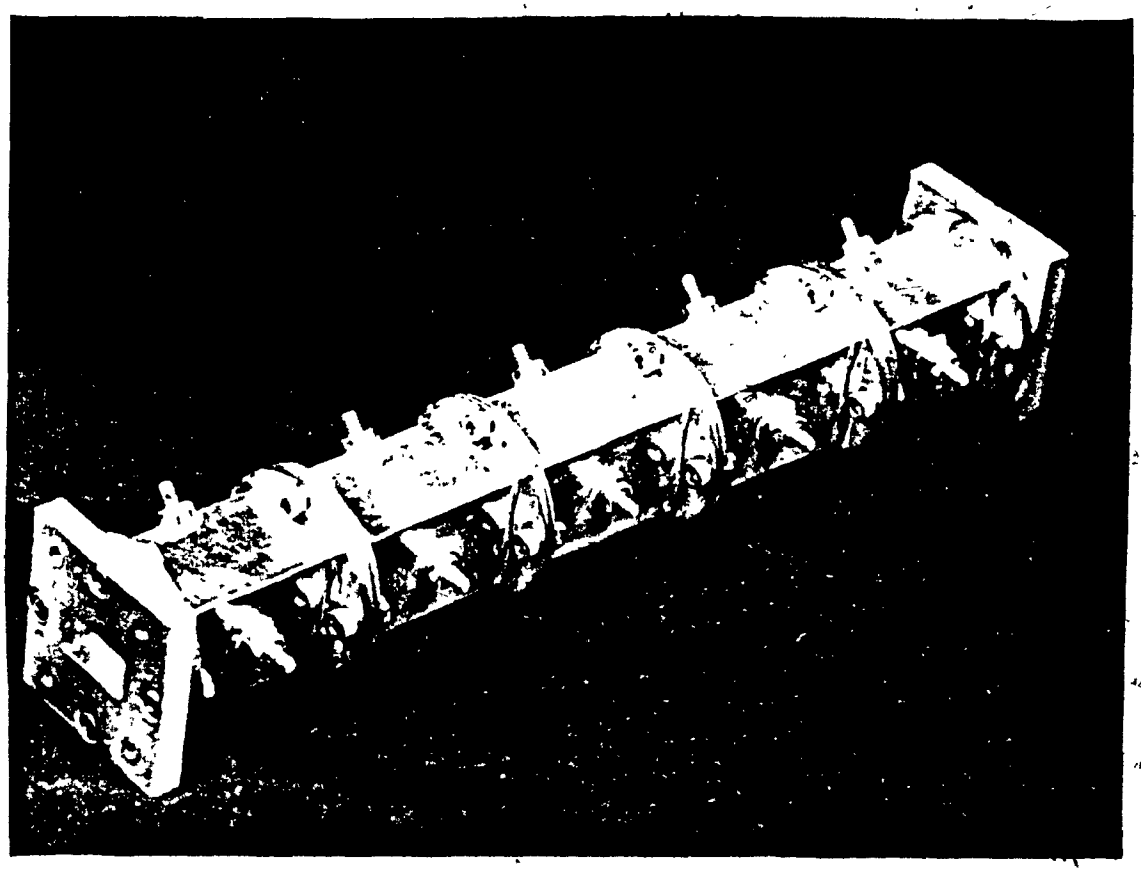

FIG.6.9 PHOTOGRAPH OF THE LINEAR PHASE FILTER

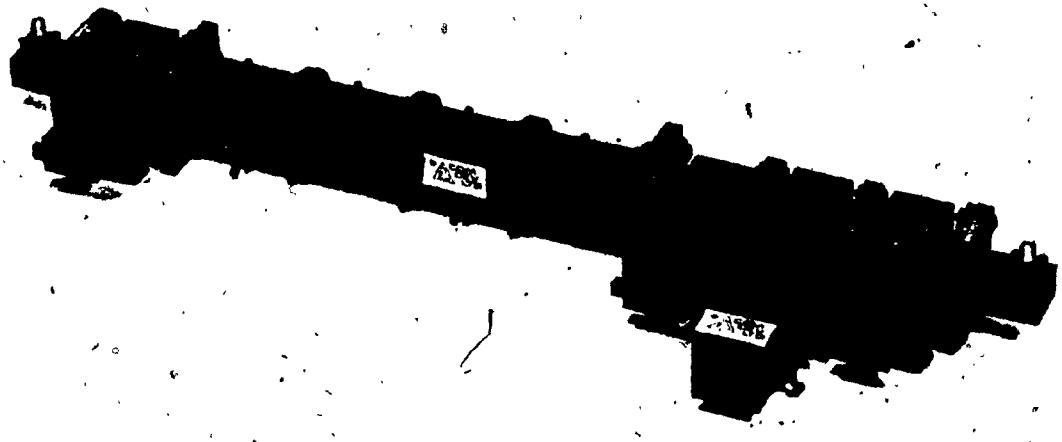

FIG.6.10 PHOTOGRAPH OF THE EXTERNALLY EQUALIZED FILTER

CHAPTER VII

CONCLUSIONS

CHAPTER VII

CONCLUSIONS

The work carried out during the course of this thesis was motivated by the continuing demands of the satellite communications industry to provide ever-more efficient filters and multiplexers at microwave frequencies. Research was directed in two specific areas:

(a) in developing techniques to analyze and synthesize the general class of lumped, doubly terminated low-pass prototype filter networks for an arbitrary set of amplitude constraints; and

(b) in improving the technique to realize the generalized filter characteristics at microwave frequencies in a dual-mode configuration.

These objectives have been met with the successful application of the results of this thesis to the design and optimization of the input and output multiplexing networks for the upcoming Canadian Domestic Satellite ANIK-C.

Synthesis of the general class of low-pass prototype filter is achieved using computer-aided optimization in conjunction with analytic techniques. The objective function is defined in terms of the practical parameters of transmission or reflection loss in decibels (dB) at frequencies of attenuation

poles and zeros-referred to as the critical frequencies of the general transmission function. The gradients of the objective and constraint functions are derived analytically. Two separate optimization programs are developed; one using the direct-search technique of the Simplex method, and the other, a gradient strategy employing new Fletcher's algorithm [51]. With the proper formulation of the problem, the gradient method has shown remarkable efficiency. Its flexibility is demonstrated by generating the known classes of filter functions such as Chebyshev and elliptic in about 2 to 6 seconds of CPU time as special cases of the general optimization problem. The effect of dissipation is examined in detail, and included in the prototype low-pass and all-pass networks. This model is then used to derive practical filters and all-pass networks.

From the optimized critical frequencies of the prototype network, practical coupled-cavity band-pass filters are synthesized, using the basic technique described by Atia et al. [14]. New closed-form relationships are derived for the couplings of even-order filters in a dual-mode configuration in terms of the eigenvalues of the symmetric coupling matrix with excess couplings, if any, as parameters. This significantly reduces the matrix manipulations and provides a ready means to optimize the couplings to realize a less sensitive practical network. For narrow-band application,

microwave filter structure can then be derived in terms of the distributed elements, as described by Cohn [1]. The theoretical work and the associated computer software developed in the thesis were put to practical test in generating filter and multiplexer trade-offs for the upcoming Canadian Domestic Satellite (ANIK-C) in the 12 GHz frequency band. The optimized designs were realized in a dual-mode configuration with TE_{103} as the mode of propagation. The measured results agree closely with the theoretical response.

As stated earlier, filter optimization is carried out with respect to amplitude constraints only. However, this does not represent a serious drawback. For minimum phase networks, phase and group delay are uniquely related to amplitude and therefore design trade-offs with respect to amplitude automatically include group delay, as well. For non-minimum phase networks, unified design charts (UDCs) are generated with real-axis zeros as parameters. By an inspection of these design charts, one can choose the near optimal values of zero-locations to achieve the lowest group delay for a given isolation response [65]. If necessary, further refinement can be obtained by computing the filter response with minor variations of these zero locations. This procedure, although less elegant than a formal optimization program involving amplitude as well as group delay constraints, is significantly simpler and suited to generating performance trade-offs.

In conclusion, it is the author's view that the work described in this thesis provides an efficient procedure to synthesize, in terms of critical frequencies, the doubly-terminated low-pass prototype networks for a given set of amplitude constraints. The treatment is completely general and encompasses the entire class of minimum phase filters consisting of loss-less reactive elements. Non-minimum phase networks (linear-phase) with real-axis zero locations are also included. When the constraint of finite conductivity of materials is included, this model has proven its versatility in generating new classes of practical filters exhibiting close correlation with theoretical response.

This work can be of help to future researchers in the following areas:

- The development of optimization procedure that includes amplitude, as well as group delay constraints for prototype filters.

- The development of synthesis techniques for the general class of filter networks with arbitrary terminations for a given set of amplitude or group delay or both types of constraints.

- Development of optimization procedure to synthesis filters with predistortion.
- Inclusion of complex zeros with quadrantal symmetry in the objective function of the prototype network.
- Use and extension of optimization methods to problems in network theory.
- Extension of closed-form relationships for susceptance matrix to odd and higher order (≥ 9) filter networks.
- Sensitivity analysis of filter realization in dual-mode configuration for transfer functions with finite zero locations.

REFERENCES

REFERENCES

[1] Cohn, S.B., "Direct-Coupled Resonator Filters", IRE, Vo.45, February 1957, pp.187-196.

[2] Matthaei, G.L., "Interdigital Band-Pass Filters", IRE Trans. on MTT, Vol.MTT-10, No.6, November, 1962, pp.479-491.

[3] Matthaei, G.L., "Comb-Line Band-Pass Filters of Narrow or Moderate Bandwidth", The Microwave Journal, Vol.6, No.9, August, 1963, pp.82-91.

[4] Wenzel, R.J., "Exact Theory of Interdigital Band-Pass Filters and Related Coupled Structures", IEEE Trans. on Microwave Theory and Techniques, Vol.MTT-13, No.5, September, 1965, pp.559-575.

[5] Rhodes, J.D., "The Stepped Digital Elliptic Filter", IEEE Trans.on Microwave Theory and Techniques, Vol.MTT-17, No.4, April, 1969, pp.178-184.

[6] Rhodes, J.D., "The Generalized Interdigital Linear Phase Filter," IEEE Trans. on Microwave Theory and Techniques, Vol.MTT-18, No.6, June, 1970, pp.301-307.

[7] Rhodes, J.D., "The Generalized Direct-Coupled Cavity Linear Phase Filter", IEEE Transmission on Microwave Theory and Techniques, MTT-18, June, 1970, pp.308-313.

[8] Levy, R., "Filters With Single Transmission Zeros at Real or Imaginary Frequencies", IEEE Trans. on MTT, Vol.24, April, 1976, pp.172-181.

[9] Kurzrok, R.M., "General Three-Resonator Filters in Waveguide," IEEE Trans. on MTT, Vol.MTT-14, Jan.1966, pp.46-47.

[10] Kurzrok, R.M., "General Four Resonator Filters at Microwave Frequencies," IEEE Trans. on MTT, Vol. MTT-14, June, 1966, plus convection, October, 1966, pp.295-296.

[11] Blachier, B.L., and Champeau, A.R., "Dual-Mode Circular and/or Square Waveguide Filters, U.S.Patent No. 3,697,898, issued October, 1972.

[12] Williams, A.E., "A Four-Cavity Elliptic Waveguide Filter," IEEE Trans. on Microwave Theory and Techniques," MTT-18, No. 12, December, 1970, pp.1109-1114.

[13] Atia, A.E., and Williams, A.E., "Narrow-Bandpass Waveguide Filters," IEEE Trans.MTT, Vol.20, April, 1972, pp.258-265.

[14] Atia, A.E., Williams, A.E., and Newcomb, R.W., "Narrow-Band Multiple-Coupled Cavity Synthesis", IEEE Trans. on Circuits and Systems, Vol.Cas-21,No.5, September, 1974, pp.649-655.

[15] Atia, A.E., and Williams, A.E., "General TE_{011}-Mode Waveguide Bandpass Filter," IEEE Trans.Microwave Theory and Techniques, Vol.24, October 1976, pp.640-648.

[16] Kallianteris, S., and O'Donovan, M.V., "Technology Advances in the Realization of Filter Networks for Communications Satellites Operating at Frequencies Above 10 GHz", AIAA 6th Communications Satellite Systems Conference, Paper No.76-242, Montreal, April, 1976.

[17] Marcuvitz, N., Waveguide Handbook, Radiation Laboratory Series, MIT, Vol.10, McGraw-Hill, 1951.

[18] Guillemin, E.A., Synthesis of Passive Networks, John Wiley & Sons, Inc., 1957.

[19] Van Valkenburg, Modern Network Synthesis, John Wiley & Sons, Inc., 1960.

[20] Weinberg, Louis, Network Analysis and Synthesis, McGraw-Hill Book Company, Inc., 1962.

[21] Saal, R., and Ulbrich, E., "On the Design of Filters by Synthesis", IRE Transactions on Circuit Theory, December, 1958.

[22] Christian, E., and Eisenmann, E., Filter Design Tables and Graphs, John Wiley & Sons, 1966.

[23] Temes, G.C., and Mitra, S.K., Modern Filter Theory and Design, John Wiley & Sons, Inc., 1973.

[24] Chitre, N.K.M., and O'Donovan, M.V., "A Unified Design Chart for Small VSWR Filters", Microwave Journal, April, 1967.

[25] Kudsia, C.M., and O'Donovan, M.V., Microwave Filters For Communications Systems, Artech House, Inc., 1974.

[26] Richard, P.I., Resistor Transmission-Line Circuits, Proc.IRE, Vol.36, February, 1948, p.217.

[27] Wenzel, R., "Exact Design of TEM Microwave Networks, Using Quarter-Wave Lines", IEEE Trans. on MTT, Vol. MTT-12, No.1, pp.94-111, January, 1964.

[28] Cristal, E.G., "A Frequency Transformation For Commensurate Transmission-Line Networks", IEEE Trans. on MTT, Vol.MTT-15, No.6, June,1967, pp.348-357.

[29] Cauer, W., "Ein Interpolations problem mit Funktionen mit Positiven Realteil", Mathematische Zeitschrift, 38, 1933, 1-44.

[30] Darlington,S., "Synthesis of Reactance 4-poles Which Produce Prescribed Insertion Loss Characteristics", J. Math. and Phys., 18, 1939, 257-353.

[31] Wanselow, R.D., "Prototype Characteristics for a Class of Dual-Mode Filters," IEEE Trans.MTT, Vol.23, August, 1975, pp.708-711.

[32] Kudsia, C.M., and Swamy, M.N.S., "Prototype Characteristics for Non-Equi-Ripple Filters for Communications Applications," IEEE, Canadian Communications and Power Conference, Montreal, Canada, October, 1976, p.196.

[33] Cohn, S.B., "Dissipation Loss in Multiple-Coupled-Resonator Filters," Proc. IRE, August, 1959, pp.1342-1348.

[34] Young, L., "Group Delay and Dissipation Loss in Transmission-Line Filters,"IEEE Trans. Microwave Theory and Techniques, Vol.MTT-11, May, 1963, pp.215-217.

[35] Microwave Engineers Handbook, Vol.1, Artech House,Inc., Mass.

[36] Dishal, M., "Design of Dissipative Band-Pass Filters Producing Desired Exact Amplitude-Frequency Characteristics," Proc.IRE, Vol.37, September, 1949, pp.1050-1069.

[37] Fubini, E.G., and Guillemin, E.A., "Minimum Insertion Loss Filters," Proc.IRE, Vol.47, January, 1959,pp.37-41.

[38] Chen, M.H., and Mahle, C., "Design of a Lossy Waveguide Filter," COMSAT Technical Review, Vol.5, Fall, 1975, pp.387-398.

[39] Bode, H.W., Network Analysis and Feedback Amplifier Design, D.Van Nostrand, New York, 1945.

[40] Cristal, E.G., "Theory and Design of Transmission Line All-pass Equalizers," IEEE Trans.Microwave Theory and Techniques, Vol.MTT-17, Jan.1969, p.28.

[41] Scanlan, J.O., and Rhodes, J.D., "Microwave All-pass Networks," IEEE Trans.Microwave Theory and Techniques, Vol.MTT-16, p.62, Feb.1968.

[42] Bandler, J.W., "Optimization Methods for Computer-Aided Design," IEEE Trans. on MTT, August 1969, pp.533-552.

[43] Jha, V.K., "Development of a User Oriented Optimization System for Computer Aided Design Packages," Master's Thesis, McMaster University, February 1971.

[44] Kowalik,J., and Osborne, M.R., Methods for Unconstrained Optimization Problems, Elsevier, New York, 1968.

[45] Fiacco, A.V., and McCormick, G.P., Non-Linear Programming, John Wiley and Sons, 1968.

[46] Carol1, C.W., "The Created Response Technique for Optimizing Non-Linear Restrained Systems," Operation Research, Vol.9, 1961, pp.169-185.

[47] Bandler, J.W., Jha, V.K., Kudsia, C.M., and Papovic, J.R., "A Microwave Network Optimiation Program," Int. Microwave Symposium, June 1973.

[48] Spendley, W., Hext, G.R., and Himsworth, F.R., "Sequential Application of Simplex Designs in Optimization and Evolutionary Operations," Technometrics, Vol.4, November, 1962, pp.441-461.

[49] Nelder, J.A., and Mead, R., "A Simplex Method for Function Minimization," Computer J., Vol.7, January, 1965, pp.308-313.

[50] Fletcher, R., and Powell, M.J.D., "A Rapidly Convergent Descent Method for Minimization," Computer Journal, Vol.6, June 1963, pp.163-168.

[51] Fletcher, R., "A New Approach to Variable Metric Algorithms," The Computer Journal, August 1970, pp.317-322.

[52] Davidon, W.C., "Variance Algorithm for Minimization", Computer Journal, Vol.10, February, 1968, pp.406-410.

[53] Bennett, B.J., "Synthesis of Electric Filters With Arbitrary Phase Characteristics", IRE International Conv. Rec., Pt.5, 1953, 19-26.

[54] Easter, B., and Powell, K.J., "Direct-Coupled-Resonator Filters Employing Additional Couplings," European Microwave Conference, London, England, Sept.1969.

[55] Saitó, M., "Synthesis Procedure for General Coupled-Resonator Transmission Networks," Electronics and Communications in Japan, Vol.53-A, No.5, 1970, pp.26-33.

[56] Atia, A.E., and Williams, A.E., "New Types of Waveguide Bandpass Filters for Satellite Transponders," Comsat Technical Review, Vol.1, No.1, Fall, 1971, pp.21-43.

[57] Christian, E., Introduction to Numerical Analysis, Massachusetts: Addison-Wesley, 1965.

[58] Fröberg, C.E., Introduction to Numerical Analysis, Massachusetts: Addison-Wesley, 1965.

[59] Atia, A., and Williams, A.E., "Dual-Mode Canonical Waveguide Filters", International Microwave Symposium, IEEE-MTT-S, June 1977, San Diego, California, pp.397-399.

[60] Pfitzenmaier, G., "An Exact Solution for a Six-Cavity Dual-Mode Elliptic Bandpass Filter," IEEE MTT International Symposium Digest, 1977, pp.400-403.

[61] Bethe, H.A., "Theory of Diffraction by Small Holes," Phys. Rev., Vol.66, 1944, pp.163-182.

[62] Matthaei,G.L., Young, L., and Jones, E.M.T., Microwave Filters, Impedance Matching Networks and Coupling Structures, McGraw-Hill Co., 1964.

[63] Kallianteris, S., "Dual-Mode Chebyshev Filters," Master's Thesis, Concordia University, Montreal, 1978.

[64] Kallianteris, S., Kudsia, C.M., and Swamy, M.N.S., "A New Class of Dual-Mode Microwave Filters for Space Application," 7th European Microwave Conference, Copenhagen, September, 1977, pp.51-58.

[65] Kudsia, C.M., Kallianteris, S., and Swamy, M.N.S., "Linear Phase versus Externally Equalized Dual-Mode Filters for Space Application," International Microwave Symposium, Ottawa, June, 1978, pp.220-222.

[66] Kudsia, C.M., "Synthesis of Optimum Reflection-Type Microwave Equalizers," RCA Review, Vol.31, No.3, September, 1970, pp.571-595.

[67] Rhodes,J.D., "A Low-Pass Prototype Network for Microwave LInear Phase Filters," IEEE Trans. on Microwave Theory and Techniques, MTT-18, June 1970, pp.290-301.

APPENDIX "A"

APPENDIX "A"

This appendix contains the unified design chart data for the non-equi-ripple Class I elliptic function filters.

TABLE A.1 UNIFIED DESIGN CHART DATA FOR NON-EQUI-RIPPLE ELLIPTIC FUNCTION (CLASS-1) FILTER

FILTER TYPE ELLIPTIC CLASS-1
NUMBER OF SECTIONS 6

MODULAR ANGLE DEGREES	CUTOFF FREQUENCY RAD/SEC	MIN ATTEN FREQUENCY RAD/SEC	F DB
20.00	.52343425	1.91045963	105.63
25.00	.58395835	1.71245091	93.74
30.00	.63799266	1.56741614	83.91
35.00	.68691252	1.45578946	75.47
40.00	.73158829	1.36688902	68.03
45.00	.77259785	1.29433444	61.31
50.00	.81033221	1.23406176	55.13
55.00	.84505139	1.18335999	49.35
60.00	.87691306	1.14036390	43.84
65.00	.90598319	1.10377324	38.48
70.00	.93222962	1.07269709	33.17
75.00	.95549151	1.04658178	27.73
80.00	.97539706	1.02522351	21.88
85.00	.99112144	1.00895810	14.98

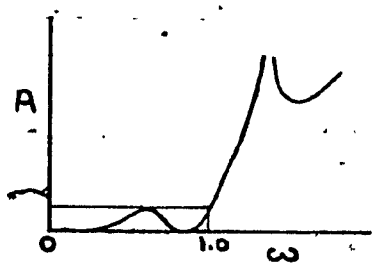

TABLE A.2 UNIFIED DESIGN CHART DATA FOR NON-EQUI-RIPPLE ELLIPTIC FUNCTION (CLASS-1) FILTER

FILTER TYPE ELLIPTIC CLASS-1
NUMBER OF SECTIONS 7

MODULAR ANGLE DEGREES	CUTOFF FREQUENCY RAD/SEC	MIN ATTEN FREQUENCY RAD/SEC	F DB	ATTEN MINIMA-2 FREQUENCY RAD/SEC	ATTEN DELTA DB
25.00	.64302730	1.55514392	104.65	2.31585871	12.85
30.00	.69998510	1.42860184	93.27	2.10105615	12.65
35.00	.75040772	1.33260889	83.53	1.93084880	12.42
40.00	.79519723	1.25754965	74.97	1.79052234	12.14
45.00	.83493989	1.19769101	67.28	1.67126152	11.81
50.00	.87002536	1.14939178	60.25	1.56741292	11.42
55.00	.90071261	1.11023205	53.71	1.47515260	10.97
60.00	.92716884	1.07855220	47.54	1.39177863	10.44
65.00	.94949421	1.05319231	41.61	1.31530929	9.79
70.00	.96773863	1.03333686	35.80	1.24424374	8.95
75.00	.98191540	1.01841767	29.95	1.17742035	7.74
80.00	.99201557	1.00804869	23.81	1.11396340	5.71
85.00	.99803015	1.00197373	16.73	1.05347144	2.45

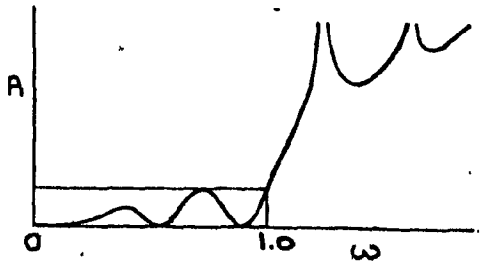

TABLE A.3 UNIFIED DESIGN CHART DATA FOR NON-EQUI-RIPPLE ELLIPTIC FUNCTION (CLASS-1) FILTER

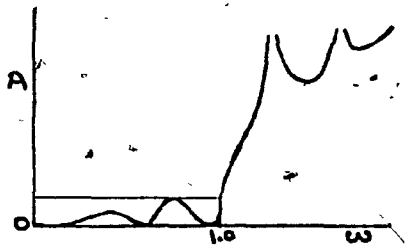

FILTER TYPE ELLIPTIC CLASS-1
NUMBER OF SECTIONS 8

MODULAR ANGLE DEGREES	CUTOFF FREQUENCY RAD/SEC	MIN ATTEN FREQUENCY RAD/SEC	F DB	ATTEN MINIMA-2 FREQUENCY RAD/SEC	ATTEN DELTA DB
30.00	.68193680	1.46641156	110.36	1.91833601	9.28
35.00	.73193582	1.36624002	99.24	1.77002406	9.10
40.00	.77671196	1.28747857	89.46	1.64911917	8.89
45.00	.81684996	1.22421503	80.68	1.54763662	8.64
50.00	.85274059	1.17268958	72.64	1.46045034	8.36
55.00	.88464319	1.13039925	65.17	1.38408683	8.03
60.00	.91272117	1.09562485	58.11	1.31608244	7.65
65.00	.93706160	1.06716570	51.32	1.25461389	7.20
70.00	.95768375	1.04418603	44.64	1.19826817	6.67
75.00	.97453724	1.02612805	37.90	1.14588079	5.99
80.00	.98748388	1.01267475	30.75	1.09638732	4.97

TABLE A.4 UNIFIED DESIGN CHART DATA FOR NON-EQUI-RIPPLE ELLIPTIC FUNCTION (CLASS-1) FILTER

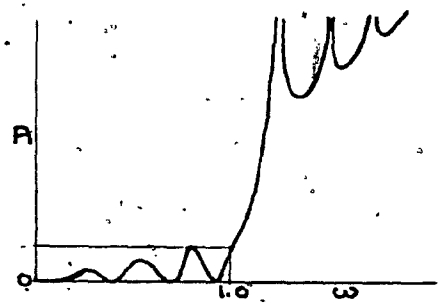

FILTER TYPE ELLIPTIC CLASS-1
NUMBER OF SECTIONS 9

MODULAR ANGLE DEGREES	CUTOFF FREQUENCY RAD/SEC	MIN ATTEN FREQUENCY RAD/SEC	F DB	ATTEN MINIMA-2 FREQUENCY RAD/SEC	ATTEN DELTA DB	ATTEN MINIMA-3 FREQUENCY RAD/SEC.	ATTEN DELTA DB
45.00	.83927998	1.19149750	92.01	1.35282927	4.87	2.18611296	18.28
50.00	.87384781	1.14436403	83.06	1.28423080	4.59	2.03348022	17.74
55.00	.90392972	1.10628069	74.75	1.22563910	4.27	1.89514455	17.10
60.00	.92972668	1.07558493	66.91	1.17510259	3.91	1.76719325	16.37
65.00	.95137940	1.05110538	59.39	1.07337665	3.50	1.64653106	15.50
70.00	.96898521	1.03200750	52.01	1.05014903	3.04	1.53043893	14.47
75.00	.98261009	1.01769767	44.58	0.00000000	2.50	1.41611386	13.20
80.00	.99229851	1.00776126	36.71	0.00000000	1.84	1.29986132	11.51
85.00	.99808336	1.00192032	27.49	0.00000000	.96	1.17454743	8.64

TABLE A.5 UNIFIED DESIGN CHART DATA FOR NON-EQUI-RIPPLE ELLIPTIC FUNCTION (CLASS-1) FILTER

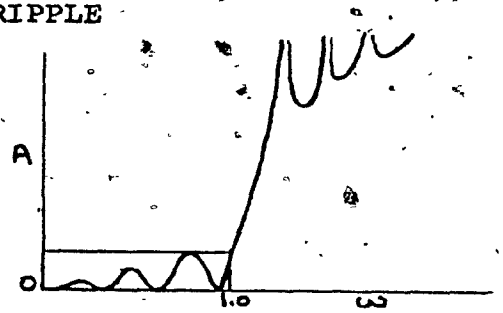

FILTER TYPE ELLIPTIC CLASS-1
NUMBER OF SECTIONS 10

MODULAR ANGLE DEGREES	CUTOFF FREQUENCY RAD/SEC	MIN ATTEN FREQUENCY RAD/SEC	F DB	ATTEN MINIMA-2 FREQUENCY RAD/SEC	ATTEN DELTA DB	ATTEN MINIMA-3 FREQUENCY RAD/SEC	ATTEN DELTA DB
45.00	.82843037	1.20710206	105.68	1.33212405	3.83	1.88872660	13.96
50.00	.86359056	1.15795616	95.68	1.26715598	3.62	1.76788637	13.50
55.00	.89450729	1.11793387	86.40	1.14602874	3.37	1.65971998	12.98
60.00	.92136828	1.08534234	77.62	1.11004525	3.09	1.56099127	12.37
65.00	.94429393	1.05899230	69.19	1.06100265	2.78	1.46919280	11.66
70.00	.96334991	1.03804442	60.90	0.00000000	2.42	1.38219810	10.83
75.00	.97855165	1.02191847	52.52	0.00000000	2.01	1.29792553	9.82
80.00	.98985859	1.01024532	43.62	0.00000000	1.52	1.21378519	8.54
85.00	.99714345	1.00286473	33.13	0.00000000	.90	1.12494343	6.61

APPENDIX "B"

APPENDIX "B"

This appendix contains:

(a) Critical frequencies and unified design chart data for filters exhibiting maximum permissible peaks in the pass-band and a single pair of transmission zeros; and

(b) critical frequencies for linear phase filters with a single or double pair of real-axis zeros.

TABLE B.1 CRITICAL FREQUENCIES AND UNIFIED DESIGN CHART DATA FOR A 4-POLE FILTER WITH FOUR EQUI-RIPPLE PEAKS IN PASS-BAND AND A SINGLE TRANSMISSION ZERO

$$K(s) = \prod_{i=1}^{2} \frac{(s^2 + a_i)^2}{(s^2 + b_1^2)}$$

a_1	a_2	b_1	b_s	F
.4752	.9582	1.2000	1.1453	27.2757
.4397	.9460	1.4000	1.3153	36.0073
.4226	.9397	1.6000	1.4902	42.3298
.4126	.9358	1.8000	1.6675	47.4297
.4060	.9333	2.0000	1.8460	51.7540
.4015	.9315	2.2000	2.0254	55.5301
.3982	.9302	2.4000	2.2052	58.8932
.3957	.9292	2.6000	2.3855	61.9312
.3938	.9284	2.8000	2.5661	64.7056
.3923	.9278	3.0000	2.7468	67.2609
.3911	.9273	3.2000	2.9278	69.6310
.3901	.9269	3.4000	3.1089	71.8421
.3892	.9266	3.6000	3.2901	73.9150
.3885	.9263	3.8000	3.4714	75.8665
.3879	.9260	4.0000	3.6527	77.7106
.3874	.9258	4.2000	3.8342	79.4588
.3870	.9257	4.4000	4.0157	81.1209
.3866	.9255	4.6000	4.1972	82.7050
.3863	.9254	4.8000	4.3788	84.2185
.3860	.9253	5.0000	4.5604	85.6674
.3858	.9251	5.2000	4.7421	87.0571

TABLE B.2 CRITICAL FREQUENCIES AND UNIFIED DESIGN CHART DATA FOR A 5-POLE FILTER WITH FIVE EQUI-RIPPLE PEAKS IN PASS-BAND AND A SINGLE TRANSMISSION ZERO

$$K(s) = s \prod_{i=1}^{2} \frac{(s^2 + a_i)}{(s^2 + b_1^2)}$$

a_1	a_2	b_1	b_s	F
.7065	.9782	1.1000	1.0727	26.9151
.6722	.9707	1.2000	1.1579	35.1766
.6530	.9663	1.3000	1.2460	41.1876
.6404	.9634	1.4000	1.3355	46.0832
.6315	.9613	1.5000	1.4259	50.2794
.6248	.9598	1.6000	1.5169	53.9833
.6197	.9586	1.7000	1.6081	57.3164
.6156	.9576	1.8000	1.6997	60.3569
.6123	.9568	1.9000	1.7915	63.1588
.6096	.9562	2.0000	1.8836	65.7615

TABLE B.3 CRITICAL FREQUENCIES WITH UNIFIED DESIGN CHART DATA FOR A 6-POLE FILTER WITH SIX EQUI-RIPPLE PEAKS IN PASS-BAND AND A SINGLE TRANSMISSION ZERO

$$K(s) = \prod_{i=1}^{3} \frac{(s^2 + a_i^2)}{(s^2 + b_i^2)}$$

a_1	a_2	a_3	b_1	b_s	F
.3177	.7989	.9832	1.1000	1.0775	32.6295
.3014	.7722	.9782	1.2000	1.1658	42.5036
.2920	.7573	.9753	1.3000	1.2563	49.7008
.2858	.7476	.9735	1.4000	1.3479	55.5675
.2813	.7407	.9722	1.5000	1.4402	60.5982
.2779	.7356	.9712	1.6000	1.5329	65.0401
.2753	.7316	.9705	1.7000	1.6260	69.0380
.2732	.7285	.9699	1.8000	1.7193	72.6852
.2715	.7259	.9694	1.9000	1.8127	76.0467
.2701	.7238	.9690	2.0000	1.9063	79.1693
.2690	.7221	.9687	2.1000	2.0000	82.0886
.2680	.7206	.9684	2.2000	2.0938	84.8322
.2671	.7193	.9682	2.3000	2.1877	87.4221
.2664	.7182	.9680	2.4000	2.2817	89.8760
.2657	.7173	.9678	2.5000	2.3757	92.2088
.2652	.7165	.9676	2.6000	2.4698	94.4326
.2647	.7157	.9675	2.7000	2.5639	96.5580
.2643	.7151	.9674	2.8000	2.6580	98.5938
.2639	.7145	.9673	2.9000	2.7522	100.5478
.2635	.7140	.9672	3.0000	2.8464	102.4266
.2632	.7136	.9671	3.1000	2.9406	104.2362

TABLE B.4 CRITICAL FREQUENCIES WITH UNIFIED DESIGN CHART DATA FOR A 7-POLE FILTER WITH SEVEN EQUI-RIPPLE PEAKS IN PASS-BAND AND A SINGLE TRANSMISSION ZERO

$$K(s) = s \prod_{i=1}^{3} \frac{(s^2 + a_i^2)}{(s^2 + b_1^2)}$$

a_1	a_2	a_3	b_1	b_s	F
.5074	.8515	.9847	1.1000	1.0809	38.0060
.4871	.8309	.9831	1.2000	1.1711	49.4751
.4753	.8195	.9811	1.3000	1.2633	57.8522
.4675	.8121	.9799	1.4000	1.3563	64.6868
.4620	.8069	.9790	1.5000	1.4499	70.5505
.4577	.8030	.9784	1.6000	1.5438	75.7294
.4545	.8001	.9779	1.7000	1.6380	80.3913
.4519	.7977	.9775	1.8000	1.7324	84.6449
.4498	.7958	.9772	1.9000	1.8269	88.5655
.4480	.7942	.9769	2.0000	1.9216	92.2078

TABLE B.5 CRITICAL FREQUENCIES WITH UNIFIED DESIGN CHART DATA FOR AN 8-POLE FILTER WITH EIGHT EQUI-RIPPLE PEAKS IN PASS-BAND AND A SINGLE TRANSMISSION ZERO

$$K(s) = \prod_{i=1}^{4} \frac{(s^2 + a_i^2)}{(s^2 + b_1^2)}$$

a_1	a_2	a_3	a_4	b_1	b_8	F
.2275	.6269	.8847	.9891	1.1000	1.0834	43.1500
.2189	.6070	.8686	.9865	1.2000	1.1751	56.2036
.2138	.5955	.8599	.9851	1.3000	1.2683	65.7568
.2104	.5880	.8542	.9842	1.4000	1.3623	73.5576
.2079	.5825	.8502	.9836	1.5000	1.4568	80.2531
.2060	.5785	.8473	.9831	1.6000	1.5516	86.1682
.2045	.5753	.8451	.9828	1.7000	1.6467	91.4938
.2034	.5728	.8433	.9825	1.8000	1.7419	96.3535
.2024	.5708	.8419	.9823	1.9000	1.8372	100.8331
.2016	.5691	.8407	.9821	2.0000	1.9326	104.9949

TABLE B.6 CRITICAL FREQUENCIES FOR A FOUR-POLE LINEAR PHASE FILTER WITH FOUR EQUI-RIPPLE PEAKS IN PASS-BAND AND A SINGLE PAIR OF REAL-AXIS ZEROS

$$K(s) = \frac{(s^2+a_1^2)(s^2+a_2^2)}{(s^2-\sigma^2)}$$

$$\sigma > 0$$

a_1	a_2	σ
.1446	.8019	.2000
.2257	.8485	.4000
.2748	.8742	.6000
.3057	.9894	.8000
.3258	.8989	1.0000
.3394	.9051	1.2000
.3489	.9094	1.4000
.3556	.9124	1.6000
.3606	.9145	1.8000
.3644	.9162	2.0000

TABLE B.7 CRITICAL FREQUENCIES FOR A SIX-POLE LINEAR PHASE FILTER WITH SIX EQUI-RIPPLE PEAKS IN PASS-BAND AND A SINGLE PAIR OF REAL-AXIS ZEROS

$$K(s) = \prod_{i=1}^{3} \frac{(s^2 + a_i^2)}{(s^2 - \sigma^2)}$$

$$\sigma > 0$$

a_1	a_2	a_3	σ
.1187	.5211	.9372	.2000
.1720	.5882	.9462	.4000
.2013	.6267	.9521	.6000
.2187	.6503	.9559	.8000
.2296	.6654	.9585	1.0000
.2368	.6755	.9603	1.2000
.2417	.6825	.9615	1.4000
.2452	.6874	.9624	1.6000
.2478	.6911	.9630	1.8000
.2497	.6938	.9635	2.0000

TABLE B.8 CRITICAL FREQUENCIES FOR AN EIGHT-POLE LINEAR PHASE FILTER WITH EIGHT EQUI-RIPPLE PEAKS IN PASS-BAND AND TWO PAIRS OF REAL-AXIS ZEROS

$$K(s) = \prod_{i=1}^{4} \frac{(s^2 + a_i^2)}{(s^2-\sigma_1^2)\,(s^2-\sigma_2^2)} \qquad \sigma_1, \sigma_2 > 0$$

a_1	a_2	a_3	a_4	σ_1	σ_2
.0899	.3353	.6811	.9588	.2000	.6000
.1344	.4248	.7389	.9669	.6000	.6000
.1474	.4558	.7630	.9707	1.0000	.6000
.1526	.4691	.7741	.9725	1.4000	.6000
.1551	.4758	.7799	.9734	1.8000	.6000
.1565	.4795	.7831	.9740	2.2000	.6000
.0961	.3641	.7122	.9640	.2000	1.0000
.1474	.4558	.7630	.9707	.6000	1.0000
.1628	.4877	.7847	.9738	1.0000	1.0000
.1690	.5015	.7947	.9754	1.4000	1.0000
.1721	.5084	.7998	.9762	1.8000	1.0000
.1738	.5122	.8027	.9766	2.2000	1.0000
.0999	.3846	.7356	.9680	.2000	2.0000
.1371	.4445	.7635	.9714	.4000	2.0000
.1559	.4779	.7817	.9737	.6000	2.0000
.1666	.4979	.7936	.9753	.8000	2.0000
.1731	.5106	.8015	.9764	1.0000	2.0000
.1773	.5189	.8068	.9772	1.2000	2.0000

TABLE B.9 CRITICAL FREQUENCIES FOR A TEN-POLE LINEAR PHASE FILTER WITH TEN EQUI-RIPPLE PEAKS IN PASS-BAND AND TWO PAIRS OF REAL-AXIS ZEROS

$$K(s) = \prod_{i=1}^{5} \frac{(s^2 + a_i^2)}{(s^2 - \sigma_1^2)(s - \sigma_2^2)}$$

a_1	a_2	a_3	a_4	a_5	σ_1	σ_2
.0802	.2816	.5484	.8131	.9778	.2000	.6000
.1146	.3543	.6093	.8408	.9811	.6000	.6000
.1239	.3778	.6336	.8535	.9828	1.0000	.6000
.1276	.3876	.6445	.8596	.9836	1.4000	.6000
.1293	.3924	.6501	.8628	.9841	1.8000	.6000
.1303	.3951	.6532	.8646	.9843	2.2000	.6000
.0850	.3017	.5764	.8291	.9799	.2000	1.0000
.1239	.3778	.6336	.8535	.9828	.6000	1.0000
.1347	.4026	.6567	.8649	.9843	1.0000	1.0000
.1390	.4130	.6672	.8704	.9850	1.4000	1.0000
.1411	.4182	.6725	.8733	.9854	1.8000	1.0000
.1423	.4210	.6755	.8749	.9856	2.2000	1.0000

APPENDIX "C"

APPENDIX "C"

This appendix contains a very brief description of the computer programs that evolved during the course of this thesis. Typical computer outputs are included.

This describes the computer software that was developed during the course of this thesis. It includes some proprietary (Com Dev Ltd) packages that are used as part of some of the programs.

The various programs with typical outputs are described as follows:

(1) Program UDC QE

This program generates the unified design charts for quazi-elliptic filters and computes the cut-off frequency with respect to the maximum ripple in the pass-band using numeric technique. Typical outputs are as described in Tables A.1 to A.5 in Appendix A.

(2) Program GEN UDC

This program generates the unified design charts and amplitude response for the general class of doubly-terminated low-pass prototype networks - for a given set of critical frequencies.

Table 4.6 in Chapter IV represents the typical output for an 8-pole filter with transmission zeros.

(3) Program GAP BPF

This program computes the amplitude and phase response and their derivatives for the general class of doubly-terminated band-pass filters for a given set of critical frequencies of the equivalent low-pass prototype network. The program can calculate transmission or reflection response, with or without dissipation and for TEM mode or wave-guide structures. The program assumes that the lumped equivalent circuit is frequency invariant.

Table C.1 shows the typical output which is for a 10-pole filter with 10 equi-ripple peaks in pass-band and two pairs of real-axis zeros in the 12 GHz frequency band. The filter is realized in a circular wave-guide of diameter 0.9 inches and having an average unloaded Q of 9,000. Critical frequencies for such a class of filter are described in Section 4.6.4.

(4) Program DM SYN

This program computes the normalized coupling and the actual susceptance matrices for the general class of symmetrical 4, 6 or 8-pole band-pass filters for a given set of critical frequencies of the equivalent low-pass prototype network and the required band-pass parameters.

Table 6.3 of Chapter VI describes the typical output which is for a 6-pole filter with six equi-ripple peaks in pass-band and a pair of transmission zeros.

(5) Program SPX OPT

This is an optimization program to synthesize in terms of the critical frequencies, the general class of doubly-terminated low-pass prototype networks for a given set of amplitude constraints using the SIMPLEX method. The program incorporates provision for equality, as well as inequality constraints on the variables.

Table C.2 depicts the typical output.

(6) Program NFL OPT

This program computes the critical frequencies for the general class of doubly-terminated low-pass prototype networks for a given set of amplitude constraints using the new Fletcher's algorithm. The gradients of the objective function and the inequality or equality constraints, if any are derived analytically.

Table 6.2 of Chapter VI depicts the typical output.

(7) Program BENT

This program generates the maximum permissible attenuation zeros for a given set of transmission zeros or real-axis zeros,or both, for the doubly-terminated filter networks, using Bennett's transformation.

Tables B.1 to B.9 in Appendix B, are the typical outputs of this program.

(8) Program BEN OPT

This is an optimization program similar to NFL OPT, except that it includes Bennett's transformation in the formulation of the objective function. It is therefore restricted to optimize the class of filters that exhibit maximum permissible peaks with equi-ripples in the pass-band.

Its output has the same basic form as that of program NFL OPT.

TABLE C.1 TYPICAL COMPUTER OUTPUT FOR THE COMPUTED RESPONSE OF A BAND-PASS FILTER, WITH THE CRITICAL FREQUENCIES OF THE EQUIVALENT LOW-PASS PROTOTYPE NETWORK AS THE INPUT PARAMETERS

FILTER CONFIG WITH 2 PAIR OF REAL-AXIS ZEROS
THE FILTER PARAMETERS FOR TRANSMISSION ARE

ORDER OF FILTER	10	
RETURN LOSS	-26.50	(DB)
FILTER BANDWIDTH	50.50	(MHZ)
CENTER FREQUENCY	11900.00	(MHZ)
LOWER LIMIT	11900.00	(MHZ)
UPPER LIMIT	11950.00	(MHZ)
UNLOADED Q	9000.00	
NUMBER OF FREQUENCY POINTS	11	

FREQUENCY MHZ	AMPLITUDE DB	RELATIVE AMPLITUDE DB	1ST DERIV DB/MHZ	PHASE RADIANS	PHASE DEVIATION DEGREES	GROUP DELAY NSEC	RELATIVE DELAY NSECS
11900.0	-1.80	.000	.000	-.023	-1.32	49.62	-.00
11905.0	-1.79	.011	.000	-1.581	-1.28	49.49	-.13
11910.0	-1.78	.018	.003	-3.129	-.73	49.17	-.46
11915.0	-1.79	.006	-.007	-4.675	-.08	49.34	-.29
11920.0	-1.86	-.056	-.025	-6.248	-1.03	51.20	1.58
11925.0	-2.08	-.276	-.074	-7.931	-8.30	57.16	7.54
11930.0	-3.25	-1.449	-.770	-10.015	-38.57	81.86	32.24
11935.0	-16.15	-14.346	-3.326	-12.251	-77.59	43.15	-6.47
11940.0	-30.64	-28.844	-2.494	-13.139	-39.45	19.02	-30.61
11945.0	-41.63	-39.835	-1.948	-13.602	23.04	11.53	-38.09
11950.0	-50.45	-48.646	-1.600	-13.903	94.75	8.00	-41.62

TABLE C.2 TYPICAL OUTPUT OF THE OPTIMIZATION PROGRAM SPX-OPT USING THE SIMPLEX METHOD*

$$K(s) = \frac{S^4(s^2+a_1^2)(s^2+a_2^2)}{(s^2+b_1^2)(s^2+b_2^2)}$$

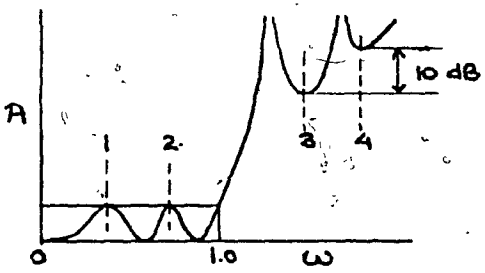

Iteration Number	U	U_{art}	Variables		
50	1.55E+00	1.94E+01	.7227	.8534	1.3066
100	1.96E-03	1.71E+01	.7288	.8610	1.2831
150	2.30E-03	1.72E+00	.7296	.8617	1.2818
200	7.21E-02	2.47E-01	.7289	.8617	1.2816

* Intermediate output for SIMPLEX method. U_{art} is the value of artificial unconstrained function at the centroid of the SIMPLEX.

Constraints: $0<a_1,a_2<1$; $1<b_1\leq 10$; $b_2=1/a_2$; F=80 dB

Objective Function: $|R(1)-R(2)|+||T(3)-T(4)|-10|$

Starting Values: $a_1=.5$, $a_2=.7$, $b_1=1.5$

Optimum Solution Found: Minimum U=1.44E-04
X:.7297,.8618,1.2817

Equality Constraint: -2.38E-03

Execution Time in Seconds: 250